HERON is jointly edited by:
STEVIN-LABORATORY of the department of Civil Engineering, Delft University of Technology, Delft, The Netherlands
and
TNO-INSTITUTE FOR BUILDING MATERIALS AND STRUCTURES. Rijswijk (ZH), The Netherlands.
HERON contains contributions based mainly on research work performed in these laboratories on strength of materials, structures and materials science.

ISSN 0046-7316

Secretary:
G. J. van Alphen
Stevinweg 1
P.O. Box 5048
2600 GA Delft, The Netherlands
Tel. 0031-15-785919
Telex 38070 BITHD

HERON vol. 31 1986 no. 4

Contents

PLASTIC DESIGN OF BURIED STEEL PIPELINES IN SETTLEMENT AREAS

A. M. Gresnigt
TNO-Institute for Building Materials and Structures, Rijswijk, The Netherlands

Publications in HERON since 1970

Plastic design of buried steel pipelines in settlement areas

1 Introduction

In the Netherlands, many rivers and canals have to be crossed by pipelines. The highest water level occurring in such watercourses is often above the level of the adjacent land, so that dykes are needed to prevent flooding. As a rule, the pipeline profile corresponds to the existing cross-section of the dyke and, after laying, is given a covering of clay and topsoil.

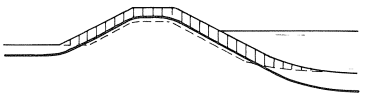

Fig. 1-1. Pipeline crossing over a dyke.
- - - - - original dyke cross-section
——— new dyke cross-section
I I I I additional covering topsoil

As the subsoil of the dyke often consists of highly compressible peat and clay strata, considerable amounts of settlement may occur. Because of the additional load on the dyke, settlement of the dyke is likely to be greater than that of the adjacent polder and of the river or canal bed.
As a result of such differential settlement, the pipeline is subjected to bending moments, normal (or direct) forces and sometimes also to torsional moments. These torsional moments occur in situations where the plane of the pipeline crossing is not vertical, as in the case (b) shown in Fig. 1-2. Because of its greater length in this case, the pipeline possesses greater flexibility and is thus better able to accommodate itself to differences in settlement.
The analysis of buried pipelines has conventionally been based on elastic theory. In the Netherlands, codes of practice embodying this approach were published in 1971 [1.1] and 1973 [1.2]. However, when these codes were applied to pipeline crossings already in existence at the time of publication, several of them were found not to satisfy the requirements. Therefore the crossings in question were judged to be deficient in safety by the dyke managers. This prompted them to call for structural measures (modification

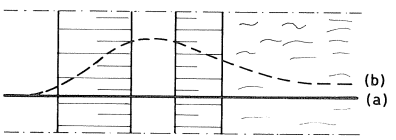

Fig. 1-2. Two possibilities for the horizontal layout of a pipeline crossing.

or replacement of existing crossings) and/or operational measures (lowering the permissible internal pressure).
In the course of subsequent discussions on the problem it was decided to carry out further research. In view of the character of the loads (imposed deformations due to differential settlement) it was expected that, by applying plastic theory, it could be shown that the actual loadbearing and deformation capacity of the pipelines are substantially greater than calculated with elastic analysis.
The principal results of the research are reported in the present publication.
It emerges that computational models based on plastic theory can provide an accurate description of the behaviour of buried steel pipelines up to failure. On applying this approach to the analysis of pipeline crossings previously considered to be deficient in safety it has been found in a number of cases that the pipelines in question are in fact safe enough. As for the other pipelines, it has proved possible to attain the desired level of safety by means of relatively minor modifications (e.g., partial removal of backfill over the pipeline). In the majority of cases replacement of the pipeline has not been necessary.
The effect of the internal pressure on the flexural behaviour is described in Chapter 2, while in Chapter 3 the effect of external loads such as earth pressure and bending upon the rupturing pressure is investigated. Chapter 4 deals with the various failure modes and indicates the limit values to be complied with.
The research has led to the development of a new design method, which is explained in Chapter 5. Rules for practical application of the method are derived in Chapters 6 and 7. In Chapter 8 the practical application possibilities for the new design method are considered and the principal conclusions summarized.

2 Bending and internal pressure in straight pipelines

In this chapter it is investigated what effect the internal pressure has upon the moment-curvature diagram, the ovalization and the buckling behaviour of straight pipelines loaded in bending. The effect of the other loads, such as earth pressure, normal force, shear force and torsional moment will be considered in Chapter 6.

2.1 *Moment-curvature diagram*

In the vicinity of bends, such as those at crossings of dykes and road embankments, the stress in the longitudinal direction caused by internal pressure (σ_{xp}) will be practically half the circumferential stress (σ_{yp}). This is the case because near bends the pipe behaves more or less in the manner of a pressure vessel in which the longitudinal strains can develop freely. In long straight pipelines, on the other hand, the longitudinal strains are zero because of the frictional restraint of the pipe by the surrounding soil. In the case of a pressure vessel the values of σ_{xp} and σ_{yp} are as follows:

$$\sigma_{xp} = \frac{\pi r^2 P}{2\pi r t} = \frac{Pr}{2t} \tag{2.1-1}$$

$$\sigma_{yp} = \frac{Pr}{t} \tag{2.1-2}$$

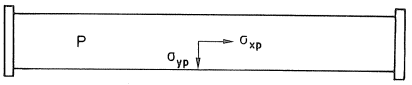

Fig. 2.1-1. Stresses due to the pressure P in a pipe with butt plates.

Bending gives rise to stresses σ_{xm} in the longitudinal direction.

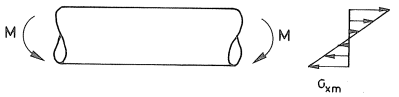

Fig. 2.1-2. Stress in longitudinal direction due to bending.

For σ_{xm} we obtain:

$$\sigma_{xm} = \frac{M}{W} = \frac{M}{\pi r^2 t} \tag{2.1-3}$$

and for σ_{xp}, σ_{xm} and σ_{yp} we can then write:

$$\sigma_x = \sigma_{xp} \pm \sigma_{xm} = 0.5\alpha\sigma_e \pm \beta\sigma_e \tag{2.1-4}$$

$$\sigma_y = \sigma_{yp} = \alpha\sigma_e \tag{2.1-5}$$

In this section: $\perp = \sigma_{yp}/\sigma_e$ and $\beta = \sigma_{xm}/\sigma_e$.
The end of the elastic range is reached when the stress combination satisfies a yield criterion. The criterion formulated by Von Mises will be adopted for this:

$$\sigma_c = \sqrt{\sigma_x^2 + \sigma_y^2 - \sigma_x\sigma_y} = \sigma_e \tag{2.1-6}$$

With (2.1-4) and (2.1-5) it follows that:

$$1 = \sqrt{(0.5\alpha \pm \beta)^2 + \alpha^2 - (0.5\alpha \pm \beta)\alpha} \tag{2.1-7}$$

$$\beta = \pm\sqrt{1 - 0.75\alpha^2} \tag{2.1-8}$$

From (2.1-8) it appears that, with increasing bending moment, the end of the elastic range is reached simultaneously on the tensile side and the compressive side. With further increase of the bending moment the region in which yielding occurs will, starting from the extreme fibres, become larger. This is indicated in Fig. 2.1-3, adopting a bilinear σ-ε diagram.
The effect of ovalization on the moment-curvature diagram will as yet not be considered in the present chapter. Its influence will be further analysed in Chapter 6.
For the bending moment it follows that:

$$M = 4\int_0^{\varphi_0} \beta\sigma_e tr\, d\varphi \frac{\sin\varphi}{\sin\varphi_0} r\sin\varphi + 4\int_{\varphi_0}^{\pi/2} \beta\sigma_e tr\, d\varphi\, r\sin\varphi \tag{2.1-9}$$

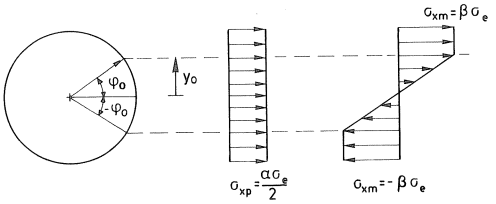

Fig. 2.1-3. Stresses in longitudinal direction due to pressure and bending.

$$M=2\beta\sigma_e tr^2\left\{\int_0^{\varphi_0}\frac{2\sin^2\varphi}{\sin\varphi_0}\,d\varphi+\int_{\varphi_0}^{\varphi/2}2\sin\varphi\,d\varphi\right\} \tag{2.1-10}$$

$$M=2\beta\sigma_e tr^2\left\{\frac{\varphi_0}{\sin\varphi_0}-\frac{\sin 2\varphi_0}{2\sin\varphi_0}+2\cos\varphi_0\right\} \tag{2.1-11}$$

After rearrangement and replacing ϕ_0 by ϕ we obtain:

$$\boxed{M=2\beta\sigma_e tr^2\left(\frac{\varphi}{\sin\varphi}+\cos\varphi\right)} \tag{2.1-12}$$

For the associated curvature it follows that:

$$\varphi=\varphi_0\rightarrow\varepsilon_x'=\frac{\sigma_e}{E}\left(\frac{\alpha}{2}+\beta-\nu\alpha\right) \tag{2.1-13}$$

$$\varphi=-\varphi_0\rightarrow\varepsilon_x''=\frac{\sigma_e}{E}\left(\frac{\alpha}{2}-\beta-\nu\alpha\right) \tag{2.1-14}$$

$$K=\frac{\varepsilon_x'-\varepsilon_x''}{2y_0}=\frac{\beta\sigma_e}{Er\sin\varphi_0} \tag{2.1-15}$$

After replacement of φ_0 by φ we obtain the following expression for the curvature associated with M according to (2.1-12):

$$\boxed{K=\frac{\beta\sigma_e}{Er\sin\varphi}} \tag{2.1-16}$$

When φ becomes equal to $\pi/2$, yielding is just attained. The bending moment is then M_{er} and the curvature K_{er}:

$$\boxed{M_{er}=\pi r^2 t\beta\sigma_e=W_e\beta\sigma_e} \tag{2.1-17}$$

$$\boxed{K_{er}=\frac{\beta\sigma_e}{Er}=\frac{W_e\beta\sigma_e}{EI}} \tag{2.1-18}$$

When φ approaches 0, the whole cross-section will be plastified and the maximum moment be reached:

$$M_{pr} = 4r^2 t\beta\sigma_e = W_p\beta\sigma_e \qquad (2.1\text{-}19)$$

$$K \rightarrow \text{tends to infinity} \qquad (2.1\text{-}20)$$

With (2.1-12) and (2.1-16) the moment-curvature diagram can be drawn for different values of the pressure P (Fig. 2.1-4). It appears from this diagram that the effect of P upon the flexural loadbearing capacity (M_{pr}), particularly at not too high values of P, is relatively slight. Anyway, with regard to buried pipelines it is to be noted that the magnitude of M_{pr} is merely of secondary importance. The deformation capacity is much more important. In this case it is the curvature to which the pipeline can be bent without giving rise to undesirable consequences such as cracking or buckling.

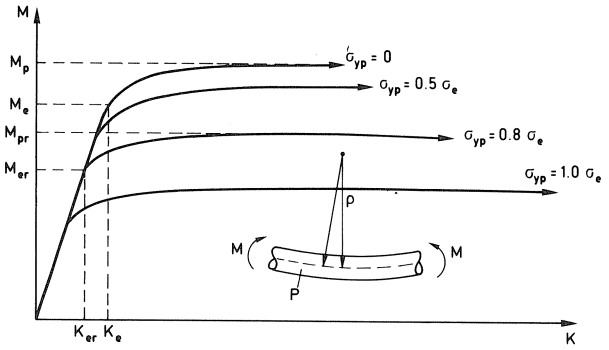

Fig. 2.1-4. Moment-curvature diagrams for pressure and bending.

At the start of the research, in 1972, little was as yet known about ovalization and the occurrence of buckling in the plastic range. The series of tests reported in Section 2.2 was carried out with a view to obtaining more information. These tests also provided a means of verifying the calculated moment-curvature diagrams.

2.2 *Tests relating to bending and internal pressure*

2.2.1 Test specimens and tests performed

Thirteen tests were performed on reduced-scale pipe specimens (152.5 mm and 122 mm external diameter, 1.55 mm wall thickness)* fabricated from hot-rolled steel plate, grade Fe 52.3, in accordance with German Standard DIN 17100. The measured yield point was about 360 N/mm^2.

In comparison with actual pipelines the specimens had a relatively large diameter/wall thickness ratio (approx. 100 and 80 respectively). This was so chosen in order to inves-

* ø 152.5–1.55 and ø 122–1.55 will be further used to denote these and similar pipe cross-sectional dimensions.

Fig. 2.2-1. Ovalization due to bending.

tigate the most unfavourable situation with regard to buckling. The bending moment M, the curvature K and the change in the vertical diameter ΔD_v (= the change of the diameter in the plane of bending) were measured (Fig. 2.2-1).
An overview of the tests performed is presented in Table 2.2-1. For further information on the test specimens and the experimental set-up the reader is referred to the photographs and to [2.10].

Table 2.2-1.

No.	D_u [mm]	t [mm]	$\frac{\sigma_{yp}}{\sigma_e} = \alpha$	P [bar]
25	152.5	1.55	0	0
26	152.5	1.55	0	0
24	152.5	1.55	0.20	14
21	152.5	1.55	0.40	29
22	152.5	1.55	0.60	43
23	152.5	1.55	0.80	58
28	152.5	1.55	1.00	72
27	152.5	1.55	−0.014	−0.99
25b	122	1.55	0	0
25c	122	1.55	0	0
29	122	1.55	0.31	28
21c	122	1.55	0.40	36
23c	122	1.55	0.80	72

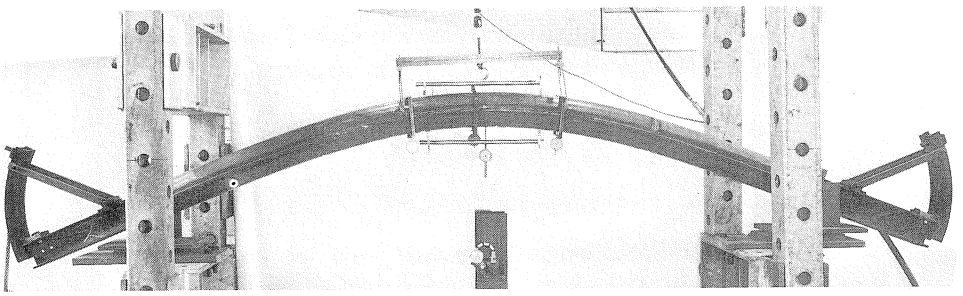

Photo 1. Experimental set-up, with test specimen 28 (bending moment + internal pressure) after the test. This pipe was initially straight; $D_u/t = 101$; $\sigma_{yp} = \sigma_e$.

2.2.2 Test results

Moment-curvature diagram; change of the diameter in the plane of bending
Fig. 2.2-2 shows the moment-curvature diagram of test 25 ($P = 0$) and Fig. 2.2-3 shows that of test 28. The measured relation between the bending moment and the change in

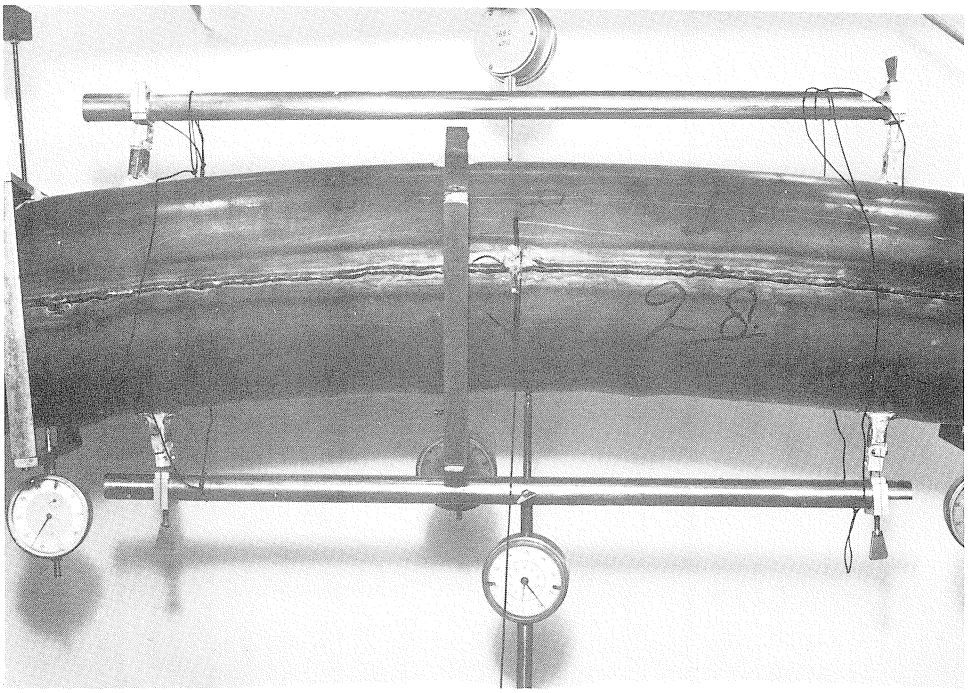

Photo 2. Detail of photo 1. Wrinkles are visible.

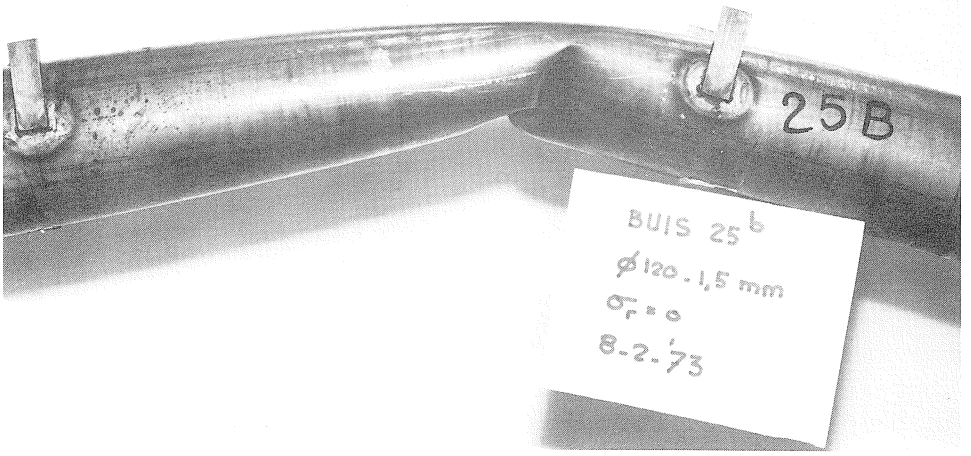

Photo 3. Test 25b with $D_u/t = 81$ and $\sigma_{yp} = 0$. The buckled shape as shown here has been accentuated by further bending of the pipe after it had buckled.

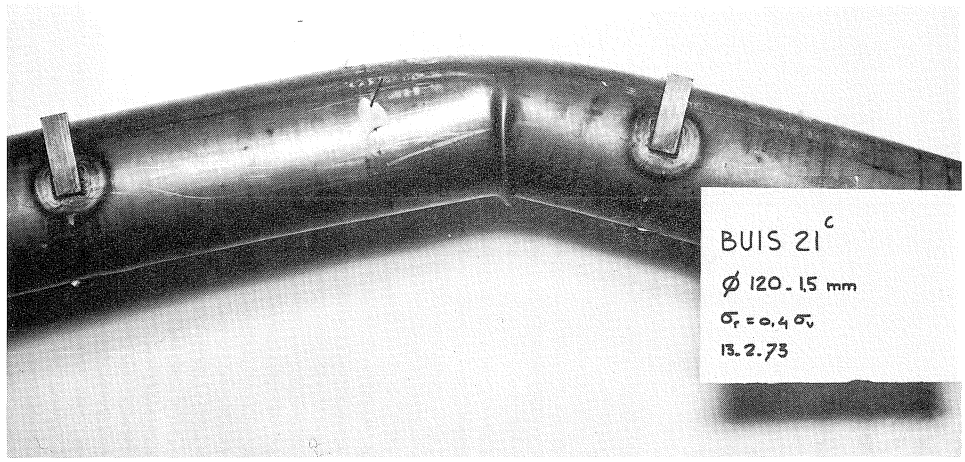

Photo 4. Test 21c with $D_u/t = 81$ and $\sigma_{yp} = 0.4\sigma_e$. In this case, too, the buckled shape has been accentuated by further bending of the pipe after it had buckled.

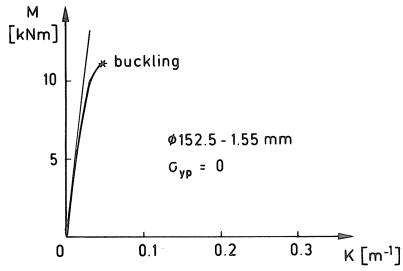

Fig. 2.2-2. Moment-curvature diagram, test 25.

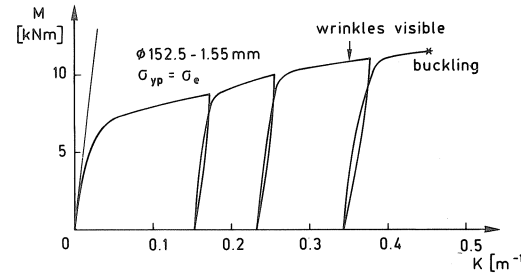

Fig. 2.2-3. Moment-curvature diagram, test 28.

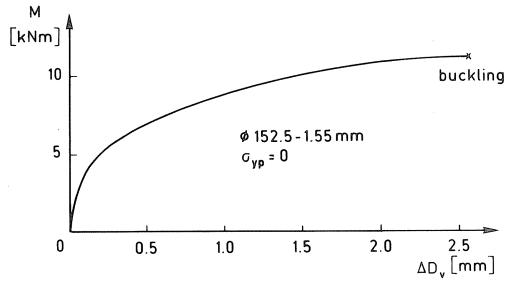

Fig. 2.2-4. Relation between moment and *decrease* in vertical diameter, test 25.

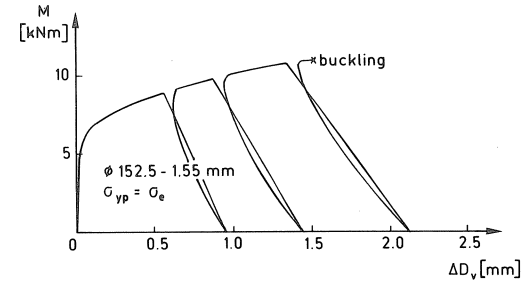

Fig. 2.2-5. Relation between moment and *increase* in vertical diameter, test 28.

the vertical diameter (= the change of the diameter in the plane of bending) in these tests is given in Figs. 2.2-4 and 2.2-5. For the other diagrams the reader is referred to [2.10].

On comparing the measured moment-curvature diagrams with Fig. 2.1-4 it is apparent that deviations from the "theoretical" diagrams in Fig. 2.1-4 occur even already at relatively low values of the bending moment.

This is due to the following causes:
- the presence of residual stresses from rolling and welding;
- the differences between the actual σ-ε diagram and the assumed bilinear diagram (limit of proportionality, strain-hardening);
- some effect of non-linear geometric behaviour.

The measured values of the maximum moment are in good agreement with the calculated values in the previous Section. Because the stresses so adjust themselves in the fully plastic state that the loadbearing capacity becomes optimal, residual stresses have no effect on the maximum moment M_{pr}.

In the test with $P=0$ the vertical diameter is found to decrease with increasing curvature. This is in agreement with what was deduced by Reissner [3.1], among others, for the elastic range. This will be further explained with reference on an equilibrium model. See Fig. 2.2-6.

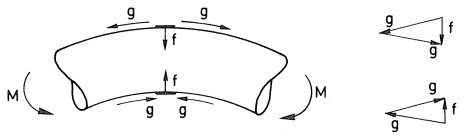

Fig. 2.2-6. "Ovalization forces".

Because of the curvature the flexural stresses, here conceived as having been compounded to forces g, will have components f which can be conceived as constituting an external load: "ovalization forces".

It is obvious that when internal pressure is acting in the pipeline the ovalization will be less than when there is zero internal pressure. That the vertical diameter increases instead of decreases in the plastic range when there is a high internal pressure (Fig. 2.2-5) is due to the fact that, besides yielding in the longitudinal direction, yielding occurs also in the circumferential direction.

This can be demonstrated with the aid of the property that in isotropic materials the direction of the strains is perpendicular (normal) to the yield surface. Fig. 2.2-7 shows the yield surface for the stresses in the pipe wall. It is the Von Mises yield criterion.

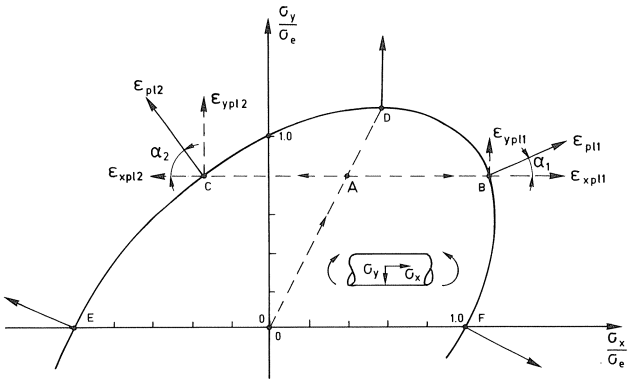

Fig. 2.2-7. Yield surface according to Von Mises.

$$f(\sigma_x, \sigma_y) = \sigma_x^2 + \sigma_y^2 - \sigma_x\sigma_y - \sigma_e^2 = 0 \qquad (2.2\text{-}1)$$

Combinations of σ_y/σ_e and σ_x/σ_e (stress points) which are located within the yield surface are in the elastic range. Stress points which are located on the yield surface satisfy the yield criterion according to (2.2-1). Stress points outside the yield surface are not possible (strain-hardening will not be considered here).
When the internal pressure is applied, the loading path OA is followed, while $\sigma_y = 2\sigma_x$. Next, bending is applied: the path AB is followed for the tensile fibres, and the path AC for the compressive fibres. Yielding is attained at the points B and C.
When, for this stress combination, the deformations - in this case the curvature - are increased, the deformation vector will be perpendicular to the yield surface. The plastic strains associated with the stresses σ_x and σ_y are ε_{xpl} and ε_{ypl}. Together they form the strain vector ε_{pl} indicated in Fig. 2.2-7.
The strains ε_{xpl} produce the additional plastic curvature. The strains ε_{ypl} produce a plastic change in the circumference of the pipe. It is apparent from Fig. 2.2-7 that the strain ε_{ypl} is positive both at the tensile fibres (point B) and at the compressive fibres (point C). Therefore bending in the plastic range in conjunction with internal pressure results in an increase in the circumference of the pipe and thus an increase in diameter.
From the above it follows that in the case of bending with internal pressure there are two factors which play a part in bringing about the change in vertical diameter:
- the reduction due to the ovalization forces;
- the increase due to yielding in the circumferential direction.

If the internal pressure is high, the second factor is the governing one. This accounts for the result of test 28 as represented in Fig. 2.2-5.
With the aid of the normality principle applied here it is possible to calculate the plastic increase in circumference as a function of the curvature, as follows:
The slope (ψ) of the yield surface is obtained by differentiation of (2.2-1) with respect to σ_x:

$$\frac{df(\sigma_x, \sigma_y)}{dx} = 2\sigma_x + 2\sigma_y \frac{d\sigma_y}{d\sigma_x} - \sigma_y - \sigma_x \frac{d\sigma_y}{d\sigma_x} = 0 \qquad (2.2\text{-}2)$$

$$\tan\psi = \frac{d\sigma_y}{d\sigma_x} = \frac{2\sigma_x - \sigma_y}{\sigma_x - 2\sigma_y} \qquad (2.2\text{-}3)$$

The direction of the strain vector ε_{pl} is:

$$\tan\alpha = -\frac{1}{\tan\psi} = \frac{\sigma_x - 2\sigma_y}{\sigma_y - 2\sigma_x} \qquad (2.2\text{-}4)$$

So this means that the plastic strain in the circumferential direction ε_{ypl} is equal to the plastic strain in the longitudinal direction ε_{xpl} multiplied by $\tan\alpha$:

$$\varepsilon_{ypl} = \tan\alpha \cdot \varepsilon_{xpl} \qquad (2.2\text{-}5)$$

For the plastic strains ε_{xpl} we obtain:

$$\varepsilon_{xpl} = \varepsilon_x - \varepsilon_{xe} \tag{2.2-6}$$

where:

$$\varepsilon_x = Kr \sin \varphi + \frac{0.5\sigma_{yp}}{E} - \frac{\nu\sigma_{yp}}{E} \tag{2.2-7}$$

$$\varepsilon_{xe} = \frac{1}{E}(\sigma_x - \nu\sigma_{yp}) \tag{2.2-8}$$

$$\sigma_{yp} = \frac{Pr}{t} \tag{2.2-9}$$

For the tensile zone (point B in Fig. 2.2-7) we obtain for σ_x with (2.2-1) and $\sigma_y = \sigma_{yp}$:

$$\sigma_{x1} = 0.5(\sigma_{yp} + \sqrt{\sigma_{yp}^2 - 4(\sigma_{yp}^2 - \sigma_e^2)}) \tag{2.2-10}$$

and for the compressive zone (point C in Fig. 2.2-7):

$$\sigma_{x2} = 0.5(\sigma_{yp} - \sqrt{\sigma_{yp}^2 - 4(\sigma_{yp}^2 - \sigma_e^2)}) \tag{2.2-11}$$

so that:

$$\varepsilon_{xe1} = \frac{1}{E}(\sigma_{x1} - \nu\sigma_{yp}) \tag{2.2-12}$$

$$\varepsilon_{xe2} = \frac{1}{E}(\sigma_{x2} - \nu\sigma_{yp}) \tag{2.2-13}$$

For the increase in circumference ($\Delta 0$) it follows that (see also Fig. 2.1-3):

$$\Delta 0 = \int_{\varphi_0}^{\pi - \varphi_0} \varepsilon_{xp} \tan \alpha_1 r \, d\varphi + \int_{\pi + \varphi_0}^{2\pi - \varphi_0} \varepsilon_{xp} \tan \alpha_2 r \, d\varphi$$

$$\Delta 0 = 2Kr^2(\tan \alpha_1 - \tan \alpha_2) \cos \varphi_0 -$$
$$- r(\pi - 2\varphi_0) \left\{ \varepsilon_{xe1} \tan \alpha_1 + \varepsilon_{xe2} \tan \alpha_2 - \right.$$
$$\left. - \frac{0.5\sigma_{yp} - \nu\sigma_{yp}}{E} (\tan \alpha_1 + \tan \alpha_2) \right\} \tag{2.2-14}$$

Where with (2.1-15), (2.1-8) and (2.1-5):

$$\varphi_0 = \arcsin \frac{\sqrt{\sigma_e^2 - 0.75\sigma_{yp}^2}}{KEr} \tag{2.2-15}$$

The plastic change in diameter due to the pressure P is:

$$\Delta D_{pl} = \frac{\Delta 0}{2\pi r} \cdot D = \frac{\Delta 0}{\pi} \tag{2.2-16}$$

From calculations for some practical cases [2.8] it appears that value of ΔD_{pl} is very small in relation to the diameter anyway. This is also apparent from the test results. For example, for $\sigma_{v\pi} = \sigma_\varepsilon$ and $K = 10K_e$ in test 28 the calculated ΔD_{pl} is only 1.3 per cent of the diameter [2.8]; see also Fig. 2.2-5.

For buried pipelines with $\sigma_{yp\,max}$ = approx. $0.7\sigma_e$ and a maximum curvature which is in general considerably less than $10K_e$ as envisaged above, the effect that ΔD_{pl} has upon the stresses is negligible.

Finally, attention must be drawn to some notable points on the yield surface in Fig. 2.2-7:

- Point D occurs when the pipe is subjected to internal pressure only. When yielding is attained, $\sigma_{yp} = 1.15\sigma_e$ and $\sigma_{xp} = 0.575\sigma_e$. As appears from the direction of the normal, then no plastic strains occur in the longitudinal direction. This is in accordance with what has been observed in rupturing tests, in which the diameter does increase, but the length of the specimen remains unchanged.
- Points E and F occur in the case of bending without internal pressure. Because the strain component ε_{ypl} at point E is positive, and is of the same magnitude but negative at point F, the total circumference will remain unchanged.
- At points E and F, where $\sigma_y = 0$, the ratio of ε_{xpl} to ε_{ypl} is as 2 : 1. This shows that Poisson's ratio in the plastic range is 0.5.

Buckling

As is to be expected, the internal pressure has a positive effect on the magnitude of the curvature $K_{buckling}$ at which buckling of the pipe occurs. This is clearly manifest in Figs. 2.2-2 and 2.2-3. In Fig. 2.2-8 the measured values of $K_{buckling}/K_e$ have been plotted against the values of $\alpha = \sigma_{yp}/\sigma_e$. The smallest measured values of $K_{buckling}$ were approx. $2.0K_e$ and occurred for $P = 0$.

In the pipes considered here, for low values of P, buckling occurs fairly suddenly when the curvature increases. It is something of a "snap-through" effect. The buckled shape is sharp and angular. Photo 3 illustrates such a case of "crease buckling". On the other hand, with high internal pressure in the pipe, buckling occurs much more gradually.

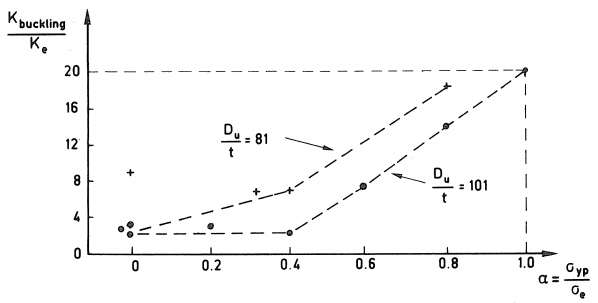

Fig. 2.2-8. Measured buckling curvature as a function of the internal pressure.

Quite often it is then not possible to determine clearly at what curvature "true" buckling develops. In this report the buckling curvature is defined as the curvature at which the highest value of the bending moment is attained. In many instances small waves in the pipe wall, occurring at lower curvatures than the buckling curvature, gave advance indication of buckling (Photo 2). The buckled shape was smooth (Photo 4).
The factors affecting the buckling curvature will be further considered in Chapter 4.

3 Effect of external loads on the rupturing pressure

The effect that the internal pressure has upon the magnitude of the maximum moment has been examined in Chapter 2. In the present chapter the effect of bending and other external loads on the rupturing pressure will be investigated. In seeking to answer this question the following basic assumptions are made:

a. The pipe material is ductile, i.e., it possesses sufficient strain capacity, so that the redistribution of stresses attended by a certain amount of yielding is possible without cracking.
b. The differential settlement affecting the buried steel pipelines under consideration is at most of such magnitude that, if the pipeline had zero flexural and/or torsional stiffness and would therefore accommodate itself completely to the differences in settlement, the strains occurring in it would not exceed the strain capacity of the material.

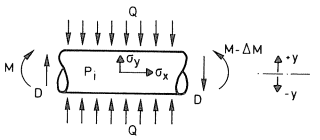

Fig. 3.1-1. Pipe loaded by internal pressure and external loads.

3.1 *Behaviour associated with increasing internal pressure*

In the following, this behaviour will be investigated with reference to a pipe loaded in bending, shear and earth pressure. These loads are indicated in Fig. 3.1-1.
The stresses due to these loads are:

$$\sigma_x = \sigma_{xp} \pm \sigma_{xm} \pm \sigma_{xq} \tag{3.1-1}$$

$$\sigma_y = \sigma_{yp} \pm \sigma_{yq} \tag{3.1-2}$$

$$\tau = \tau_d \tag{3.1-3}$$

where:

σ_{xp} = stress in x-direction due to P
σ_{yp} = stress in y-direction due to P
σ_{yq} = stress in y-direction due to Q

σ_{xq} = stress in x-direction due to Q; because of lateral contraction, the (flexural) stresses σ_{yq} also give rise to stresses in the x-direction

σ_{xm} = stress in x-direction due to M

τ_d = shear stress due to shear force D

With increasing internal pressure, yielding will occur when the stress combination satisfies the yield criterion. The Von Mises criterion will be adopted:

$$\sigma_c = \sqrt{\sigma_x^2 + \sigma_y^2 - \sigma_x\sigma_y + 3\tau^2} = \sigma_e \tag{3.1-4}$$

When yielding occurs, Poisson's ratio is $\nu = 0.5$. For σ_x, σ_y and τ according to (3.1-1), (3.1-2) and (3.1-3) it follows that:

$$\sigma_x = 0.5\sigma_{yp} \pm \sigma_{xm} \pm 0.5\sigma_{yq} \tag{3.1-5}$$

$$\sigma_y = \sigma_{yp} \pm \sigma_{yq} \tag{3.1-6}$$

$$\tau = \tau_d \tag{3.1-7}$$

With these expressions (3.1-4) becomes:

$$\sigma_e^2 = 0.75(\sigma_{yp} \pm \sigma_{yq})^2 + \sigma_{xm}^2 + 3\tau_d^2 \tag{3.1-8}$$

With further increase of P, after incipient yielding at the extreme fibres, yielding will gradually develop in all parts of the cross-section. This will be accompanied by some stress redistribution, because σ_{xm} will have to decrease when P and σ_{yp} increase, the reason being that the yield criterion as stated in (3.1-8) must always be satisfied. This redistribution of stresses is associated with some yielding. The curvatures will increase somewhat.

If the internal pressure increases further after yielding has developed in all parts of the cross-section, the yield criterion can be satisfied only if σ_{xm} further decreases. This means that the moment which can be resisted becomes smaller and that the pipe therefore offers less resistance to the deformations due to differential settlement. If P is sufficiently high, σ_{xm} and therefore also M will become zero, so that the pipeline will then accommodate itself "passively", as it were, to the differences in settlement.

When M decreases, the shear force will of course decrease at the same time, and for $M = 0$ the value of τ_d will likewise be zero.

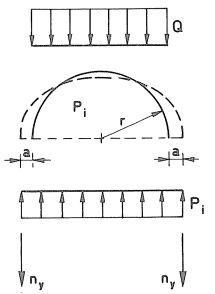

Fig. 3.1-2. Earth pressure Q "carried" by the internal pressure P_i.

As for the flexural stresses due to q, these will decrease due to the "rerounding" effect when the internal pressure increases.
In view of the above, (3.1-8) becomes:

$$\sigma_e^2 = 0.75(\sigma_{yp} \pm \sigma_{yq})^2 \tag{3.1-9}$$

$$\sigma_{yp} \pm \sigma_{yq} = \pm 1.15\sigma_e \tag{3.1-10}$$

If P is still further increased until $\sigma_{yp} = 1.15\sigma_e$, the value of σ_{yq} will gradually have to become zero.
The stress σ_{yp} is equated to:

$$\sigma_{yp} = \frac{P_p r}{t} = 1.15\sigma_e \tag{3.1-11}$$

For reasons of equilibrium, Fig. 3.1-2:

$$2n_y + Q = 2P_p(r + a) \tag{3.1-12}$$

For n_y we obtain:

$$n_y = t\sigma_{yp} = P_p r \tag{3.1-13}$$

so that (3.1-12) becomes:

$$Q = 2P_p a \tag{3.1-14}$$

This means that the earth pressure Q is, as it were, supported by the internal pressure. The wall of the pipe resists no bending moments. The situation that thus arises is comparable to that of a fire-hose loaded by internal pressure. A hosepipe in that condition is able to support an imposed external load.
In consequence of these circumstances, the only stresses which act in the pipe subjected to the pressure P_p in accordance with (3.1-11) are due to this pressure P_p itself. This means that, if the pressure in the pipe is further raised above the yield pressure P_p, a situation will be reached which is similar to that of a pipe not subjected to external loads. In connection with this the rupturing pressure of a pipe which is subjected also to external load will be no different from that of a pipe loaded by internal pressure only. This leads to the conclusion that, provided the conditions as to the pipe material and the imposed loads are satisfied, the rupturing pressure is not adversely affected by external loads.
The foregoing considerations can be applied also to other external loads than those envisaged here and will lead to the same conclusion.

3.2 *Direct derivation of the above with the aid of plastic theory*

For this purpose the stress distribution is so chosen that Prager's third theorem is satisfied. For the present case this theorem implies that, provided the chosen stress distribution fulfils a number of conditions, the associated load is the failure load. Since

Prager refers his theorems to the yielding stage, here the yield pressure P_p will provisionally be regarded as the failure load.
The chosen stress distribution is as follows:

$$\sigma_y = \sigma_{yp} = \frac{P_p r}{t} \tag{3.2-1}$$

$$\sigma_x = \sigma_{xp} = \frac{P_p r}{2t} \tag{3.2-2}$$

where:

$$P_p = \frac{1.15\sigma_e t}{r} \tag{3.2-3}$$

The conditions to be satisfied by the chosen stress distribution according to (3.2-1), (3.2-2) and (3.2-3) are:

a. The stress distribution must satisfy the requirements of equilibrium. This condition is satisfied. The stresses $\sigma_{yp} = 1.15\sigma_e$ and $\sigma_{xp} = 0.57\sigma_e$ are of such magnitude that the load can be supported by the yield pressure P_p. The load due to the earth pressure is supported by the internal pressure, while the bending moment and shear force are zero. Because the pipeline is buried and the differential settlement is of limited magnitude, no bending moment, no torsional moment, no normal force and no shear force are necessary for equilibrium.
b. The stress combination must everywhere be so constituted that the Von Mises comparison stress is not exceeded. This condition is satisfied in the case of the stresses σ_{yp} and σ_{xp}, since:

$$\sigma_c = \sqrt{1.15\sigma_e^2 + 0.57\sigma_e^2 - 1.15 \cdot 0.57\sigma_e^2} = \sigma_e \tag{3.2-4}$$

c. The stress combination must everywhere be in conformity with the strains that occur. Having regard to the tensile stresses and the corresponding strains this condition is likewise satisfied.
d. A plastic mechanism must be formed. This is indeed the case because at every point in the pipe wall the stress combination satisfies the yield criterion. A small increase in P produces a large increase in the circumferential strains.

In this way it has been proved that the yield pressure according to (3.2-3) is the "failure load". This failure load is not affected by the external loads.
That the "true" failure load, namely, the rupturing pressure, is higher than the yield pressure is due to the occurrence of strain hardening after the strains have attained the appropriate magnitude for this. Hence it follows that if the maximum working pressure is linked to the yield pressure, the actual safety against rupturing is greater according as the ratio between the tensile strength σ_t and σ_e is higher. The strain at which σ_t occurs also plays a part. According as this strain is greater, the increase in diameter at which σ_t is attained is likewise, so that, for equal σ_t, the rupturing pressure associated with a greater strain is less.

3.3 *Experimental verification*

3.3.1 Tests on reduced-scale pipes

By means of a series of rupturing tests [2.8], [2.12] it has also been shown experimentally that external loads do not adversely affect the rupturing pressure. The tests in question were always based on two specimens as nearly identical as possible. This was achieved by making the two specimens from the same length of pipe (⌀ 108 – 2 mm) or from the same bend (⌀ 114 – 3.8 mm) with a radius of 270 mm.

The following load combinations were investigated:

a. *Straight pipes*
   a1. earth pressure $(Q_d + Q_i)$ + bending (M) + internal pressure (P_i)
   a2. bending (M) + torsion (M_t) + internal pressure (P_i)
b. *Smooth bends*
   b1. earth pressure (Q_i) + bending (M) + internal pressure (P_i)
   b2. bending (M) + torsion (M_t) + internal pressure (P_i)
c. *Mitred bends*
   c1. earth pressure (Q_i) + bending (M) + internal pressure (P_i)

The procedure adopted was as follows:
First, at $P = 0$, the external loads were applied to one of the two specimens until the deformations (ovalization, curvature, rotation) were so great that the limit states defined in Chapter 4 had amply been exceeded. In many cases buckling occurred.
After these deformations had been imposed, the specimens were maintained in the deformed condition, and the deformed specimen as well as the non-deformed specimen were connected to the same pump. This set-up is shown diagramatically, for test (a1), in Fig. 3.3-1.

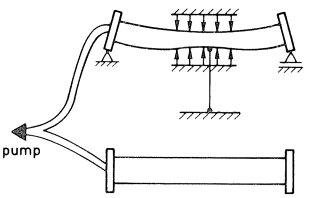

Fig. 3.3-1. Schematic set-up of the rupturing test a_1.

In nearly all the tests the first rupturing was found to occur in the specimen not deformed by external loads. In those cases where this was not so, the difference between the two rupturing pressures was negligible.
What had theoretically been deduced with the aid of plastic theory was thus experimentally confirmed for all kinds of load combinations, for straight pipes as well as for smooth bends and mitred bends. Photos 5 to 14 show the experimental set-up and specimens employed.

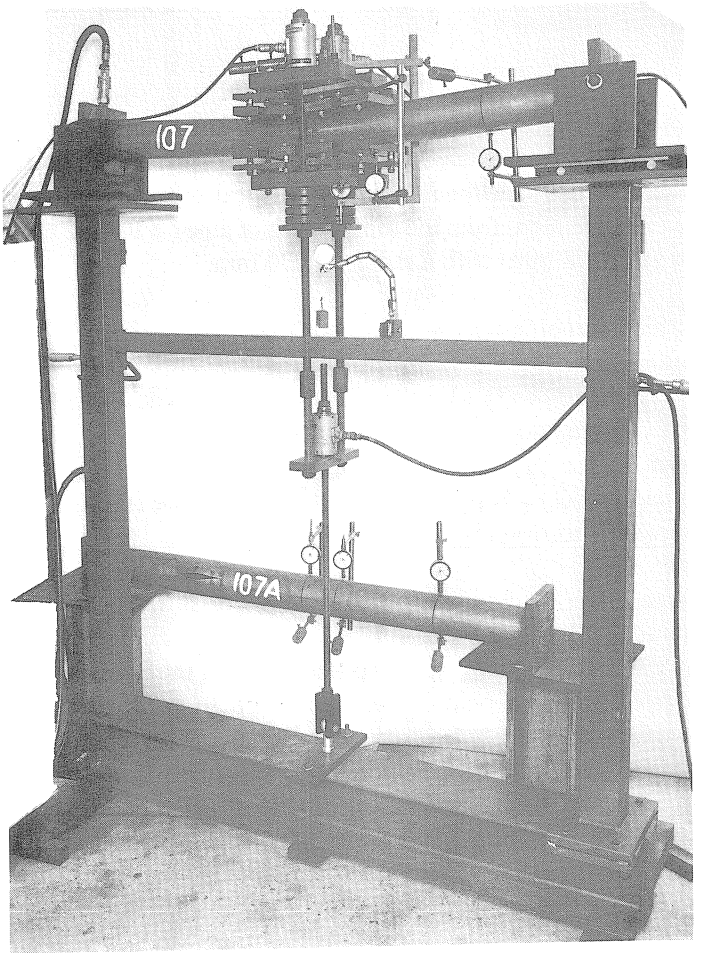

Photo 5. Rupturing test under the action of "earth pressure" ($Q_d + Q_i$) and bending (M) upon straight pipes (Nos. 107 and 107A, test a1).

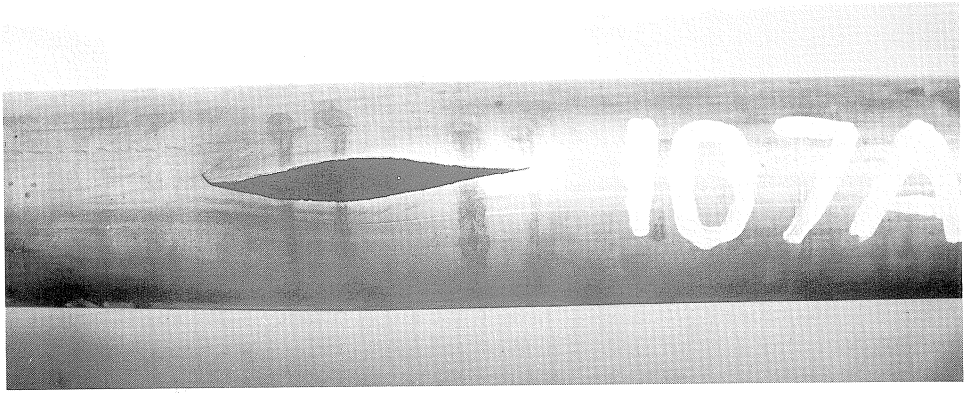

Photo 6. Detail of ruptured pipe (No. 107A).

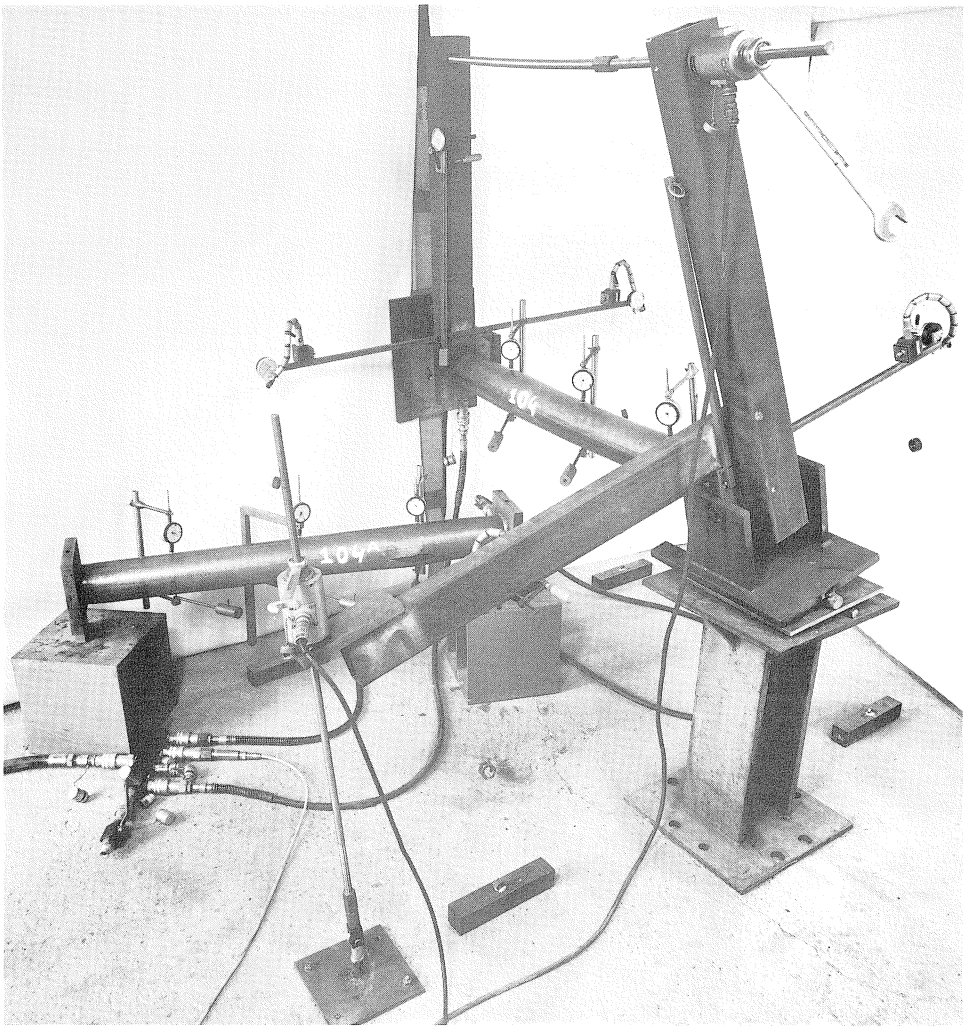

Photo 7. Rupturing test under the action of bending (M) and torsion (M_t) on straight pipes (Nos. 104 and 104A, test a2).

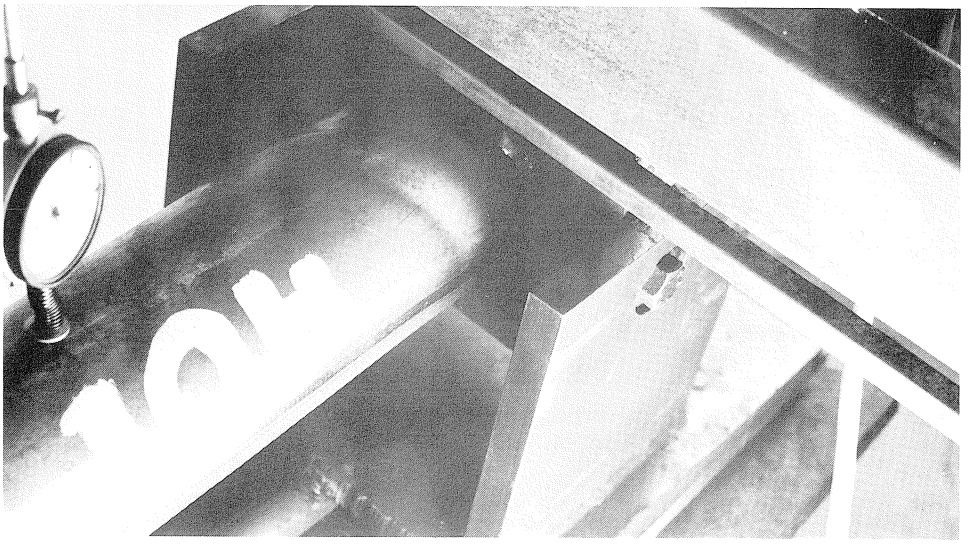

Photo 8. Detail of pipe No. 104: buckling due to bending and torsion (before internal pressure was applied).

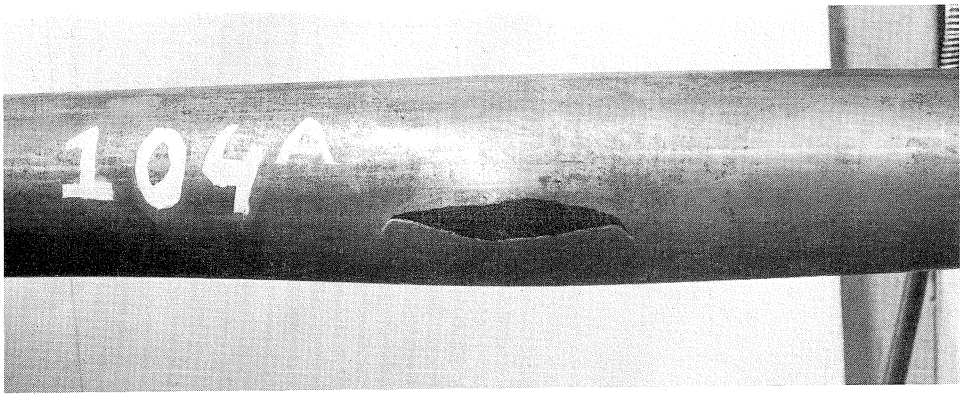

Photo 9. Detail of ruptured pipe No. 104A.

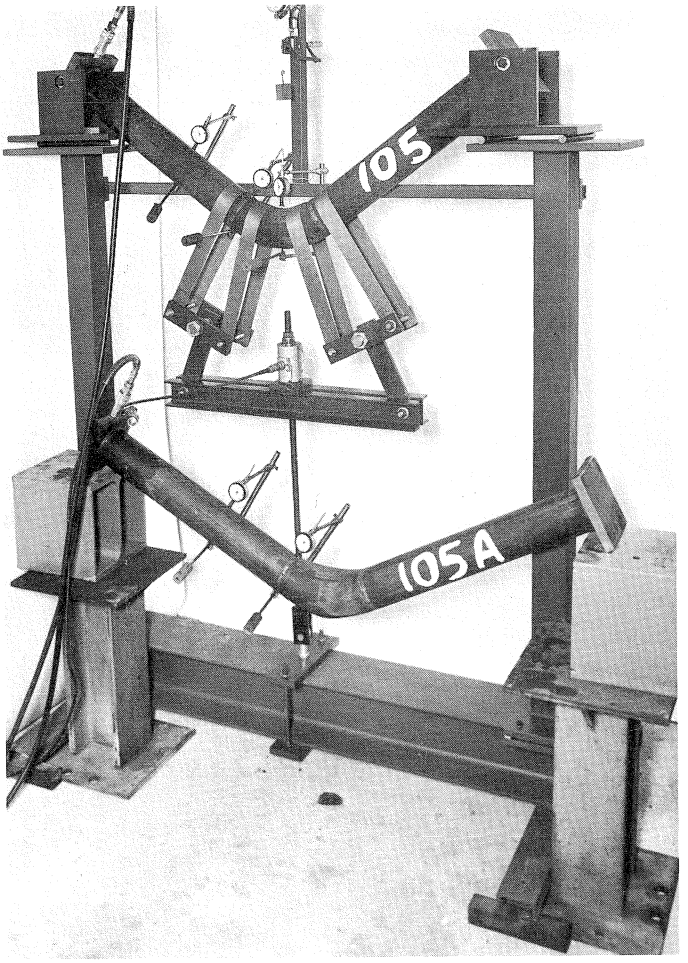

Photo 10. Rupturing test on smooth bends under the action of "earth pressure" (Q_i) and bending (M) (Nos. 105 and 105A, test b1).

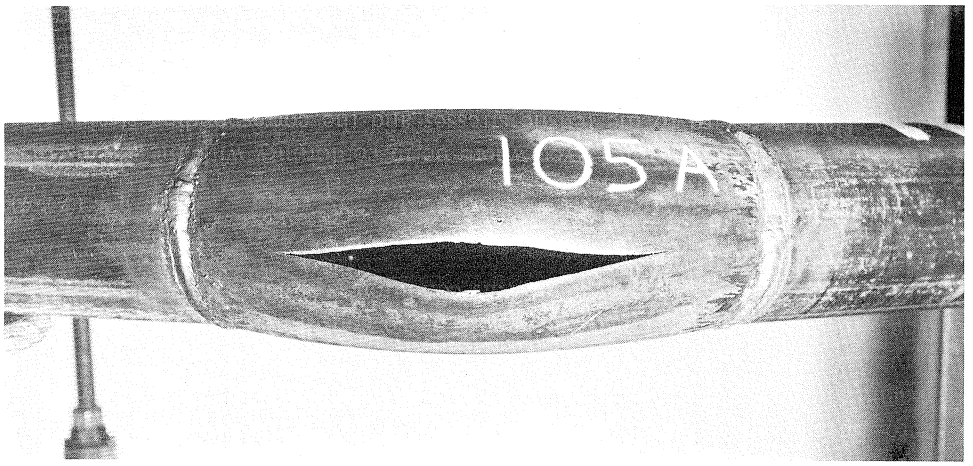

Photo 11. Detail of ruptured bend No. 105A (rupture on outside of bend).

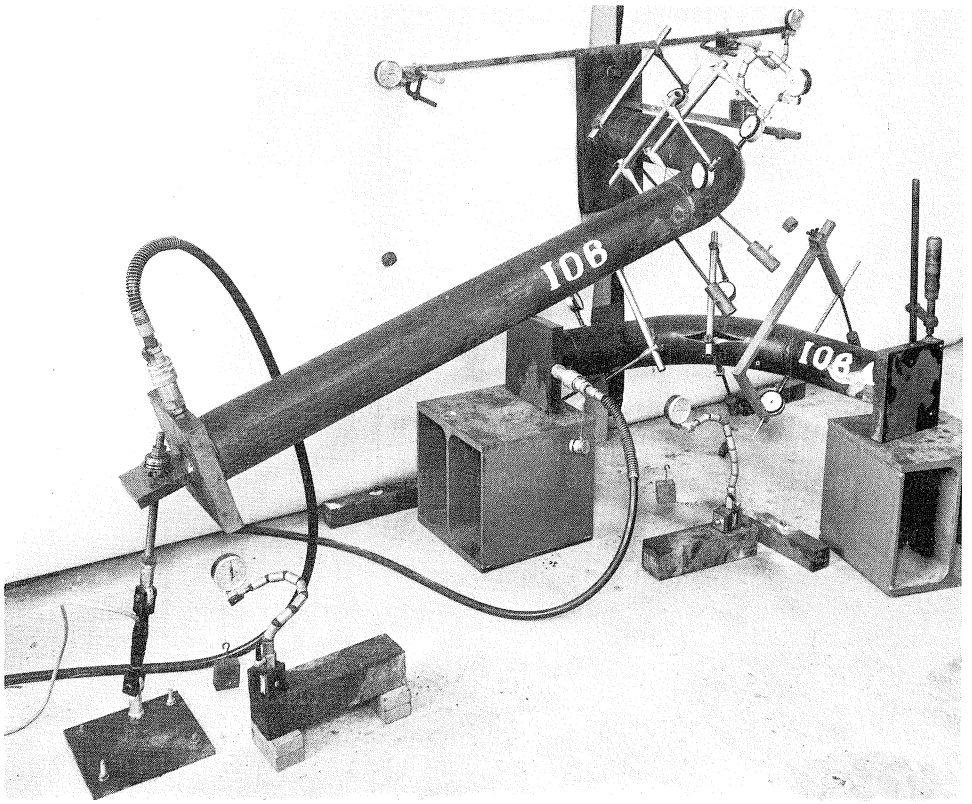

Photo 12. Rupturing test on smooth bends under the action of bending (M) and torsion (M_t) (Nos. 106 and 106A, test b2).

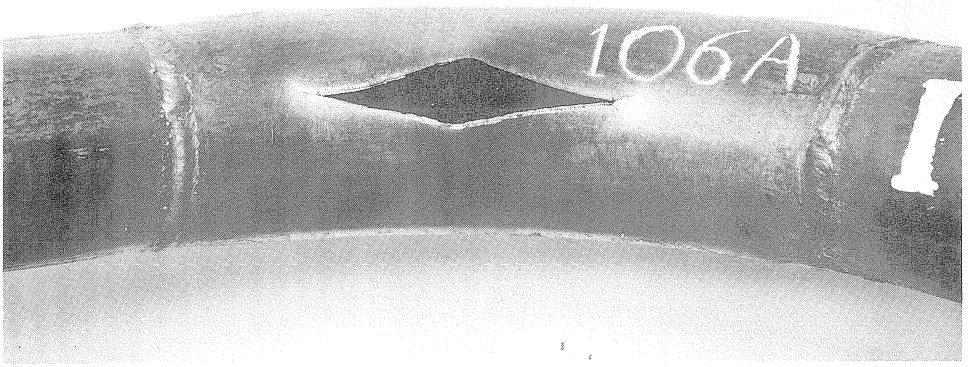

Photo 13. Detail of ruptured bend No. 106A (rupture on inside of bend).

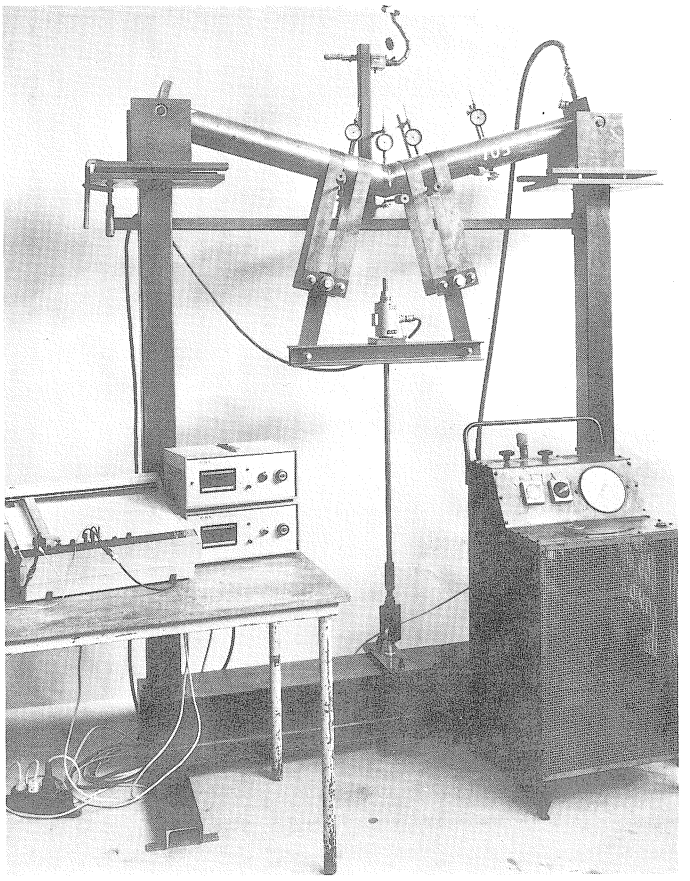

Photo 14. Rupturing test on mitred bends under the action of "earth pressure" (Q_i) and bending (M) (test c1).

3.3.2 Full-scale tests

Purpose of the tests

With the exception of the full-scale tests mentioned here, reduced-scale pipes were used for all the approximately 70 tests performed within the scope of the research (scale factor 1 : 4 to 1 : 8). Provided that the laws of similarity and scaling-down are duly taken into account, the conclusions to be drawn from these tests on reduced-scale specimens are validly applicable also to full-size pipes.

In connection with the acceptance of these conclusions by the licensing authorities for the management of dykes and flood defences* bending tests followed by rupturing tests were moreover performed on two full-scale specimens.

Specimens and tests performed

The tests were substantially similar to those described in the preceding section. After being subjected to a bending test, the buckled pipe together with a pipe not deformed by external loads was loaded by internal pressure until rupturing occurred. The test specimens were fabricated from pipes ($\varnothing$ 609.6 – 6.4 mm) made from steel whose specifications complied with API 5LX 52. The measured yield point of this steel was 360–380 N/mm^2 in the longitudinal direction. The tensile strength both in the longitudinal and in the circumferential direction was 500–510 N/mm^2, and the elongation at fracture in the d_{p5} tensile test bars was 30–35 per cent. A circumferential (girth) weld was located in the middle of the measuring zone (Fig. 3.3-2).

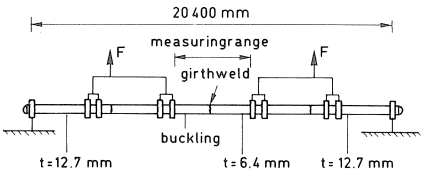

Fig. 3.3-2. Schematic set-up of the full-scale bending test.

The experimental set-up for the bending test is shown schematically in Fig. 3.3-2. The loads F were applied to the pipe by means of thin steel straps (see Photo 15). By employing a thicker-walled pipe at those locations where these forces were largest, the occurrence of buckling at those point of load application was prevented.

During the bending test a negative pressure of about – 1 bar was maintained in the pipe by means of a vacuum pump. This was the most unfavourable situation from the point of view of buckling. While the test was being performed the curvature was measured at various points, as was also the change in the vertical and in the horizontal diameter (Photo 15).

---

* Technical Advisory Committee for Dykes and Flood Defences (Technische Adviescommissie voor de Waterkeringen: TAW); the Provincial Civil Engineering Works Departments; the Polder Management Boards; etc.

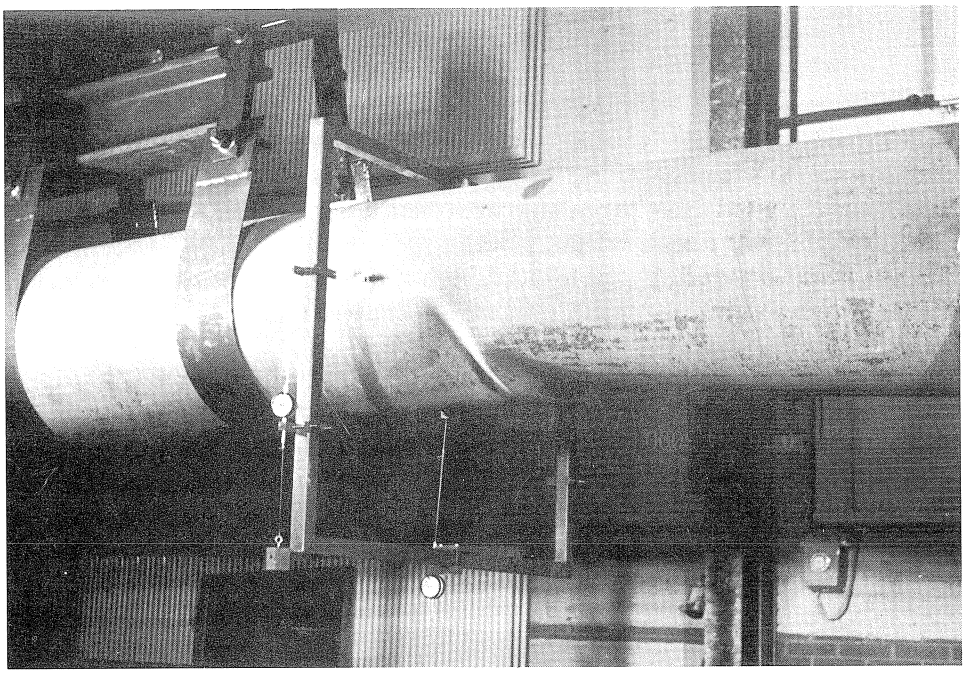

Photo 15. Buckled pipe in the full-scale test.

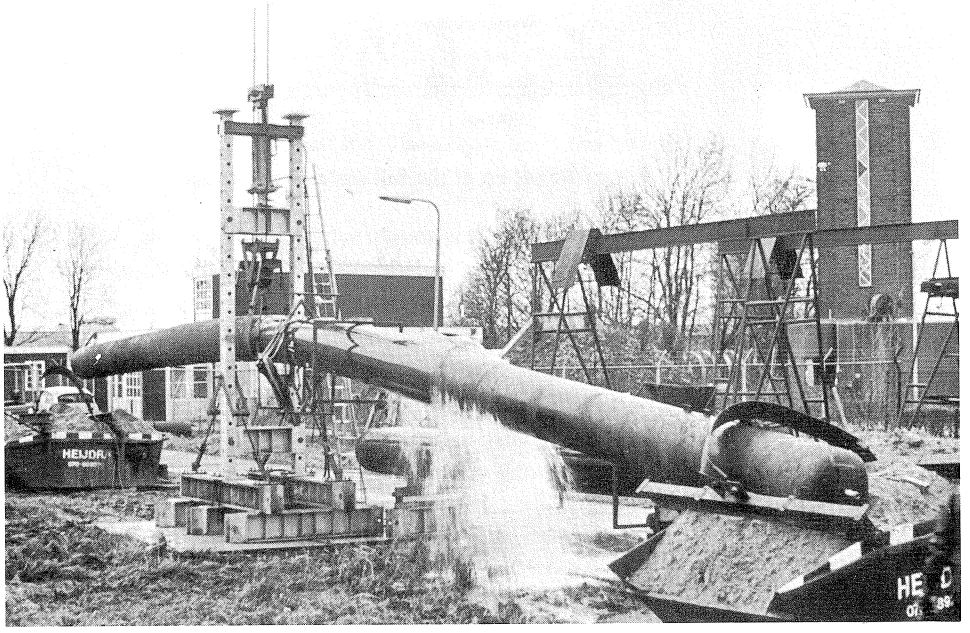

Photo 16. Full-scale rupturing test set-up.

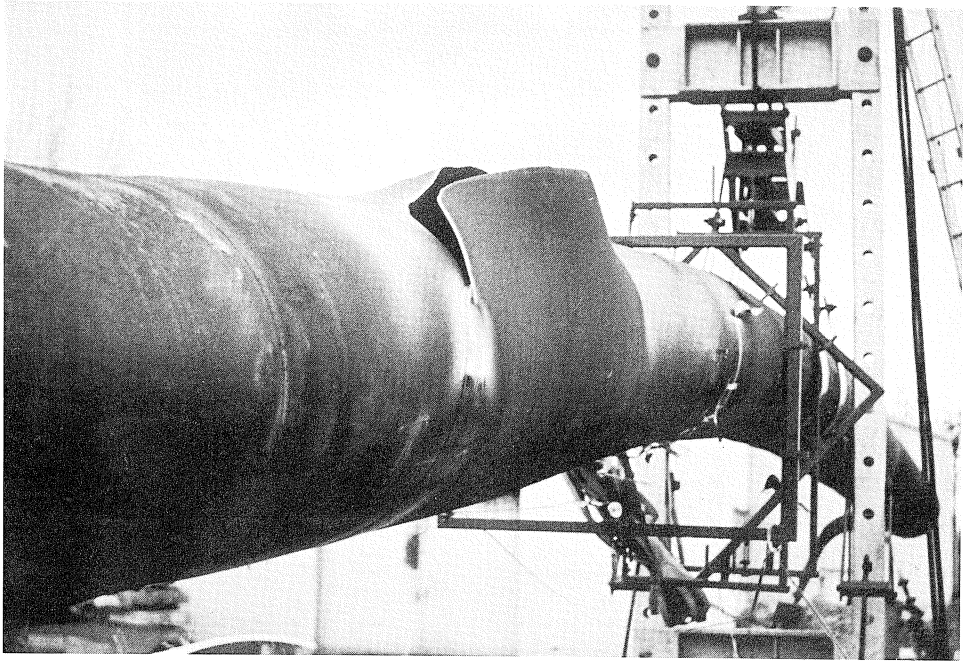

Photo 17. Ruptured pipe in the full-scale test.

After buckling had occurred the pipe was removed to an outdoor testing site, where it was subjected to further deformation (deeper buckling). The deflection was thereafter maintained (fixed) in the condition that had been attained. The rupturing test was then performed. The set-up is shown schematically in Fig. 3.3-3; see also Photo 16.

Result of bending test

The measured moment-curvature diagram is given in Fig. 3.3-4, while Fig. 3.3-5 gives the relation between the moment and the ovalization. The buckled pipe is shown in Photo 15.

The buckling curvature was approximately $1.5K_e$, which was less than had been obtained in the reduced-scale tests (Section 2.2). The difference was, however, within the range of scatter associated with such tests. The following causes of scatter may be mentioned:

- Variation in the stress-(compressive) strain properties of the steel used: more particularly the limit of proportionality and the strain-hardening modulus [2.8], [2.11]. The

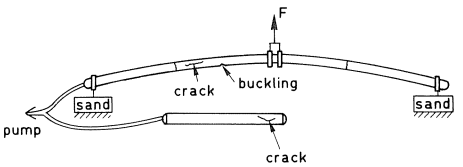

Fig. 3.3-3. Schematic set-up of the full-scale rupturing test.

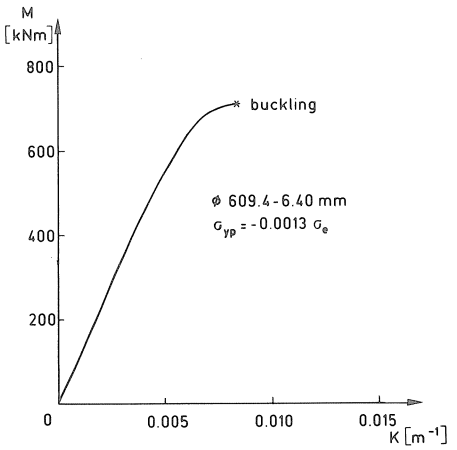

Fig. 3.3-4. Measured moment-curvature diagram.

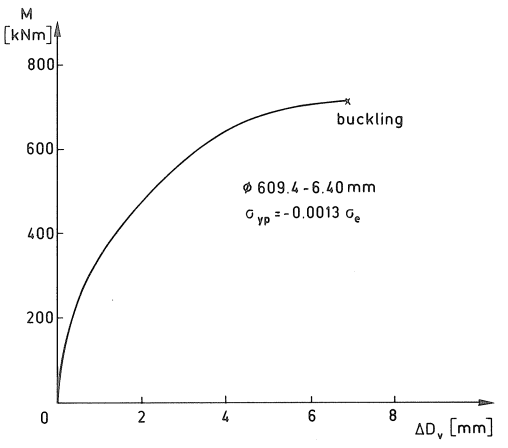

Fig. 3.3-5. Measured moment-ovalization diagram. ΔD_v is the change (decrease) in diameter in the plane of bending.

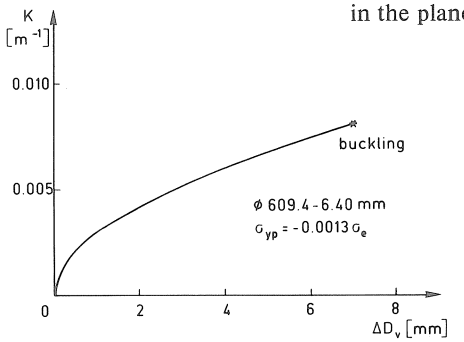

Fig. 3.3-6. Measured curvature-ovalization diagram. ΔD_v is the change (decrease) in diameter in the plane of bending.

applied steel had virtually no limit of proportionality. This is of major influence particularly in cases where the critical compressive buckling strain is not much greater than ε_e.

- Variation in the geometric deviations from the ideal circular shape.
- Variation in the mechanical properties in the circumferential direction in relation to the longitudinal direction (σ-ε diagram).
- Variation in the magnitude of the residual stresses.

The absence of the limit of proportionality is probably the main reason for the present test result.

Result of rupturing test

In the rupturing test the rupturing pressure in both test specimens was approximately 110.1 bar. On the basis of the nominal diameter of the pipes and the minimum measured wall thickness the stress σ_{yp} was:

$$\sigma_{yp} = \frac{110.1 \times 10^{-1}(609.6 - 2 \times 6.35)}{2 \times 6.35} = 517 \text{ N/mm}^2$$

On the basis of the actual diameter at the instant of rupturing the value of σ_{yp} was:

$$\sigma_{yp} = \frac{110.1 \times 10^{-1}(609.6 - 2 \times 6.35 + \text{approx. } 55)}{2 \times 6.35} = 565 \text{ N/mm}^2$$

This latter value is larger than the measured failure stress by a factor 565/510 = approx. 1.11. The reason is that, besides σ_{yp}, there also acts a stress σ_{xp} in the longitudinal direction (biaxial state of stress).
While the internal pressure increased, the bending moment was found to decrease, as had been expected. At high values of the internal pressure the tensile force at the bearings became zero and the ends of the pipe rested on the sand-filled containers, i.e., the curvature further increased. Moreover, the buckle that had formed in the pipe gradually disappeared with increasing internal pressure. The rupturing that ultimately occurred was in a different location from the buckle (see Fig. 3.3-3 and Photo 17).
In these full-scale tests it was again confirmed experimentally that under the stated conditions the rupturing pressure is not affected by the external loads.

4 Limit states and limit values

4.1 *Introduction*

The failure modes that may occur in buried pipelines are:
- Development of leakage due to cracking or rupturing.
- Development of inadmissible large deformations, such as excessive out-of-roundness and buckling. This failure mode is especially important from the pipeline manager's point of view. Since buckling may, for example, be associated with very large local strains, buckling increases the danger of cracking and leakage. Thus the failure mode "inadmissible deformations" is also of importance to the dyke manager.

When either of these two failure modes occurs, a so-called limit state is attained. This is a state in which the structure is deemed to have become unserviceable or in which one or more of its parts have ceased to perform the function for which they were designed.
In the "Technical principles for the design of buried steel pipelines" (TGSL - 1986) [2.1] the above possibilities of failure have been worked out to the following five limit states and their associated limit values. With regard to the limit values stated there, it is to be noted that they relate to the design loads given in the TGSL. These are the service loads multiplied by factors incorporating the required margin of safety.

4.2 *Limit state "stresses"*

This is the limit state where the calculated stress exceeds the limit value represented by the yield point σ_e.

4.3 *Limit state "strains"*

The material of which the pipeline is made must be able to withstand the strains due to the design loads and design settlements without giving rise to cracking. The material

(parent metal and welds) must therefore possess sufficient strain capacity. In judging whether sufficient strain capacity is available it is necessary to take account of possible discontinuities that may be present, e.g., in the form of weld imperfections.
One consequence of applying plastic theory is that, by more deliberately making use of the plastic properties of steel, the strains occurring in the pipeline material will in general be greater than when elastic theory is applied. This gives rise to the question whether the pipe wall with the possible discontinuities it contains, can suitably take up these greater strains. The research undertaken in response to this question led to the report [2.9], in which it is proposed that the "Crack Tip Opening Displacement" (CTOD) approach to the problem be adopted.

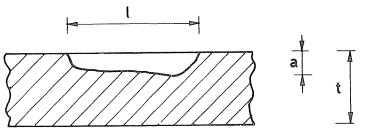

Fig. 4.3-1. Dimensions of a discontinuity assumed to be present in the material.

PD 6493 [1.8] has been used in [2.9]. With the CTOD approach a quantitative relation can be established between:

a. the *CTOD value,* which is a toughness parameter of the material considered and is determinable by means of a standard test;
b. the *dimensions of a discontinuity* assumed to be present in the material, e.g., a welding flaw with dimensions a and l;
c. the *minimum strain capacity* available in the material in question.

4.4 *Limit state "deformations"*

This limit state is attained when the ovalization becomes unacceptably large. A second possibility is the occurrence of buckling of the pipe wall (local buckling, with "wrinkling" or "creasing") and a third possibility is the occurrence of overall buckling (lateral instability of the pipeline, in the manner of a strut).

4.4.1 Ovalization

The limit value of the change in diameter in the design state is put at $0.15D_u$:

$$\Delta D_g = 0.15 D_u \tag{4.4-1}$$

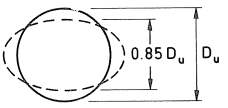

Fig. 4.4-1. Limit value for the ovalization in the design state.

4.4.2 Local buckling

Bending, normal force and pressure P

The value calculated in [3.3] for the critical buckling stress for $P = 0$ in the elastic range ($\nu = 0.3$) is:

$$\sigma_{cr} = 0.605E\frac{t}{r} \tag{4.4.2}$$

Tests have shown that the actually occurring buckling stresses are considerably smaller than the values given by (4.4-2) and moreover exhibit considerable scatter. The causes of this scatter have already been stated in Section 3.3.2.

On the basis of the available experimental results the following limit values have been adopted, both for the elastic range and for the plastic range:

- for $t/r' > 1/60$:

$$\varepsilon_{cr} = 0.25\frac{t}{r'} - 0.0025 + 3000\left(\frac{Pr}{Et}\right)^2 \cdot \frac{|P|}{P} \tag{4.4-3}$$

- for $t/r' < 1/60$:

$$\varepsilon_{cr} = 0.10\frac{t}{r'} + 3000\left(\frac{Pr}{Et}\right)^2 \cdot \frac{|P|}{P} \tag{4.4-4}$$

where:

$$r' = \frac{r}{1 - \frac{3a}{r}} \tag{4.4-5}$$

a = ovalization at $\varphi = \pi/2, 3\pi/2$ (Fig. 4.4-2)

In [2.11] these formulae for ε_{cr} have been compared with the available experimental results from the present writer's own research and from research reported by Sherman [3.4], Kato [3.5], Murphey [3.6], Reddy [3.7], Korol [3.8], Kimura [3.9] and Bouwkamp [3.10]. In practically all cases (4.4-3) and (4.4-4) give lower (= safe) values for ε_{cr}. In Fig. 4.4-2 the formulae given for ε_{cr} are compared with some experimental results [3.7]. The latter relate to pipes which were subjected to bending and/or normal force in conjunction with $P = 0$.

In the case of a buried pipeline the pipe cross-section will become oval due to the action of earth pressure. As a result of this, the radius of curvature of the pipe wall in the zone where buckling will ultimately occur (compressive zone) is increased to r'.

Formula (4.4-5) has been derived as follows. The ovalization w is assumed to be:

$$w = -a\cos 2\varphi \tag{4.4-6}$$

The additional curvature ΔK of the pipe wall is:

$$\Delta K = \frac{d^2w}{r^2\,d\varphi^2} + \frac{w}{r^2} \tag{4.4-7}$$

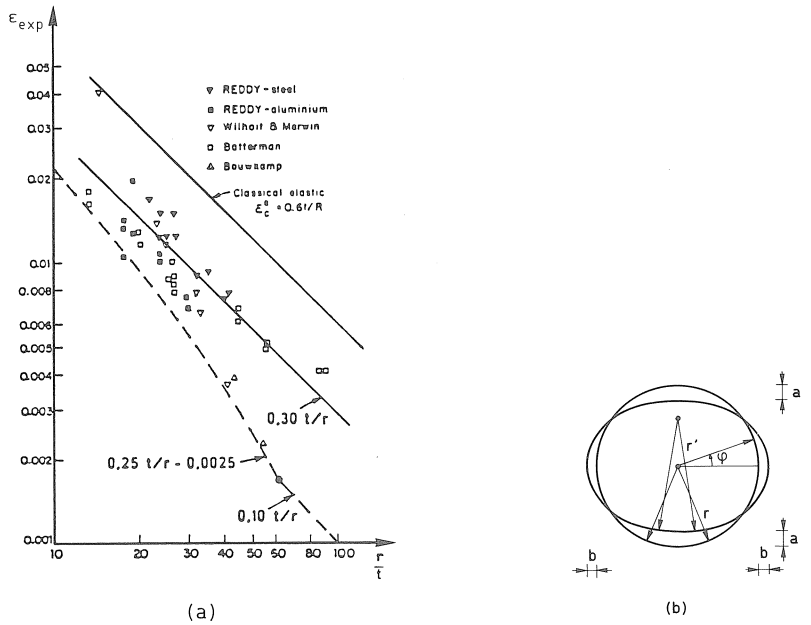

Fig. 4.4-2. a. Results of buckling tests [3.7]
b. Ovalized pipe.

so that

$$\Delta K = \frac{3a \cos 2\varphi}{r^2} \tag{4.4-8}$$

For $\varphi = \pi/2$ and $-\pi/2$ it follows for the total curvature of the pipe wall:

$$K = \frac{1}{r} - \frac{3a}{r^2} \tag{4.4-9}$$

so that the radius of curvature r' becomes

$$r' = \frac{1}{K} = \frac{r}{1 - \frac{3a}{r}} \tag{4.4-10}$$

Comparison with the available test results in Chapter 6 reveals good agreement.

Torsion

In [3.3] the critical buckling stress, for $P = 0$, in the elastic range (with $\nu = 0.3$) has been calculated as

$$\tau_{cr} = 0.253E \frac{t}{r} \sqrt{\frac{t}{r}} \tag{4.4-11}$$

The values of τ_{cr} thus calculated are found to be in good agreement with the available test results. There is little scatter, certainly in comparison with that associated with bending. With (4.4-11) the critical rotation is found to be:

$$\theta_{cr} = \frac{\tau_{cr}}{Gr} = \frac{0.253E}{Er(2+2\nu)} \frac{t}{r} \sqrt{\frac{t}{r}}$$

$$\theta_{cr} = 0.66 \frac{t}{r^2} \sqrt{\frac{t}{r}} \tag{4.4-12}$$

If a pressure P is acting, then:

$$\theta_{cr} = 0.66 \frac{t}{r^2} \sqrt{\frac{t}{r}} + \frac{3000}{r} \left(\frac{Pr}{Et}\right)^2 \frac{|P|}{P} \tag{4.4-13}$$

In the case of a pipe which has ovalized (due to earth pressure) the radius r is replaced by r' according to (4.4-10). On comparing (4.4-13) with results obtained from tests, including tests in the plastic range, there is found to be good agreement [2.8], [2.11].

Bending, normal force, pressure P, torsion
The following interaction formula for bending and torsion is given in [3.15]:

$$\left(\frac{M_{p\,buckling}}{M_{cr}}\right)^{1.5} + \left(\frac{M_{t\,buckling}}{M_{tcr}}\right)^2 = 1 \tag{4.4-14}$$

where:

M_{cr} = buckling moment for bending only
M_{tcr} = buckling moment for torsion only

This interaction formula is based on experimentally obtained data and is valid for the elastic range. For the deformations this formula can be transformed into:

$$\left(\frac{\varepsilon_{buckling}}{\varepsilon_{cr}}\right)^{1.5} + \left(\frac{\theta_{buckling}}{\theta_{cr}}\right)^2 = 1 \tag{4.4-15}$$

On checking this formula against available test results it appears that it can be validly applied also in the plastic range, the values of ε_{cr} and θ_{cr} for this purpose being those given by (4.4-3) or (4.4-4) and (4.4-13).

4.4.3 Lateral buckling

The (overall) lateral buckling stability of a buried pipeline subjected to normal force (i.e., direct or axial force) is favourably influenced by the restraint of the surrounding soil, which acts as an elastic support [3.3]. If the critical compressive strain ε_{cr} associated with local buckling of the pipe wall is less than the yield strain, the notational yield point σ'_e is introduced [3.16]:

$$\sigma'_e = \varepsilon_{cr} E \tag{4.4-16}$$

Curves for the analysis of lateral buckling are contained in publications issued by the ECCS [1.9], [3.16].

4.5 *Limit state "alternate yielding"*

Variations in the pressure P and in the temperature give rise to stress variations. So long as the stress points remain within the yield surface shown in Fig. 4.5-1, no yielding will occur. In the event of variation of the pressure and/or the temperature after a certain flexural deformation has been imposed, there will, the first time that such variation occurs, generally be some stress redistribution attended by yielding. After the first pressure and/or temperature variation the stress system will have so established itself that all the phenomena associated with subsequent variations will be elastic unless stress paths such as AB and CD do not fit within the yield surface. In this latter case alternate yield will occur.

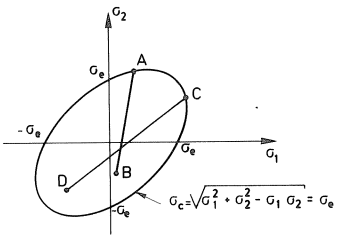

Fig. 4.5-1. Yield surface with possible stress paths within it.

4.6 *Limit state "fatigue"*

The procedure for fatigue analysis of buried steel pipelines is described in [2.6], where the German Standard DIN 2413 is adopted as the basis [1.6]. In developing this analysis, some fresh insights have been taken into account, as also the importance of the dyke concerned (damage factor) and the number of pipeline crossings of the dykes around the polder in question.

5 Outline of the new method of analysis

What has been stated in the preceding chapters leads to the conclusion that three principal aspects are to be distinguished in connection with the analysis and assessment of buried steel pipelines - namely, the calculation of the strength, the calculation of the strains and deformations, and the calculation of the effect of load variations. These aspects will be further considered in this chapter.
In this context, attention is drawn to Section 4.1, stating that the calculations are based on design loads obtained by multiplying the service loads (e.g., the maximum operating pressure and the settlements) by factors incorporating the required margin of safety.

5.1 *Strength*

Because the rupturing pressure is not affected by the external loads and imposed deformations, the design value of the pressure P must satisfy:

$$\sigma_{yp} = f\frac{Pr}{t} \leqslant \sigma_e \tag{5.1-1}$$

where for straight pipes $f = 1$ and
- for the inner (concave) side of bends:

$$f = f_{bi} = \frac{R - r/3}{R - r} \tag{5.1-2}$$

- for the outer (convex) side of bends:

$$f = f_{bu} = \frac{R + r/3}{R + r} \tag{5.1-3}$$

The radius R of the bend is indicated in Fig. 5.1-1.

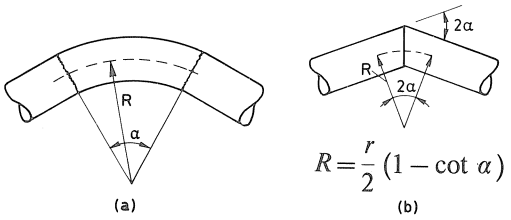

$$R = \frac{r}{2}(1 - \cot\alpha) \tag{5.1-4}$$

Fig. 5.1-1. Bend angle and bend radius for a smooth and for a mitred bend respectively.

5.2 *Deformations and strains*

Pipeline crossings as shown in Figs. 1-1 and 1-2 can be conceived as elastically supported beams of three-dimensional configuration. In the calculations the properties of the soil are generally schematized as actual springs, as indicated in Fig. 5.2-1. In analysing this system it is necessary to take account of the nonlinear character of the

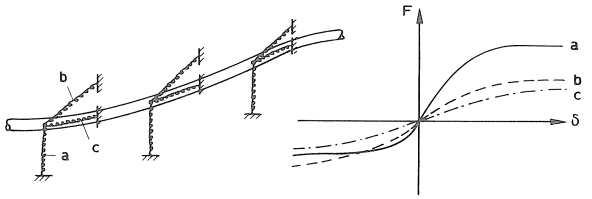

Fig. 5.2-1. Schematization of a pipeline with "earth springs".
a = vertrical earth spring
b = horizontal earth spring
c = frictional earth spring

various "earth springs". In general, a finite element computer program is necessary for carrying out the analysis of this system. The input data are the soil properties, the imposed settlement differences and other loads, and the properties of the pipeline. These properties relate more particularly to the bending moment-curvature diagram and the torsional moment-rotation diagram. In Chapter 6 these diagrams and the effect thereon of, for example, earth pressure will be calculated for straight pipes and for smooth bends respectively. For mitred bends the reader is referred to [2.4].
The result of the "beam-analysis" as envisaged above is that at every cross-section of the pipeline the following are known:
- bending moment and curvature;
- torsional moment and rotation;
- normal force and lengthening or shortening;
- shear force and shear deformation;
- earth pressure and displacements.

Finally, by means of supplementary "cross-section analyses" the deformations such as ovalization, strains, rotations etc. can be calculated and be checked against the limit values given in Chapter 4.
These calculations will be dealt with in greater detail in the following chapters.

5.3 *Load variations*

In this stage of the analysis it is investigated what effect the anticipated variations in pressure and temperature will have upon the strains in the longitudinal and in the circumferential direction. Particularly in greatly ovalized pipes the variations in pressure may produce considerable strain variations.
In the following chapters, computational models for the calculation of these variations will also be considered.

6 Derivation of design rules for buried straight steel pipelines

In Section 6.1 the maximum bending moment M_m that can be resisted is calculated as a function of the properties of the pipe and of the other loads such as earth pressure, torsional moment, etc.
In Section 6.2 the ovalization distortions which occur are calculated as a function of earth pressure, curvature (bending) and rotation (torsion).
In the calculations presented in Sections 6.1 and 6.2 it is presupposed that the pipe cross-section has become fully plastic under the influence of the loads.
The transition between the elastic range and the fully plastic range is considered in Section 6.3. Sections 6.4 and 6.5 deal with the effect of the pressure upon ovalization and with the calculation of the strains. Finally, in Section 6.6 some results of tests are compared with the results obtained by applying the design rules established here.

6.1 *Maximum bending moment M_m that can be resisted*

The formulae which are derived in Sections 6.1.2 to 6.1.4 are summarized in Section 6.1.5.

6.1.1 Overview of the loads

The maximum moment M_m that can be resisted by the pipeline conceived as a beam is influenced by the magitude of:

a. the earth pressure $Q_d + Q_i$;
b. the difference between internal and external pressure P;
c. the normal force F;
d. the shear force D;
e. the torsional moment M_t;
f. the ovalization a;
g. the curvature K.

The loads that possibly act on the pipeline are indicated in Fig. 6.1-1, where Q_d is the directly transferred earth pressure and Q_i the indirectly transferred earth pressure. It is in fact due to this latter earth pressure that the pipeline acts as a beam and undergoes bending: Q_i causes a change in the shear force by an amount ΔD.

The effect of earth pressure, curvature, internal pressure and ovalization is calculated in Section 6.1.2. Section 6.1.3 deals with the effect of normal force, while the effect of shear force and torsional moment is considered in Section 6.1.4. Finally, Section 6.1.5 gives a summary of the interaction formulae with which the effect of all the above-mentioned factors on the maximum moment M_m can be calculated.

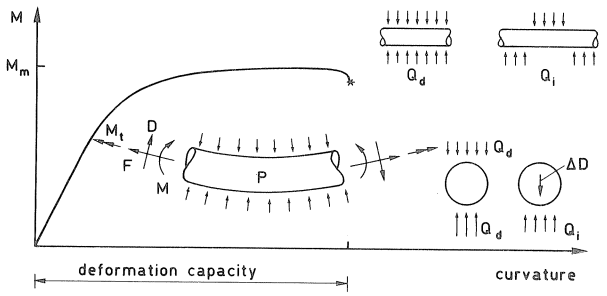

Fig. 6.1-1. Moment-curvature diagram with the other loads acting on the pipe. The force ΔD provides an indication of the shear force contribution due to Q_i per unit length of the pipe.

6.1.2 Effect of earth pressure Q_d and Q_i, curvature K, pressure P and ovalization a on the magnitude of M_m

The earth pressure, the curvature, the ovalization and the pressure in the pipeline give rise to so-called plate forces in the pipe wall: bending moments m_x and m_y, normal forces n_x and n_y. The plate forces acting on a wall element are indicated in Fig. 6.1-2.

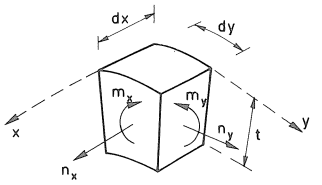

Fig. 6.1-2. Plate forces on a pipe wall element $dx \cdot dy \cdot t$. The x-direction is the longitudinal direction of the pipe, the y-direction is the circumferential direction.

The normal forces n_x are responsible for the bending moment M and normal force F acting on the pipeline (Fig. 6.1-1). The maximum magnitude of m_x is affected by the magnitude of the other plate forces. In Section 6.1.2.1, m_y and n_y are calculated, and in Section 6.1.2.2, m_x, n_x and the maximum moment M_m that can be resisted are considered.

6.1.2.1 Moments and normal forces m_y and n_y in the pipe wall

Due to Q_d and Q_i

The plate moments which are produced by Q_d and Q_i at the top (m_{yt}) the side (m_{ys}) and the bottom (m_{yb}) are indicated in Fig. 6.1-3. In this report, Q_d and Q_i are in N/mm, the plate moments in Nmm/mm, and the plate normal forces in N/mm.

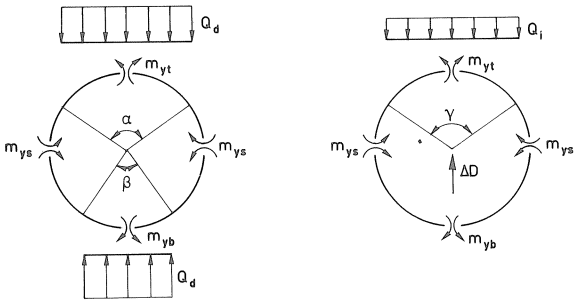

Fig. 6.1-3. Plate moments due to Q_d and Q_i.

From the conditions of equilibrium (Fig. 6.1-2) it follows for the load Q_d:

$$|m_{yt}| + 2|m_{ys}| + |m_{yb}| = Q_d r \left\{1 - \frac{1}{4}\left(\sin\frac{\alpha}{2} + \sin\frac{\beta}{2}\right)\right\} \tag{6.1-1}$$

For the average moment at the top, the side and the bottom:

$$m_{yqd} = \frac{1}{4} Q_d r \left\{1 - \frac{1}{4}\left(\sin\frac{\alpha}{2} + \sin\frac{\beta}{2}\right)\right\} \tag{6.1-2}$$

Similarly, for the load Q_i:

$$m_{yqi} = \frac{1}{4} Q_i r \left\{\frac{1}{2} - \frac{1}{4}\sin\frac{\gamma}{2}\right\} \tag{6.1-3}$$

The sum of m_{yqd} and m_{yqi} can be written as:

$$m_{yq} = m_{yqd} + m_{yqi} \tag{6.1-4}$$

For n_{yq} at the sides it can be written approximately:

$$n_{yqs} = 0.5Q_d + 0.25Q_i \tag{6.1-5}$$

At the top and at the bottom the value of n_{yq} is much less. The average n_{yq} at top, sides and bottom is approximately:

$$n_{yq} = 0.25Q_d + 0.125Q_i \tag{6.1-6}$$

Formula (6.1-6) gives too high a value for the top and bottom, and too low a value for the sides. Because these differences have only a negligible effect on M_m, they will, for the sake of simplicity, not be further considered.
With (6.1-3) and (6.1-2) it is possible to express Q_i in an equivalent earth pressure Q_{eq} which gives the same m_{yq} as Q_d does:

$$Q_{eq} = Q_i \frac{2 - \sin \gamma/2}{4 - \sin \alpha/2 - \sin \beta/2} \tag{6.1-7}$$

The quantity Q_{eq} will be used in Sections 6.5 and 6.6 and also in Chapter 7.

Due to the curvature K
With the aid of the equilibrium model considered in Section 2.2.2 the ovalization forces and plate forces can be calculated as follows.

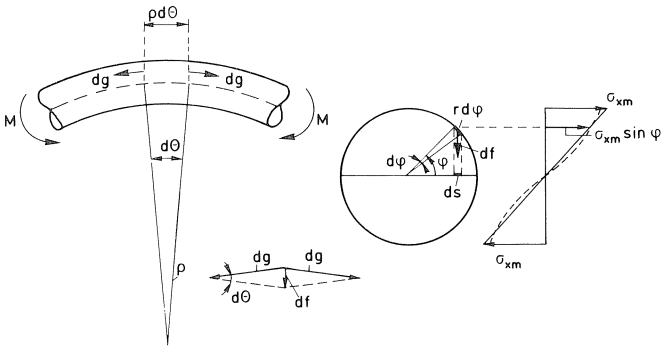

Fig. 6.1-4. Calculation of ovalization forces.
——— geometrically linear
- - - - - geometrically non-linear

The stress $\sigma_{xm} \sin \varphi$ due to the bending moment M acts in the axial direction. Over a distance $r\,d\varphi$ there acts the force:

$$dg = rt\sigma_{xm} \sin \varphi \, d\varphi \tag{6.1-8}$$

where:

$$\sigma_{xm} = \varepsilon_{xm} E = \frac{r}{\varrho} E \tag{6.1-9}$$

The force dg has a component df directed towards the diameter of the pipe:

$$\mathrm{d}f = \mathrm{d}g\, \mathrm{d}\theta = \frac{r^2 tE}{\varrho} \sin\varphi\, \mathrm{d}\varphi\, \mathrm{d}\theta \tag{6.1-10}$$

The length ds shown in Fig. 6.1-4 is:

$$\mathrm{d}s = r\, \mathrm{d}\varphi \sin\varphi \tag{6.1-11}$$

The forces df can be conceived as a uniformly distributed load q shown in Fig. 6.1-5:

$$q = \frac{\mathrm{d}f}{\varrho\, \mathrm{d}\theta\, \mathrm{d}s} = \frac{rtE}{\varrho^2} \tag{6.1-12}$$

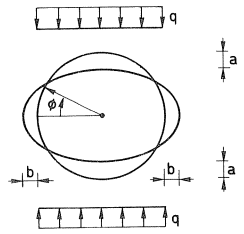

Fig. 6.1-5. Equivalent load q due to the ovalization forces.

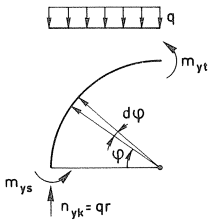

Fig. 6.1-6. Calculation of moments m_{yt} and m_{ys} due to q.

For $m_{y\varphi}$ is obtained on the basis of equilibrium:

$$m_{y\varphi} = m_{ys} + qr(r - r\cos\varphi) - 0.5q(r - r\cos\varphi)^2$$
$$m_{y\varphi} = m_{ys} + qr^2(0.5 - 0.5\cos^2\varphi) = m_{ys} + 0.25qr^2(1 - \cos 2\varphi) \tag{6.1-13}$$

The condition that the angular rotation at the top and at the sides is zero can be written as:

$$\int_0^{\pi/2} \frac{m_{y\varphi}}{EI} \frac{\partial m_{y\varphi}}{\partial m_{ys}} r\, \mathrm{d}\varphi = 0 \tag{6.1-14}$$

Now m_{ys} can be determined with the aid of this formula, giving:

$$\int_0^{\pi/2} \{m_{ys} + 0.25qr^2(1 - \cos 2\varphi)\}\, \mathrm{d}\varphi = 0$$

$$[m_{ys}\varphi + 0.25qr^2(\varphi - 0.5\sin 2\varphi)]_0^{\pi/2} = 0$$

so that:

$$m_{ys} = -0.25qr^2 \tag{6.1-15}$$

For the associated ovalization it follows, for $P = 0$ and neglecting the lateral contraction:

$$a = \int_0^{\pi/2} \frac{m_{y\varphi}}{EI} r^2 \sin\varphi \, d\varphi$$

$$a = \frac{qr^4}{EI} \int_0^{\pi/2} (-0.25 \cos 2\varphi \sin\varphi) \, d\varphi$$

$$a = \frac{qr^4}{EI} \int_0^{\pi/2} \{-0.25(2\cos^2\varphi \sin\varphi - \sin\varphi)\} \, d\varphi$$

$$a = \frac{qr^4}{EI} \left[0.25 \left(\frac{2}{3} \cos^3\varphi - \cos\varphi \right) \right]^{\pi/2}$$

$$a = \frac{qr^4}{12EI} = \frac{qr^4}{12E \frac{1}{12} t^3} \tag{6.1-16}$$

With (6.1-12) is obtained:

$$a = r \left(\frac{r^2}{\varrho t} \right)^2 \tag{6.1-17}$$

The distribution of the stresses σ_x is changed in consequence of ovalization. The stress distribution which develops in the longitudinal direction in consequence of this geometrically non-linear behaviour is indicated in Fig. 6.1-4. Reissner and Weinitschke have taken this into account in [3.1]. For $P = 0$ and neglecting lateral contraction, the following expressions are obtained according to [3.1]:

$$\left.\begin{aligned} a &= r \left(\frac{\alpha^2}{12} + \frac{71\alpha^4}{8640} + \frac{44551\alpha^6}{7560 \cdot 7200} + \ldots \right) \\ b &= -r \left(\frac{\alpha^2}{12} + \frac{\alpha^4}{960} - \frac{2059\alpha^6}{168 \cdot 7200} + \ldots \right) \end{aligned}\right\} \tag{6.1-18}$$

where:

$$\alpha = \frac{r^2}{\varrho t} \sqrt{12} = \frac{Kr^2}{t} \sqrt{12} \tag{6.1-19}$$

For buried pipelines the ratio diameter to wall thickness (D/t) is between about 10 and about 120. With these values of D/t the second and following terms in (6.1-18) are very small in relation to the first term. They are therefore neglected:

$$a = -b = r \left(\frac{r^2}{\varrho t} \right)^2 \tag{6.1-20}$$

This result is in agreement with that of the geometrically linear analysis with the ovalization forces. In the further treatment of the subject the effect of the above-mentioned non-linear behaviour will not be considered.

For the bending moment at the sides we obtain with (6.1-12), (6.1-15) and (6.1-9):

$$m_{ys} = -0.25 \frac{r^2 t}{\varrho} \sigma_{xm} \tag{6.1-21}$$

where:

$$\sigma_{xm} = \frac{M}{\pi r^2 t} \tag{6.1-22}$$

From (6.1-13) and (6.1-21) it follows that the moments at the top, the sides and the bottom are all equal in absolute value.
For the average moment due to curvature we can write:

$$m_{yk} = 0.25 \frac{r^2 t}{\varrho} \cdot \frac{M}{\pi r^2 t} = 0.080 MK \tag{6.1-23}$$

For n_{yk} (Fig. 6.1-6) it follows with (6.1-12), (6.1-9) and (6.1-22) that:

$$n_{yk} = qr = \frac{r^2 tE}{\varrho^2} = \frac{rt}{\varrho} \sigma_{xm} = 0.32 \frac{MK}{r} \tag{6.1-24}$$

Similarly, for the fully plastic cross-section, m_{yk} can be derived by replacing $\sigma_{xm} \sin \varphi$ in (6.1-8) by σ_e. We then obtain:

$$m_{yk} = 0.285 \frac{r^2 t}{\varrho} \sigma_e \tag{6.1-25}$$

With

$$\sigma_e = \frac{M_p}{4 r^2 t} \tag{6.1-26}$$

this gives:

$$m_{yk} = 0.071 \frac{M_p}{\varrho} = 0.071 M_p K \tag{6.1-27}$$

If M_p is reduced to M_m by earth pressure, the pressure P, etc., it is assumed that the following expression may be adopted for m_{yk}:

$$m_{yk} = 0.071 M_m K \tag{6.1-28}$$

The normal force at the top and at the bottom due to curvature is zero. The normal force at the sides in a fully plastic cross-section is a little greater than n_{yk} in the elastic range as expressed by (6.1-24). The average for the fully plastic cross-section is taken as:

$$n_{yk} = 0.20 \frac{M_m K}{r} \tag{6.1-29}$$

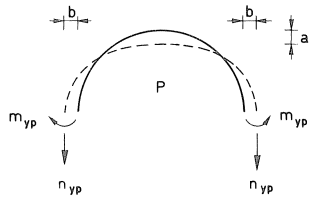

Fig. 6.1-7. Plate forces in y-direction due to the pressure P.

Due to the pressure P

In a pipe of circular cross-section the pressure P produces normal forces n_{yp} and n_{xp} in the pipe wall. In an oval-section pipe the moments m_{yp} will additionally occur.
For a circular-section pipe:

$$n_{yp} = Pr \tag{6.1-30}$$

For an oval-section pipe, for reasons of simplicity, n_{yp} is also taken as equal to Pr according to (6.1-30). For m_{yp} we then obtain:

$$m_{yp} = -Pra \tag{6.1-31}$$

The magnitude of n_{xp} depends on the boundary conditions. For example, in the case of a pipe which is free to deform longitudinally:

$$n_{xp} = 0.5Pr \tag{6.1-32}$$

Influence of ovalization on m_y

As a result of ovalization the moments m_{yq} and m_{yk} are increased by a factor f_0 according to:

$$f_0 = 1 - \frac{b}{r} \tag{6.1-33}$$

Because of $a \approx -b$ the factor f_0 can alternatively be written as:

$$f_0 = 1 + \frac{a}{r} \tag{6.1-34}$$

In Fig. 6.1-5, a is shown as having a positive and b a negative value. For small amounts of ovalization: $|a| \approx |b|$. For larger amounts of ovalization the difference between $|a|$ and $|b|$ increases, while then $|a| > |b|$. On adopting (6.1-34), values that are somewhat too high are obtained for m_{yq} and m_{yk}. For buried pipelines this is on the safe side because the calculated values of M_m will be lower in consequence. For further calculation it is advantageous to work with (6.1-34) because only one parameter need be considered for ovalization.
The calculation of ovalization will be dealt with in Section 6.2.

Totals

The totals of the plate moments and plate normal forces are:

$$m_y = m_{yq} + m_{yk} + m_{yp} \tag{6.1-35}$$

$$n_y = n_{yq} + n_{yk} + n_{yp} \tag{6.1-36}$$

$$n_x = n_{xk} + n_{xp} \tag{6.1-37}$$

$$m_x = \text{(see the next section)} \tag{6.1-38}$$

The plate forces n_{xk} and m_x will be calculated in the next section.

6.1.2.2 Maximum moment M_m that can be resisted

The plate forces acting on an element of the pipe wall are shown in Fig. 6.1-2. According to plastic theory the stresses associated with these plate forces are allowed to be so chosen that the largest possible values for Q_d, Q_i, P and M are obtained. The conditions are that the yield point must not be exceeded, that there is equilibrium and that the stresses are in reasonably good agreement with the strains that occur. The chosen stress distribution is shown in Fig. 6.1-8.

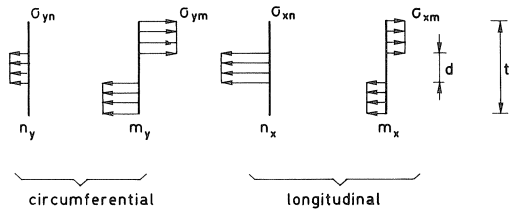

Fig. 6.1-8. Chosen stress distribution in the pipe wall.

Applying the Von Mises criterion, the condition that the yield point must not be exceeded gives:

$$\sigma_{ym}^2 + \sigma_{xm}^2 - \sigma_{ym}\sigma_{xm} = \sigma_e^2 \tag{6.1-39}$$

and

$$\sigma_{yn}^2 + \sigma_{xn}^2 - \sigma_{yn}\sigma_{xn} = \sigma_e^2 \tag{6.1-40}$$

With the stress distributions in Fig. 6.1-8 it follows that:

$$m_x = 0.25t^2\sigma_{xm} - 0.25d^2\sigma_{xm} \tag{6.1-41}$$

$$m_y = 0.25t^2\sigma_{ym} - 0.25d^2\sigma_{ym} \tag{6.1-42}$$

$$n_x = \mathrm{d}\sigma_{xn} \tag{6.1-43}$$

$$n_y = \mathrm{d}\sigma_{yn} \tag{6.1-44}$$

With

$$m_p = 0.25 t^2 \sigma_e \tag{6.1-45}$$

$$n_p = t\sigma_e \tag{6.1-46}$$

it follows that:

$$\frac{m_x}{m_p} = \frac{\sigma_{xm}}{\sigma_e}\left(1 - \frac{d^2}{t^2}\right)$$

$$\sigma_{xm} = \frac{m_x}{m_p}\left(1 - \frac{d^2}{t^2}\right)^{-1} \sigma_e \tag{6.1-47}$$

$$\sigma_{ym} = \frac{m_y}{m_p}\left(1 - \frac{d^2}{t^2}\right)^{-1} \sigma_e \tag{6.1-48}$$

$$\frac{n_y}{n_p} = \frac{\sigma_{yn}}{\sigma_e} \cdot \frac{d}{t}$$

$$\sigma_{yn} = \frac{n_y}{n_p} \cdot \frac{t}{d} \sigma_e \tag{6.1-49}$$

$$\sigma_{xn} = \frac{n_x}{n_p} \cdot \frac{t}{d} \sigma_e \tag{6.1-50}$$

Substitution of (6.1-47) to (6.1-50) into (6.1-39) and (6.1-40) gives:

$$\left(\frac{m_x}{m_p}\right)^2 + \left(\frac{m_y}{m_p}\right)^2 - \left(\frac{m_x}{m_p}\right)\left(\frac{m_y}{m_p}\right) = \left\{1 - \left(\frac{d}{t}\right)^2\right\}^2 \tag{6.1-51}$$

$$\left(\frac{n_x}{n_p}\right)^2 + \left(\frac{n_y}{n_p}\right)^2 - \left(\frac{n_x}{n_p}\right)\left(\frac{n_y}{n_p}\right) = \left(\frac{d}{t}\right)^2 \tag{6.1-52}$$

Elimination of d/t gives:

$$\left(\frac{m_x}{m_p}\right)^2 + \left(\frac{m_y}{m_p}\right)^2 - \frac{m_x m_y}{m_p^2} - \left\{1 - \left(\frac{n_x}{n_p}\right)^2 - \left(\frac{n_y}{n_p}\right)^2 + \frac{n_x n_y}{n_p^2}\right\}^2 = 0 \tag{6.1-53}$$

The plate moment m_x can still be freely chosen, since m_x is not essential to equilibrium. The bending moment M and the normal force F acting on the pipeline conceived as a beam have maximum values when n_x reaches its maximum in the tensile zone and n_x reaches its minimum in the compressive zone. This means that the first three terms of (6.1-53) must have minimum values, which will be the case if the following equation is satisfied:

$$\frac{\partial}{\partial m_x}\left\{\left(\frac{m_x}{m_p}\right)^2 + \left(\frac{m_y}{m_p}\right)^2 - \left(\frac{m_x m_y}{m_p^2}\right)\right\} = 2\frac{m_x}{m_p^2} - \frac{m_y}{m_p^2} = 0 \tag{6.1-54}$$

so that:

$$m_x = 0.5 m_y \tag{6.1-55}$$

The result $m_x = 0.5 m_y$ is in agreement with the normality principle. This means that the deformation vector is perpendicular to the yield surface. The yield surface for the plate moments m_x and m_y according to (6.1-51) is shown in Fig. 6.1-9.
The normal to the yield surface indicates the direction of the associated deformations – in this case, the plate curvatures.
Since the plate curvature in the longitudinal direction k_x is virtually zero, this means that the ratio m_x/m_y in this situation is represented by the points A and A′ in Fig. 6.1-9.

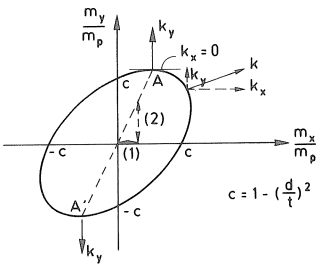

Fig. 6.1-9. Yield surface for the moments m_x and m_y in the direction of the curvatures occurring in the pipe wall.

From (6.1-53) it follows with $m_x = 0.5 m_y$ that:

$$(0.25 + 1 - 0.5)\left(\frac{m_y}{m_p}\right)^2 = \left\{1 - \left(\frac{n_x}{n_p}\right)^2 - \left(\frac{n_y}{n_p}\right)^2 + \frac{n_x n_y}{n_p^2}\right\}^2 \tag{6.1-56}$$

$$n_x = 0.5\left(n_y \pm n_p \sqrt{4 - 3\left(\frac{n_y}{n_p}\right)^2 - 2\sqrt{3}\frac{|m_y|}{m_p}}\right) \tag{6.1-57}$$

A possible curve for n_x as a function of φ and m_y and n_y is shown in Fig. 6.1-10. The bending moment M and the normal force F are obtained by integration over the cross-section of the pipe.
The average of the absolute values of m_y at the top, the sides and the bottom has been calculated in Section 6.1.2.1. This average will be adopted in the further treatment of the subject. This is in accordance with plastic theory, since the moment distribution obtained in this way is in agreement with equilibrium and with the direction of deformations that occur.

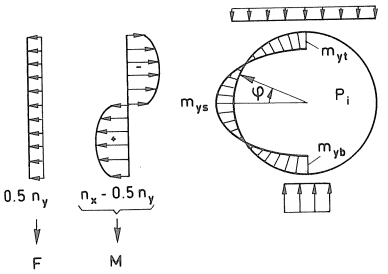

Fig. 6.1-10. Distribution of the plate forces n_x and m_y.

However, the distribution for which:

$$|m_{yt}| = |m_{ys}| = |m_{yb}| = m_y \tag{6.1-58}$$

need not necessarily be the most favourable, i.e., optimum, distribution. Comparative calculations [2.2] have established that the differences in M associated with other distributions of m_y are only a few per cent of M.
To calculate M, it is necessary first to determine n_x as a function of φ. With (6.1-58) the following expression for n_x according to (6.1-57) can be written for $\varphi = 0$, $\pi/2$, π and $3\pi/2$:

$$n_x = 0.5 n_y \pm 0.5 n_p c_1 \tag{6.1-59}$$

where:

$$c_1 = \sqrt{4 - 3\left(\frac{n_y}{n_p}\right)^2 - 2\sqrt{3}\,\frac{|m_y|}{m_p}} \tag{6.1-60}$$

For $\varphi = \pi/4$, $3\pi/4$, $5\pi/4$, $7\pi/4$ it is assumed that the plate moment m_y is zero. For n_x according to (6.1-57) the following expression can be written for these values of φ:

$$n_x = 0.5 n_y \pm 0.5 n_p c_2 \tag{6.1-61}$$

where:

$$c_2 = \sqrt{4 - 3\left(\frac{n_y}{n_p}\right)^2} \tag{6.1-62}$$

For intermediate values of φ a sine function is adopted:

$$n_{x\varphi} = 0.5 n_y \pm 0.5 n_p \{c_1 + (c_2 - c_1) \sin 2\varphi\} \tag{6.1-63}$$

Integration of (6.1-63) yields expressions for the associated bending moment M and normal force F:

$$M = 0.5 n_p r^2 \cdot 4 \int_0^{\pi/2} \{c_1 + (c_2 - c_1) \sin 2\varphi\} \sin \varphi \, d\varphi$$

$$M = 4 n_p r^2 \left(\frac{c_1}{6} + \frac{c_2}{3}\right) = M_p \left(\frac{c_1}{6} + \frac{c_2}{3}\right) \tag{6.1-64}$$

$$F = \int_0^{2\pi} n_{x\varphi} r t \, d\varphi$$

$$F = 2\pi r \cdot 0.5 n_y = \pi r n_y \tag{6.1-65}$$

In the integrals on which (6.1-64) and (6.1-65) are based a circular cross-section has been adopted for the pipe. In [2.2] it has been calculated that, in consequence of ovalization, the bending moment is reduced by a factor h:

$$h = 1 - \frac{2}{3}\frac{a}{r} \tag{6.1-66}$$

so that (6.1-64) becomes:

$$M_m = hM_p\left(\frac{c_1}{6} + \frac{c_2}{3}\right) \tag{6.1-67}$$

The ovalization a to be introduced into (6.1-66) is calculated in Section 6.2.
The formulae (6.1-65) and (6.1-67) are valid for one particular distribution of n_x around the cross-section (Fig. 6.1-10). For other distributions of n_x other combinations of M_m and F are found. This will be considered in the next section, and the influence of an arbitrary normal force on the bending moment will be calculated.

6.1.3 Influence of an arbitrary normal force on M_m

In the preceding section the normal force acting in the pipeline was, for the chosen distribution of n_x, found to be equal to F according to (6.1-65). It will now be investigated what effect an arbitrary normal force F has.
This force can be written as:

$$F = \pi r n_y + N \tag{6.1-68}$$

where N is called the effective normal force:

$$N = F - \pi r n_y \tag{6.1-69}$$

In Fig. 6.1-11 it is shown how, in consequence of a different distribution of n_x from that considered in the preceding section, the effective normal force N can be resisted.

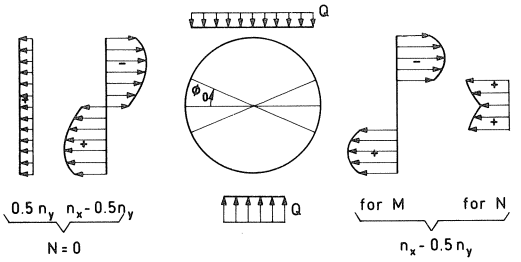

Fig. 6.1-11. Distribution of n_x in response to the bending moment and the effective normal force N.

With (6.1-63) and (6.1-66) we obtain for M:

$$M = h \cdot 0.5 n_p r^2 \cdot 4 \int_{\varphi_0}^{\pi/2} \{c_1 + (c_2 - c_1) \sin 2\varphi\} \sin \varphi \, d\varphi$$

$$M = 0.5 h M_p \left[-c_1 \cos \varphi + (c_2 - c_1) \frac{2}{3} \sin^3 \varphi \right]_{\varphi_0}^{\pi/2}$$

$$M = hM_p \left\{ \frac{1}{3}(c_2 - c_1) + \frac{1}{2} c_1 \cos \varphi_0 - \frac{1}{3}(c_2 - c_1) \sin^3 \varphi_0 \right\} \tag{6.1-70}$$

With (6.1-63) we obtain for N:

$$N = \pm 0.5 n_p r \cdot 4 \int_0^{\varphi_0} \{c_1 + (c_2 - c_1) \sin 2\varphi\} \, d\varphi$$

$$N = \pm 2 n_p r [c_1 \varphi - 0.5(c_2 - c_1) \cos 2\varphi]_0^{\varphi_0}$$

$$N = \pm N_p \left\{ \frac{c_1}{\pi} \varphi_0 + \frac{1}{2\pi} (c_2 - c_1) - \frac{1}{2\pi} (c_2 - c_1) \cos 2\varphi_0 \right\} \tag{6.1-71}$$

where:

$$N_p = 2\pi r n_p \tag{6.1-72}$$

The maxima for M and N according to (6.1-70) and (6.1-71) are M_{pr} and N_{pr}. They are obtained by successively equating φ_0 to 0 and $\pi/2$.
For $\varphi_0 = 0$:

$$M_{pr} = h M_p \left(\frac{c_1}{6} + \frac{c_2}{3} \right) \tag{6.1-73}$$

For $\varphi_0 = \pi/2$:

$$N_{pr} = \pm N_p \left(\frac{c_1}{5.50} + \frac{c_2}{3.14} \right) \tag{6.1-74}$$

The terms in parentheses in the formulae (6.1-73) and (6.1-74) are very similar. For $c_1 = c_2$ the numerical values of these respective terms are equal; the greatest difference occurs when $c_1 = 0$ and $c_2 = 2$:

$$\left(\frac{c_1}{6} + \frac{c_2}{3} \right) = \frac{2}{3} = 0.667 \tag{6.1-75}$$

$$\frac{c_1}{5.50} + \frac{c_2}{3.14} = \frac{2}{3.14} = 0.637 \tag{6.1-76}$$

The differences turn out to be very small. For the sake of simplicity the formula for N_{pr} can therefore be written as follows:

$$N_{pr} = \pm N_p \left(\frac{c_1}{6} + \frac{c_2}{3} \right) \tag{6.1-77}$$

M_{pr} according to (6.1-73) is applicable when $N = 0$, while N_{pr} according to (6.1-77) is applicable when $M = 0$. The following expression can be written to represent the interaction:

$$\frac{M_m}{M_{pr}} + \left(\frac{N}{N_{pr}} \right)^{1.7} = 1 \tag{6.1-78}$$

This formula has been derived in [3.11] for pipes loaded in bending and normal force. In

[2.2] it has been shown that (6.1-78) yields good results also for the load combinations considered here.

Finally, some comments are offered on the effective normal force N. In the case of a pipe which can deform freely and is not subjected to external normal forces (Fig. 6.1-12) the value of N according to (6.1-69) is very small in relation to that of N_p according to (6.1-72). This is so because the contributions made by n_{yq} and n_{yk} in n_y according to (6.1-36) are very small in relation to $n_p = t\sigma_e$. If n_{yq} and n_{yk} in (6.1-36) are neglected, this has no significant effect on the value of M_m that is ultimately calculated. This being so, instead of (6.1-69) the following formula can be adopted for N:

$$N = F - \pi r n_{yp} = F - P\pi r^2 \tag{6.1-79}$$

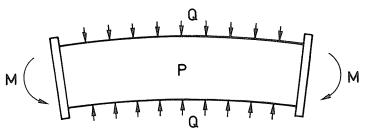

Fig. 6.1-12. For a pipe which can deform freely in the longitudinal direction it is permissible to take N as zero.

6.1.4 Influence of shear force and torsional moment on M_m

The maximum shear force D_p that can be resisted by a pipe is:

$$D_p = 4 \int^{\pi/2} tr \, d\varphi \, \tau_e \cos \varphi = 4tr\tau_e \tag{6.1-80}$$

With

$$A = 2\pi rt \tag{6.1-81}$$

the following expression can alternatively be written for D_p:

$$D_p = \frac{2}{\pi} A\tau_e \tag{6.1-82}$$

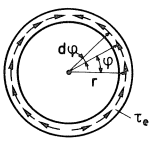

Fig. 6.1-13. Distribution of the shear stresses for D_p.

If other loads are present, such as Q_d and Q_i, P and M, it is assumed that the shear force is resisted by that part of the pipe wall which was originally intended to resist bending. This approach is in analogy with the treatment of the normal force as indicated earlier on.

With reference to (6.1-77), the area available for the purpose is:

$$A_d = \frac{N_{pr}}{\sigma_e} = 2\pi rt\left(\frac{c_1}{6} + \frac{c_2}{3}\right) \tag{6.1-83}$$

With (6.1-82) and (6.1-83) writing τ for τ_e, D for D_p and A_d for A the following approximate expression is obtained for the average shear stress:

$$\tau = \frac{\pi}{2}\frac{D}{A_d} \tag{6.1-84}$$

Thus the stresses σ_x and τ act in the part of the pipe wall intended for M, N and D. According to Von Mises:

$$\sigma_x^2 + 3\tau^2 = \sigma_e^2 \tag{6.1-85}$$

$$\sigma_x = \sigma_e\sqrt{1 - \frac{3\tau^2}{\sigma_e^2}} \tag{6.1-86}$$

With $\tau_e = \sigma_e/\sqrt{3}$ we obtain:

$$\sigma_x = \sigma_e\sqrt{1 - \left(\frac{\tau}{\tau_e}\right)^2} \tag{6.1-87}$$

which can alternatively be written as:

$$\sigma_x = \sigma_e\sqrt{1 - \left(\frac{D}{D_{pr}}\right)^2} \tag{6.1-88}$$

where:

$$D_{pr} = \frac{2}{\pi}\tau_e A_d = \frac{2}{\pi}\cdot\frac{2\pi rt\sigma_e}{\sqrt{3}}\left(\frac{c_1}{6} + \frac{c_2}{3}\right) = D_p\left(\frac{c_1}{6} + \frac{c_2}{3}\right) \tag{6.1-89}$$

In (6.1-88), D_{pr} is the maximum shear force that a pipe loaded by Q_d, Q_i and P is able to resist. With reference to (6.1-88) it appears that σ_x and thus the moment M_{pr} and force N_{pr} according to (6.1-73) and (6.1-77) are reduced by the shear force D:

$$M_{pdr} = hM_p\left(\frac{c_1}{6} + \frac{c_2}{3}\right)\sqrt{1 - \left(\frac{D}{D_{pr}}\right)^2} \tag{6.1-90}$$

$$N_{pdr} = \pm N_p\left(\frac{c_1}{6} + \frac{c_2}{3}\right)\sqrt{1 - \left(\frac{D}{D_{pr}}\right)^2} \tag{6.1-91}$$

The torsional moment can be taken into account in similar fashion. The formulae are given in the summary of the interaction formulae in the next section.
Finally, it is to be noted that in practical cases the reduction due to normal force and especially shear force is fairly small.

6.1.5 Summary of interaction formulae

The interaction formulae derived in the preceding sections are summarized in this section:

$$\frac{M_m}{M_{pdtr}} + \left(\frac{N_m}{N_{pdtr}}\right)^{1.7} = 1 \tag{6.1-92}$$

where:

M_m = maximum bending moment
N_m = maximum effective normal force $= F - P\pi r^2$ (6.1-93)

$$M_{pdtr} = M_{pr}\sqrt{1 - \left(\frac{D}{D_{pr}} + \frac{M_t}{M_{tpr}}\right)^2} \tag{6.1-94}$$

$$N_{pdtr} = \pm N_{pr}\sqrt{1 - \left(\frac{D}{D_{pr}} + \frac{M_t}{M_{tpr}}\right)^2} \tag{6.1-95}$$

$$M_{pr} = ghM_p \tag{6.1-96}$$

$$g = \left(\frac{c_1}{6} + \frac{c_2}{3}\right) \tag{6.1-97}$$

$$h = \left(1 - \frac{2}{3}\frac{a}{r}\right) \tag{6.1-98}$$

$$N_{pr} = gN_p \tag{6.1-99}$$

$$D_{pr} = gD_p \tag{6.1-100}$$

$$M_{tpr} = gM_{tp} \tag{6.1-101}$$

$$M_p = 4r^2 t\sigma_e \tag{6.1-102}$$

$$N_p = 2\pi rt\sigma_e \tag{6.1-103}$$

$$D_p = 4rt\sigma_e/\sqrt{3} \tag{6.1-104}$$

$$M_{tp} = 2\pi r^2 t\sigma_e/\sqrt{3} \tag{6.1-105}$$

$$c_1 = \sqrt{4 - 3\left(\frac{n_y}{n_p}\right)^2 - 2\sqrt{3}\left|\frac{m_y}{m_p}\right|} \tag{6.1-106}$$

$$c_2 = \sqrt{4 - 3\left(\frac{n_y}{n_p}\right)^2} \tag{6.1-107}$$

$$n_y = n_{yq} + n_{yk} + n_{yp} \tag{6.1-108}$$

$$n_{yq} = 0.25Q_d + 0.125Q_i \tag{6.1-109}$$

$$n_{yk} = 0.20\frac{M_m K}{r} \tag{6.1-110}$$

$$n_{yp} = Pr \tag{6.1-111}$$

$$n_p = t\sigma_e \tag{6.1-112}$$

$$m_y = m_{yq} + m_{yk} + m_{yp} \tag{6.1-113}$$

$$m_{yq} = m_{yqd} + m_{yqi} \tag{6.1-114}$$

$$m_{yqd} = 0.25 Q_d r \left\{1 - 0.25 \left(\sin\frac{\alpha}{2} + \sin\frac{\beta}{2}\right)\right\} \cdot f_0 \tag{6.1-115}$$

$$m_{yqi} = 0.25 Q_i r \left\{0.5 - 0.25 \sin\frac{\gamma}{2}\right\} \cdot f_0 \tag{6.1-116}$$

$$m_{yk} = 0.071 M_m K \cdot f_0 \tag{6.1-117}$$

$$m_{yp} = -Pra \tag{6.1-118}$$

$$m_p = 0.25 t^2 \sigma_e \tag{6.1-119}$$

$$f_0 = 1 + \frac{a}{r} \tag{6.1-120}$$

The following are furthermore of importance:

$$Q_{eq} = Q_i \frac{2 - \sin\frac{\gamma}{2}}{4 - \sin\frac{\alpha}{2} - \sin\frac{\beta}{2}} \tag{6.1-121}$$

$$M_e = \pi r^2 t \sigma_e \tag{6.1-122}$$

$$m_e = \frac{1}{6} t^2 \sigma_e \tag{6.1-123}$$

6.2 *Ovalization of the fully plastic cross-section and the relation between bending moment and torsional moment*

The set-up of the new method of design and analysis has been outlined in Chapter 5. Hence follows the need for a relation between the deformations obtained from the "beam analysis" (curvature, rotation, etc.) and the ovalization that occurs. In the present Section 6.2 this relation is derived for a fully plastic section, while in Section 6.3 an approximation is given for the case where the section is only partly plastic. In Section 6.2, too, the relation between the bending moment and the torsional moment is determined as a function of the imposed flexural deformation and torsional deformation. The formulae derived in the present Section 6.2 are summarized at the end thereof. The calculations in this report are always based on a bilinear stress-strain diagram, without strain-hardening.

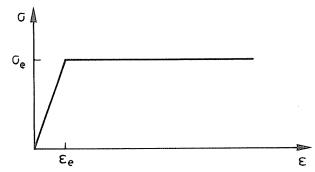

Fig. 6.2-1. Assumed stress-strain diagram.

In the fully plastic section there is, for the stress-strain diagram of Fig. 6.2-1, no direct relation between the stress and the strain and therefore no direct relation between the forces acting on the section and the deformations. This being so, the analysis will make use of the principle of virtual work and of the normality principle already applied in Sections 2.2 and 6.1. A condition for the application thereof is that geometrically linear behaviour must be presumed. For this reason the determination of the ovalization is based on a somewhat modified formula for the maximum moment:

$$M=\left(\frac{c_1}{6}+\frac{c_2}{3}\right) f M_p = g f M_p \tag{6.2-1}$$

where:

$$f=\sqrt{1-\left(\frac{D}{D_{pr}}+\frac{M_t}{M_{tpr}}\right)^2 \cdot \left\{1-\left(\frac{N_m}{N_{pdtr}}\right)^{1.7}\right\}} \tag{6.2-2}$$

For the relation between M according to (6.2-1) and M_m according to (6.1-92) we have:

$$M_m=\left(1-\frac{2}{3}\frac{a}{r}\right) M = h M \tag{6.2-3}$$

The equation of virtual work for the loads acting on the pipe cross-section can be written as follows:

$$M \cdot \delta K + M_t \cdot \delta\theta + D \cdot \delta\gamma + N \cdot \delta\varepsilon_x + P \cdot \delta A + 2Q_d \cdot \delta a_d + Q_i \cdot \delta a_i + 2q \cdot \delta a_q = \delta A_i \tag{6.2-4}$$

where:

δK = variation in the curvature
δA = variation in the cross-sectional area (πr^2)
$\delta\theta$ = variation in the torsional deformation
$\delta\gamma$ = variation in the shear deformation
$\delta\varepsilon_x$ = variation in the change in length
δa_d = variation in the average displacement of Q_d
δa_i = variation in the average displacement of Q_i
δa_d = variation in the average displacement of q
q = ovalization forces (see Fig. 6.1-5)
δA_i = variation in the internal work

This equation of virtual work is valid for any variation of the degrees of freedom. For ovalization:

$$P \cdot \delta A + 2Q_d \cdot \delta a_d + Q_i \cdot \delta a_i + 2q \cdot \delta a_q = \delta A_{i0} \tag{6.2-5}$$

where δA_{i0} is the variation in the internal work associated with ovalization.
Ovalization is assumed to occur in consequence of rotation at the plastic hinges marked by the heavy dots in Fig. 6.2-2 ($\varphi = 0, \pi/2, \pi, 3\pi/2$). No deformations are assumed to occur in the intermediate parts of the circumference of the pipe cross-section.

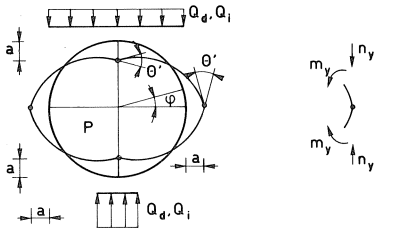

Fig. 6.2-2. Model for the calculation of ovalization.

The right-hand side of (6.2-5) can now be written as follows:

$$\delta A_{i0} = 4m_y \cdot \delta\theta' + 4n_y \cdot \delta\varepsilon_y \tag{6.2-6}$$

With (6.2-5) and (6.2-6) the following can be written for (6.2-4):

$$M \cdot \delta K + M_t \cdot \delta\Theta + D \cdot \delta\gamma + N \cdot \delta\varepsilon_x + 4m_y \cdot \delta\theta' + 4n_y \cdot \delta\varepsilon_y = \delta A_i \tag{6.2-7}$$

Next, an adjacent loading situation will be considered which is associated with the same deformation mechanism and does the same internal work. The equation of virtual work for this loading situation is:

$$\begin{aligned}&(M + \mathrm{d}M) \cdot \delta K + (M_t + \mathrm{d}M_t) \cdot \delta\theta + (D + \mathrm{d}D) \cdot \delta\gamma + (N + \mathrm{d}N) \cdot \delta\varepsilon_x + \\ &+ 4(m_y + \mathrm{d}m_y) \cdot \delta\theta' + 4(n_y + \mathrm{d}n_y) \cdot \delta\varepsilon_y = \delta A_i\end{aligned} \tag{6.2-8}$$

From (6.2-7) and (6.2-8) follows:

$$\mathrm{d}M \cdot \delta K + \mathrm{d}M_t \cdot \delta\theta + \mathrm{d}D \cdot \delta\gamma + \mathrm{d}N \cdot \delta\varepsilon_x + 4\ \mathrm{d}m_y \cdot \delta\theta' + 4\ \mathrm{d}n_y \cdot \delta\varepsilon_y = 0 \tag{6.2-9}$$

Equation (6.2-9) gives the formulation for the condition of normality within the limits of the deformation mechanism envisaged here.
In the further analysis of the problem the pressure P is assumed to be constant during the further application of the flexural and the torsional deformation. Moreover, the terms $\mathrm{d}D \cdot \delta\gamma$, $\mathrm{d}N \cdot \delta\varepsilon_x$ and $4\ \mathrm{d}n_y \cdot \delta\varepsilon_y$ in (6.2-9) will be neglected in relation to the other terms. In fact this means that D, N and n_y are assumed to be constant.
Having regard to the above, (6.2-9) becomes:

$$\mathrm{d}M \cdot \delta K + \mathrm{d}M_t \cdot \delta\theta + 4\ \mathrm{d}m_y \cdot \delta\theta' = 0 \tag{6.2-10}$$

$$4\delta\theta' = -\frac{dM}{dm_y}\delta K - \frac{dM_t}{dm_y}\delta\theta \tag{6.2-11}$$

For the relation between $\delta\theta'$ and δa it follows from Fig. 6.2-2 that:

$$\delta a = \frac{\delta\theta'}{2} r \tag{6.2-12}$$

With this relation, equation (6.2-11) becomes:

$$\delta a = \frac{r}{8}\left(-\frac{dM}{dm_y}\delta K - \frac{dM_t}{dm_y}d\theta\right) \tag{6.2-13}$$

For calculating the ovalization as a function of the imposed flexural deformation δK and torsional deformation $\delta\theta$ it remains to determine the quotients dM/dm_y and dM_t/dm_y. These quotients can be determined by making use of (6.2-1) and (6.2-2) and of the normality condition. For the sake of simplicity, in this report the normal force N and the shear force D will be equated to zero. A derivation in which the effect of D and N has been incorporated is given in [2.2] and [2.7]. However, comparative calculations have shown the effect of D and N on the ultimate ovalization of buried pipelines to be of only very limited magnitude.
As a result of the above, (6.2-1) and (6.2-2) become:

$$\left(\frac{M}{M_p}\right)^2 + \left(\frac{M_t}{M_{tp}}\right)^2 = g^2 \tag{6.2-14}$$

where:

$$g = \frac{c_1}{6} + \frac{c_2}{3} \tag{6.2-15}$$

In Fig. 6.2-3 the relation between M, M_t and m_y (g is a function of m_y) according to (6.2-14) is shown for $P=0$ and only for positive values of M, M_t and m_y. The surface represented in this diagram is called the yield surface. For $P \neq 0$ other yield surfaces are

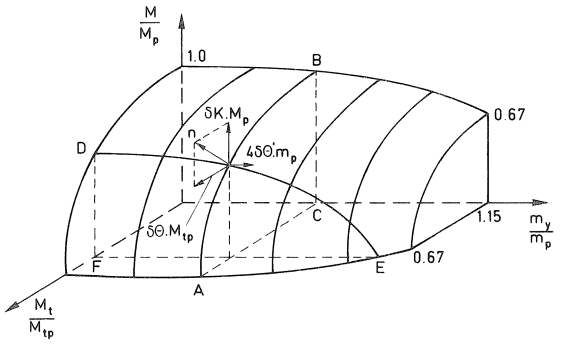

Fig. 6.2-3. Yield surface for M, M_t and m_y, with directions of the deformations.

obtained, which lie within the surface represented in Fig. 6.2-3. For constant m_y the sections through the yield surface are always circles, for in that case g in (6.2-14) is constant and this equation then represents a circle. The following derivation is therefore valid also for values of P other than $P=0$.
For determining the interrelation of M and M_t the term $4\ \mathrm{d}m_y \cdot \mathrm{d}\theta'$ in (6.2-10) can be put equal to zero, so that:

$$\mathrm{d}M \cdot \delta K + \mathrm{d}M_t \cdot \delta\theta = 0 \tag{6.2-16}$$

On differentiating (6.2-14) with respect to M we obtain:

$$\frac{2M}{M_p^2} + \frac{2M_t}{M_{tp}^2} \cdot \frac{\mathrm{d}M_t}{\mathrm{d}M} = 0 \tag{6.2-17}$$

From (6.2-16) and (6.2-17) it follows that:

$$\frac{\delta K}{\delta\theta} = \frac{M}{M_t} \cdot \frac{M_{tp}^2}{M_p^2} \tag{6.2-18}$$

After some rearrangement this gives:

$$\left(\frac{M}{M_p}\right)^2 = \left(\frac{\delta K}{\delta\theta}\right)^2 \cdot \left(\frac{M_t}{M_{tp}}\right)^2 \cdot \left(\frac{M_p}{M_{tp}}\right)^2 \tag{6.2-19}$$

From (6.2-19) and the yield condition (6.2-14) it follows that:

$$\left(\frac{\delta K}{\delta\theta}\right)^2 \cdot \left(\frac{M_t}{M_{tp}}\right)^2 \cdot \left(\frac{M_p}{M_{tp}}\right)^2 + \left(\frac{M_t}{M_{tp}}\right)^2 = g^2 \tag{6.2-20}$$

so that:

$$\boxed{M_t = \frac{g \cdot M_{tp} \cdot \delta\theta}{\sqrt{(\delta\theta)^2 + (\delta K)^2 \cdot c}}} \tag{6.2-21}$$

where:

$$c = \left(\frac{M_p}{M_{tp}}\right)^2 = \left(\frac{4r^2 t\sigma_e}{2\pi r^2 t\sigma_e/\sqrt{3}}\right)^2 = \left(\frac{2\sqrt{3}}{\pi}\right)^2 = 1.22 \tag{6.2-22}$$

We similarly obtain:

$$\boxed{M = \frac{g \cdot M_p \cdot \delta K}{\sqrt{(\delta K)^2 + (\delta\theta)^2/c}}} \tag{6.2-23}$$

With (6.2-21), (6.2-22) and (6.2-23) the values of M and of M_t are determined as functions of $\delta K/\delta\theta$ and of m_y (g is a function of m_y). For a particular value of $\delta K/\delta\theta$ and of m_y the point of intersection of the curves AB and DE in Fig. 6.2-3 determines M and M_t.

The deformation vectors at that point are also shown in the diagram. They are obtained from (6.2-16). For the interrelation of δK and $\delta\theta$ we can write:

$$\frac{\delta K \cdot M_p}{\delta\theta \cdot M_{tp}} = -\frac{dM_t/M_{tp}}{dM/M_p} \tag{6.2-24}$$

The right-hand side of (6.2-24) indicates the direction of the normal (perpendicular line) with respect to the section ABC through the yield surface shown in Fig. 6.2-3. The left-hand side of the equation relates to the components of the deformation vector $[\delta K \cdot M_p;\ \delta\theta \cdot M_{tp}]$ indicated in Fig. 6.2-3.
For the interrelation of the ovalization parameter $\delta\theta'$ and δK and of $\delta\theta'$ and $\delta\theta$ we similarly obtain:

$$\frac{\delta K \cdot M_p}{4\delta\theta' \cdot m_p} = -\frac{dm_y/m_p}{dM/M_p} \tag{6.2-25}$$

$$\frac{\delta\theta \cdot M_{tp}}{4\delta\theta' \cdot m_p} = -\frac{dm_y/m_p}{dM_t/M_{tp}} \tag{6.2-26}$$

With the values of M and M_t which are now known - according to (6.2-23) and (6.2-21) - and with the yield condition (6.2-14) the quotients dM/dm_y and dM_t/dm_y in (6.2-13) can then be determined, so that the relation between δa and δK and $\delta\theta$ is known.
Formula (6.2-13) can alternatively be written as follows:

$$\delta a = -\frac{r}{8}\left(\frac{dM/M_p}{dm_y/m_p}\cdot\frac{M_p}{m_p}\cdot\delta K + \frac{dM_t/M_{tp}}{dm_y/m_p}\cdot\frac{M_{tp}}{m_p}\cdot\delta\theta\right) \tag{6.2-27}$$

Substituting:

$$\frac{M_p}{m_p} = \frac{4r^2 t\sigma_e}{0.25t^2\sigma_e} = 16\frac{r^2}{t} \tag{6.2-28}$$

and:

$$\frac{M_{tp}}{m_p} = \frac{2\pi r^2 t\sigma_e/\sqrt{3}}{0.25t^2\sigma_e} = \frac{8\pi}{\sqrt{3}}\frac{r^2}{t} \tag{6.2-29}$$

it follows that:

$$\boxed{\delta a = -\frac{r^3}{t}\left(2\psi_m\cdot\delta K + \frac{\pi}{\sqrt{3}}\psi_t\cdot\delta\theta\right)} \tag{6.2-30}$$

where:

$$\psi_m = \frac{dM/M_p}{dm_y/m_p} \tag{6.2-31}$$

and:

$$\psi_t = \frac{dM_t/M_{tp}}{dm_y/m_p} \tag{6.2-32}$$

are the slopes of the yield surface shown in Fig. 6.2-3. These slopes depend on the magnitude of m_y. The maximum value for m_y is reached if c_1 according to (6.1-106) is zero:

$$m_{ym} = 1.15 m_p \left\{1 - 0.75 \left(\frac{n_y}{n_p}\right)^2\right\} \tag{6.2-33}$$

With increasing m_y the slopes ψ_m and ψ_t become greater and thus also the rate at which ovalization occurs. For $m_y = m_{ym}$ the values of ψ_m and ψ_t become very large. In Fig. 6.2-3 with $n_{yp} = 0$ and $n_y \approx 0$ this is the point where $m_y \approx 1.15 m_p$. This means that in response to a small increase in the curvature and/or the rotation the ovalization undergoes a very considerable increase. This failure mode is called failure due to progressive ovalization. In reality this failure mode is not very likely to occur, the reason being that with increasing ovalization the buckling stability is lowered (Chapter 5), so that buckling then usually becomes the governing mode.

Summary of formulae presented in Section 6.2 (see also the formulae in Section 6.1.5)

$$M_m = \left(1 - \frac{2}{3}\frac{a}{r}\right) M = h\,M \tag{6.2-3}$$

$$M = \left(\frac{c_1}{6} + \frac{c_2}{3}\right) f M_p = g f M_p \tag{6.2-1}$$

$$f = \sqrt{1 - \left(\frac{D}{D_{pr}} + \frac{M_t}{M_{tpr}}\right)^2 \cdot \left\{1 - \left(\frac{N_m}{N_{pdtr}}\right)^{1.7}\right\}} \tag{6.2-2}$$

If D and N are neglected, the following formulae for δa and the relation between M and M_t apply*.

$$M = \frac{g \cdot M_p \cdot \delta K}{\sqrt{(\delta K)^2 + (\delta\theta)^2/1.22}} \tag{6.2-23}$$

$$M_t = \frac{g \cdot M_{tp} \cdot \delta\theta}{\sqrt{(\delta\theta)^2 + (\delta K)^2 \cdot 1.22}} \tag{6.2-21}$$

$$\delta a = -\frac{r^3}{t}\left(2\psi_m \cdot \delta K + 1.81\psi_t \cdot \delta\theta\right) \tag{6.2-30}$$

$$\psi_m = \frac{dM/M_p}{dm_y/m_p} \tag{6.2-31}$$

$$\psi_t = \frac{dM_t/M_{tp}}{dm_y/m_p} \tag{6.2-32}$$

* Formulae with the effect of D and N incorporated are given in [2.1], [2.2] and [2.7].

$$m_y < m_{ym} = 1.15 m_p \left\{1 - 0.75 \left(\frac{n_y}{n_p}\right)^2\right\} \tag{6.2-33}$$

In Section 6.1 it has been shown that m_y depends upon, among other quantities, the magnitude of the curvature and of the ovalization. For $P = 0$, increasing curvature and ovalization cause m_y to increase. This means that the calculation must be performed stepwise, since ψ_m and ψ_t are dependent on m_y.
The effect of the pressure upon the ovalization that occurs will be further considered in Section 6.4.

6.3 *Elastic-plastic range*

In Sections 6.1 and 6.2 the loads that the pipe can support and the ovalizations have been calculated for the fully plastic section. The present section examines the situation where the section is only partly plastic.

6.3.1 Moment-curvature diagram

Two moment-curvature diagrams are shown in Fig. 6.3-1.
In the elastic range the flexural stiffness is reduced in consequence of ovalization. This has been derived in [2.2]:

$$EI_{red} = E\pi r^3 t \left(1 - 1.5 \frac{a}{r}\right) \tag{6.3-1}$$

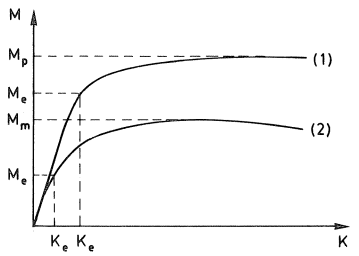

Fig. 6.3-1. Moment-curvature diagrams: (1) bending only; (2) bending + other loads.

For $K = K_e$ the end of the elastic range is reached. On a conservative estimate this is the case when:

$$\frac{M}{M_e} + \frac{M_t}{M_{tp}} + \frac{m_y}{m_e} + \frac{n_y}{n_p} + \frac{D}{D_p} + \frac{N}{N_p} = 1 \tag{6.3-2}$$

For the situation comprising bending and other loads the moment-curvature diagram of Fig. 6.3-1 is again presented in Fig. 6.3-2, together with the curve representing M_m according to the formulae of Section 6.1. M_m has been calculated from the end of the elastic range. In calculating M_m according to Section 6.1 it has been assumed that the section is fully plastic, i.e., that yielding has developed in every part of it. Since m_y

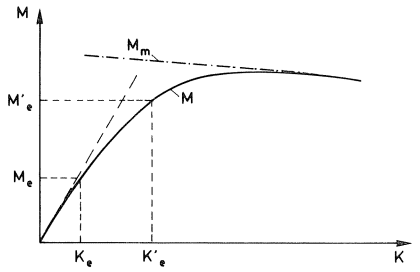

Fig. 6.3-2. Moment-curvature diagram for bending and other loads, together with the relationship for M_m. It is to be noted that strain-hardening has been left out of account in the calculation of M_m. If strain-hardening occurs, the line representing M_m will show less downward slope with increasing curvature or may indeed slope upward.

increases with increasing curvature, M_m will decrease with increasing curvature. In the actual pipe the cross-section will, for curvatures exceeding K_e, gradually develop plastic behaviour, so that the bending moment will increase until the section has become fully plastic and M_m is attained.

A theoretical derivation of the moment-curvature diagram in the region between M_e and the attainment of M_m is, when bending and other loads are acting, a very complicated problem. For this reason the following approximation will be adopted:

$$M'_e = \frac{M_e}{M_p} M_m \approx \frac{M_m}{1.27} \tag{6.3-3}$$

$$K'_e = \frac{M'_e}{EI_{red}} \tag{6.3-4}$$

$$EI_{red} = E\pi r^3 t \left(1 - 1.5 \frac{a'}{r}\right) \tag{6.3-5}$$

$$\varphi = \text{arc sin} \frac{K'_e}{K} \tag{6.3-6}$$

$$M = M_m \cdot 0.5 \left(\frac{\varphi}{\sin \varphi} + \cos \varphi\right) \tag{6.3-7}$$

In these formulae:

K = the curvature for which M is calculated
M_m = the maximum moment, according to Section 6.1, associated with K
a' = the ovalization on attainment of K'_e; this ovalization is calculated in Section 6.3.2

The formulae (6.3-6) and (6.3-7) have already been derived in Section 2.1.

The approximation presented here for the elastic-plastic range is in reasonably good agreement with the experimental results. An important advantaged of the computational model that has here been adopted for the elastic-plastic range is the relatively simple application of the "beam analysis" described in Section 5.2. By introducing

notional values for the modulus of elasticity E' and the yield point σ_e' it is possible to simulate the actual moment-curvature diagram quite simply:

$$E' = \frac{E}{1 - 1.5\,\frac{a'}{r}} \tag{6.3-8}$$

$$\sigma_e' = \frac{M_m}{M_p}\,\sigma_e \tag{6.3-9}$$

In the "beam analysis" the "standard" moment-curvature diagram for a pipe cross-section, as described in Section 2.1, can then further be employed.

6.3.2 Curvature-ovalization diagram

Because the cross-section is not yet fully plastic in the elastic-plastic range, there will be a gradual transition from the "elastic" rate of ovalization to the "fully plastic" rate. To link this behaviour pattern to M/M_m appears an obvious choice:

$$a_2 = a_1 + \delta a\,\frac{M}{M_m} \tag{6.3-10}$$

where:

δa = ovalization that occurs when the curvature increases by δK and/or torsion by $\delta\theta$

a_1, a_2 = ovalization at the end of the previous step and the new ovalization

M = M according to (6.3-7)

6.3.3 Torsional moment-rotation diagram

The reduction of the torsional stiffness in the elastic range is negligible. For the elastic-plastic branch ($\theta_e < \theta < \theta_p$) we have approximately:

$$M_t = \theta \cdot GI_t \left(1 - \frac{(\theta - \theta_e)(M_{tp} - M_{tm})}{(\theta_p - \theta_e)M_{tp}}\right) \tag{6.3-11}$$

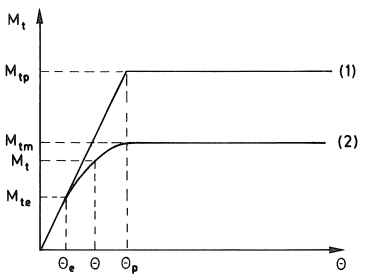

Fig. 6.3-3. Torsional moment-rotation diagram.
1. Only torsional moment
2. Torsional moment + other loads

The quantities M_{te}, M_{tp}, M_{tm}, θ_e and θ_p are indicated in Fig. 6.3-3.

6.4 *Further consideration of the effect of pressure on ovalization*

If an internal excess pressure ($P = P_i - P_u > 0$) is acting, with increasing curvature and therefore also increasing ovalization the magnitude of m_{yp} will also increase. Because m_{yp} differs in its algebraic sign from m_{yq} and m_{yk}, the value of m_y will, if P is sufficiently high, not increase with increasing curvature but will instead decrease. When m_y decreases, the slope of the yield surface also decreases, so that the "rate of ovalization" diminishes.
The minimum value for m_y is zero. When this value has been reached, the equilibrium condition (6.1-113) determines the magnitude of the ovalization:

$$(6.1\text{-}113) \rightarrow m_y = m_{yq} + m_{yk} + m_{yp} = 0 \tag{6.4-1}$$

With (6.1-118) it then follows that:

$$a = \frac{m_{yq} + m_{yk}}{Pr} \tag{6.4-2}$$

This means therefore that as soon as this situation has been attained, the formulae derived in Section 6.2 for the calculation of the ovalization are no longer applicable. Then the earth pressure and the ovalization forces are, as it were, supported by the internal pressure.

6.5 *Calculation of the strains*

For the longitudinal direction the strains are relatively simple to determine from the curvatures and rotations obtained from the "beam analysis" calculations. For the circumferential strains it is in general necessary to use a finite element computer program with which both the geometric and the physical non-linear behaviour can be taken into account. In the context of this research a special computer program designated as REK*, based on the finite difference method has been developed for the purpose. The result of a calculation of this kind is shown in Fig. 6.5-1.

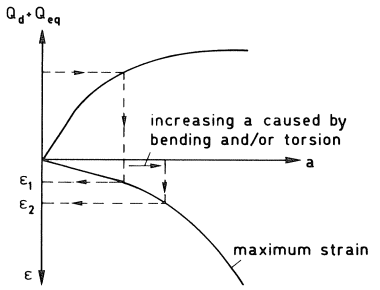

Fig. 6.5-1. Calculation of the strains.

* REK is the Dutch word for STRAIN.

6.6 *Experimental verification*

6.6.1 Overview of the tests performed

The design rules have been incorporated in the IBBC-TNO's computer program RECHT* by means of which the results of the following tests have been analysed:

- 8 tests on pipes ø 152.5–1.55 mm: bending + pressure;
- 5 tests on pipes ø 122 –1.55 mm: bending + pressure;
- 10 tests on pipes ø 152.5–1.55 mm: bending + torsion + pressure;
- 1 test on pipe ø 609.6–6.4 mm: bending + pressure (full-scale test, Section 3.3.2);
- 5 tests on pipes ø 149 –1.62 mm: earth pressure + bending + pressure;
- 2 tests on pipes ø 12″ –9.5 mm: earth pressure + bending.

There is found to be good agreement between the measured and the calculated values for the bending moment, the torsional moment and the earth pressure. The same is true of the ovalization. It is to be noted that in nearly all cases the calculated ovalizations were higher than the measured values and the calculated curvatures and rotations with respect to buckling were lower than the measured values. Hence it can be concluded that the design rules yield results that are on the safe side.
By way of illustration one of the tests of the series earth pressure + bending + internal pressure that were performed will be described in the next section.

6.6.2 Test 112: earth pressure, bending, $P = -1$ bar

The test set-up employed is shown diagrammatically in Figs. 6.6-1 and 6.6-2. See also Photographs 18 and 19. With the aid of the equipment adopted for applying the bending load it was ensured that the moment acting at the circumferential welds was a little smaller than in the measuring region in the middle of the test specimen. Premature buckling at the non-representative welds was thus prevented. In the case of the specimens purpose-made under our own control it was, with the available equipment, not possible to avoid a relatively pronounced "high-low" situation at the welds.
The deformation was determined from the displacements measured with the aid of the displacement transducers K_1 and K_2 mounted in steel frames welded to the pipe. The

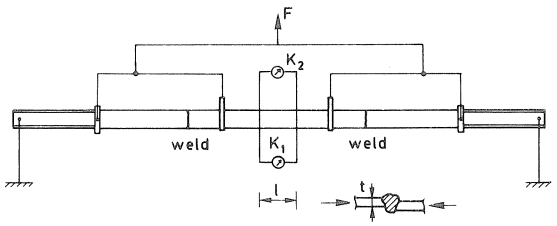

Fig. 6.6-1. Schematic set-up with the equipment for the bending moment and measuring devices for the curvature (ø 149–1.62).

* RECHT is the Dutch word for STRAIGHT.

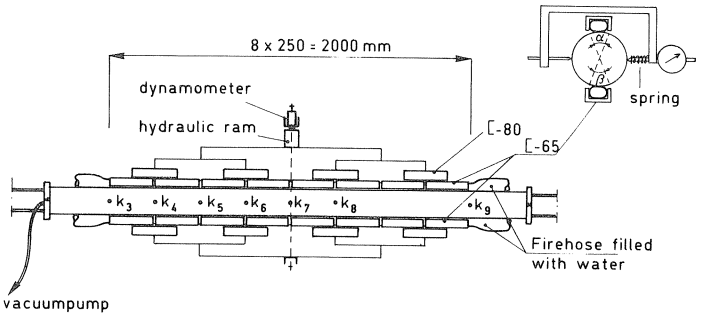

Fig. 6.6-2. Schematic set-up with the equipment for the "earth pressure" load and measuring devices for the change in the horizontal diameter in the points k_1 through k_9.

earth pressure was simulated by means of the loading system shown in Fig. 6.1-2, where it is also indicated that air was extracted from the pipe by a vacuum pump so as to obtain a pressure P practically equal to -1 bar. The loading angle α and the bearing angle β were 30°. The measured yield point was about 354 N/mm^2.
The testing sequence was as follows:
a. apply $P = -1$ bar (air pump);
b. apply earth pressure Q_d;
c. apply bending moment M.

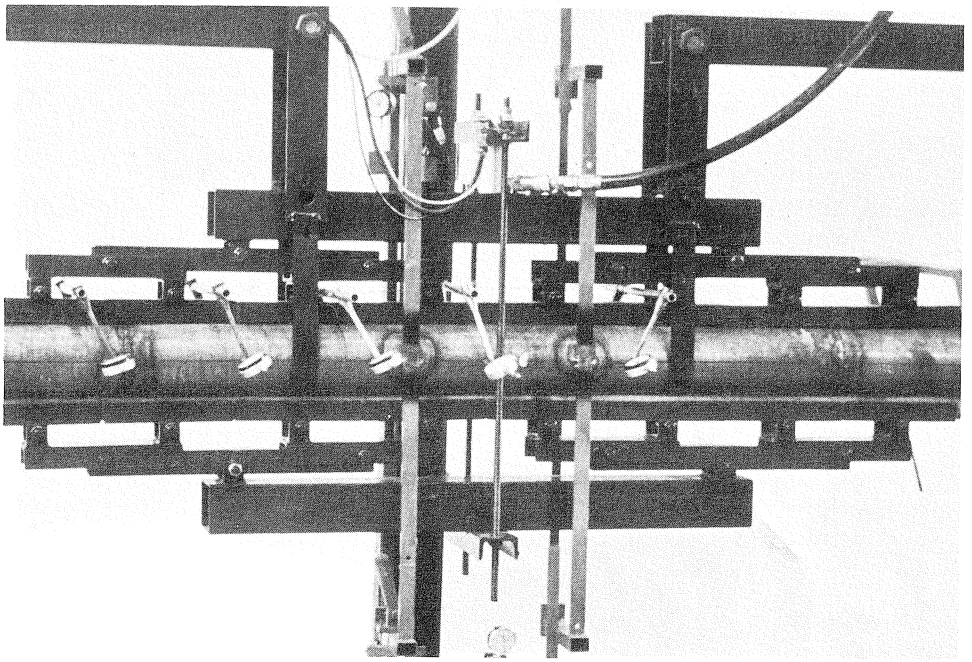

Photo 18. Central part of the testing arrangement for the load combination of earth pressure and bending.

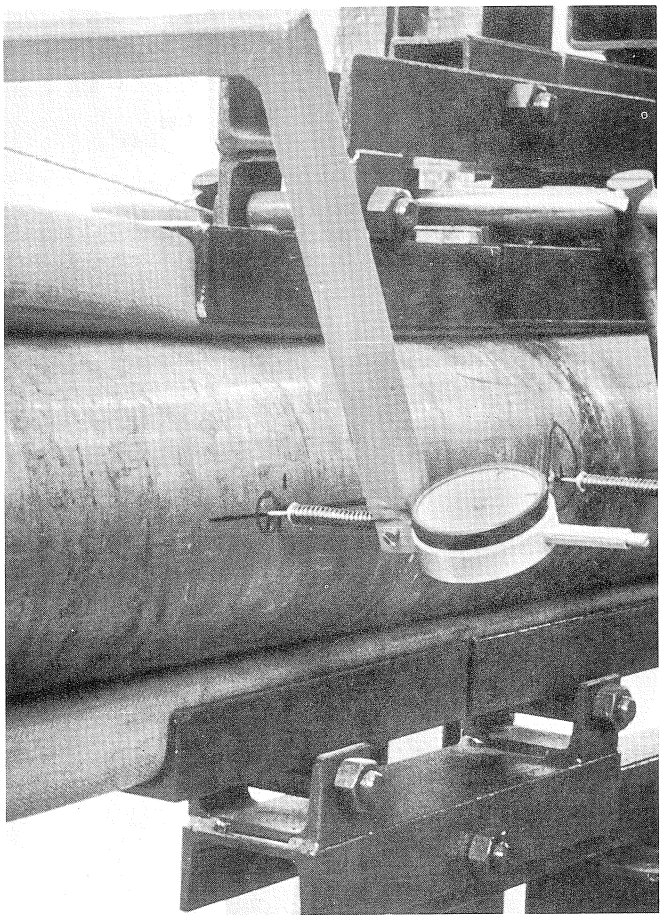

Photo 19. Testing arrangement with the fire-hose for the application of "earth pressure" and the measuring device for determining the change in the horizontal diameter.

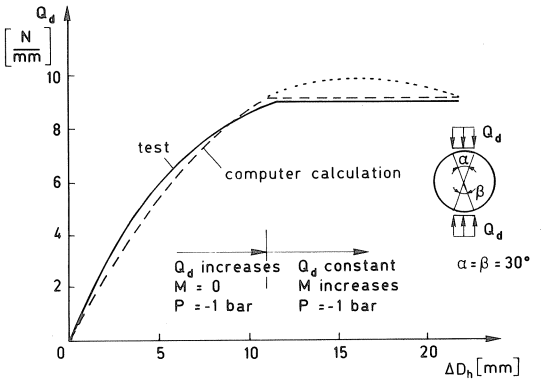

Fig. 6.6-3. Earth pressure-ovalization diagram. ΔD_h is the change (increase) in diameter perpendicular to the plane of bending (= horizontal diameter).

The measured results together with the results calculated with the aid of the RECHT computer program, already mentioned, are indicated in Figs. 6.6-3, 6.6-4 and 6.6-5.

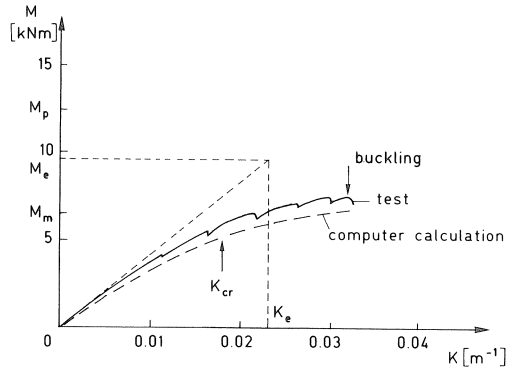

Fig. 6.6-4. Moment-curvature diagram.

As shown in Fig. 6.6-3, a very high value of Q_d was applied in this test (equal to about 90 per cent of the ultimate value for failure due to Q_d alone in conjunction with $P = -1$ bar). This large Q_d accordingly brings about a considerable reduction of the maximum moment (Fig. 6.6-4).

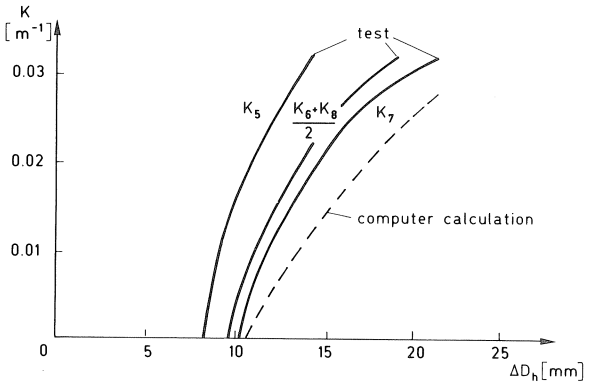

Fig. 6.6-5. Curvature-ovalization diagram. ΔD_h is the change (increase) in diameter perpendicular to the plane of bending.

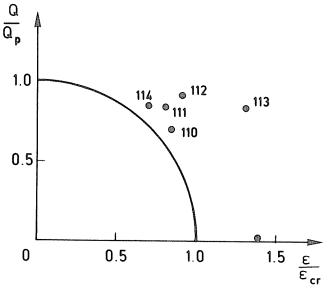

Fig. 6.6-6. Interaction formula and test results.

6.6.3 Interaction formula

The interaction formula (6.6-1) has been established on the basis of the calculations performed. It can be used to make a quick assessment of whether particular combination of earth pressure and imposed curvature will comply with the limit value with respect to buckling:

$$\left(\frac{Q}{Q_{dp}}\right)^2 + \left(\frac{\varepsilon}{\varepsilon_{cr}}\right)^2 = 1 \qquad (6.6\text{-}1)$$

where:

$$Q = Q_d + Q_{eq} \tag{6.6-2}$$

Q_{eq} = the design value of Q_i converted into an equivalent earth pressure (Section 6.1.2.1)

Q_{dp} = the load-carrying capacity with regard to Q_d for the pressure P under consideration

ε = the compressive strain calculated in the design state

ε_{cr} = the critical compressive strain according to Section 4.4.2

Formula (6.6-1) is represented in Fig. 6.6-1, together with the results obtained in the test series on ⌀ 149–1.62 mm pipes.
In the case of test 113 (Fig. 6.6-1) the loading sequence was reversed. First, the pipe was loaded in bending and then Q_d was applied. With the aid of the normality principle, already referred to, it can be shown that this latter loading sequence leads to more favourable buckling curvatures [2.11].

7 Derivation of design rules for smooth bends in buried steel pipelines

The design rules for smooth bends, as embodied in the various codes of practice ([1.7], for example), have been derived for the elastic range. An extension of the rules to comprise the plastic range is therefore necessary. Besides, the existing design rules do not take account of various influences - more particularly, the influence of earth pressure, of the stiffening effect of the straight lengths of pipe to which the bend is connected, and of ovalization of the cross-section.
An approximate description of elastic-plastic behaviour is given in Section 7.1. In Sections 7.2 and 7.3 the above-mentioned influences are calculated in the case of elastic and of plastic material behaviour respectively. Next, the influence of variations in pressure and the calculation of strains are considered. Finally, some test results are reported.
Only bending within the plane of curvature of the pipe is treated in this report. Design rules for bending not confined to this plane are given in [2.3].

7.1 *Approximate description of elastic-plastic behaviour; sign conventions*

Among others, the following insights were gained form the investigations:

a. The bend may be substantially stiffened by the straight pipes to which it is connected. As a result, the stiffness factor k is reduced, especially in the case of bends with a small central angle α. Also, the ovalization associated with bending is reduced by the connected straight pipes.
b. In consequence of the ovalization that occurs the flexural stiffness of the bend changes. For positive bending, i.e., the bend becomes more sharply curved (see

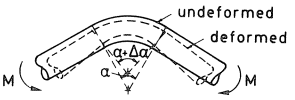

Fig. 7.1-1. Deformation of a pipe bend due to bending (flexural deformation).

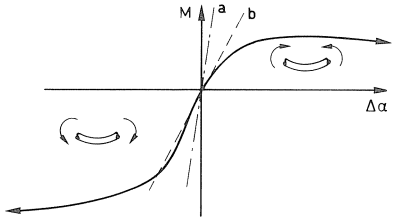

Fig. 7.1-2. Moment-angular rotation diagram for positive and for negative bending respectively.

Fig. 7.1-1), the flexural stiffness decreases with increasing ovalization and bending moment. For negative bending, i.e., the bend becomes less sharply curved ("straightens"), the flexural stiffness increases with increasing ovalization and bending moment. In Fig. 7.1-2 the line "a" represents the linearly elastic behaviour of a straight pipe with the same diameter and wall thickness as the bend. The line "b" is the tangent at the origin to the M-$\Delta\alpha$ diagram of the bend.

c. Because of the phenomenon described in point b, the plastic moment M_{pbo} of the bend is dependent also on the direction in which bending occurs (see Fig. 7.1-2).
d. A displacement of the M-$\Delta\alpha$ diagram occurs in consequence of the earth pressure (see Fig. 7.1-3).
e. The flexural deformation capacity with regard to buckling is considerably greater in bends than in straight pipes of the same diameter and wall thickness.

Sign conventions

The positive directions of the forces and deformations are indicated in Figs. 7.1-4 to 7.1-6.

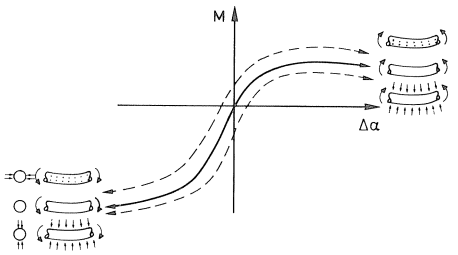

Fig. 7.1-3. Effect of earth pressure on the moment-angular rotation diagram.

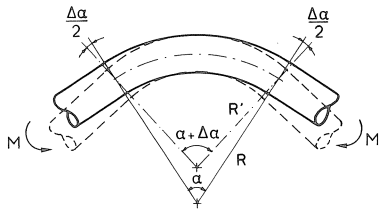

Fig. 7.1-4. Angular rotation $\Delta\alpha$ and change of the bend radius R to R' in the case of positive bending.

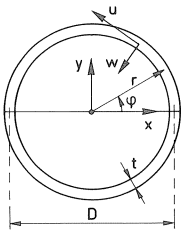

Fig. 7.1-5. Displacements u and w and other quantities in the cross-section.

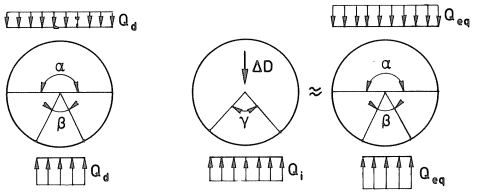

Fig. 7.1-6. Earth pressures and loading and bearing angles. The force ΔD provides an indication of the shear force contribution due to Q_i per unit length of the pipe. Q_i can be conceived as replaced by Q_{eq} according to (6.1-7) and (7.2-7).

7.2 *Elastic range*

Von Karman and other investigators have derived formulae for describing the behaviour of bends loaded in bending and pressure P. Their derivation makes use of the principle of minimum strain energy [3.12], [3.13].

In the theory elaborated in [3.12], [3.13] and other publications the following assumptions and simplifications have in general been adopted:

a. The derivations are valid for an "infinitely" long bend. The effect of the straight pipes to which it is connected is not taken into account.
b. The ratio of the radius of the pipe cross-section to the radius of the bend is treated as negligible in relation to unity ($r/R + 1 \approx 1$).
c. The circumferential strain at mid-thickness of the pipe wall is taken to be zero.
d. Plane sections are assumed to remain plane and perpendicular to the axis of the pipe after it has been subjected to bending (Bernoulli's assumption).

e. The derivations are valid for a bending moment which is constant along the bend.
f. The effect of the change in geometry such as ovalization and the change in the radius of the bend is not taken into account.
g. The derivations are only valid for the elastic range and the load combination of bending and pressure P.

Within the context of investigations reported here the assumptions and simplifications stated in points b, c, d, and e were adopted. The effects associated with points a, f and g have been given due consideration, however.

7.2.1 Potential energy equation

In [2.3] the following potential energy equation has been derived for a long bend loaded in bending, pressure P and earth pressure $Q = Q_d + Q_{eq}$. The derivation in this section is based on linearly elastic material behaviour and on the assumptions and simplifications listed in points a to f:

$$
\begin{aligned}
E_{pot} = {} & \frac{rtE}{2R^2} \int_0^{2\pi} \left(r\eta \sin\varphi - \frac{du}{d\varphi} \sin\varphi + u \cos\varphi \right)^2 d\varphi + \\
& + \frac{Et^3}{24r^3} \int_0^{2\pi} \left(\frac{d^3u}{d\varphi^3} + \frac{du}{d\varphi} \right)^2 d\varphi - \\
& - M \frac{\eta}{L} + \\
& + \frac{1}{2} P \int_0^{2\pi} \left\{ 2r \frac{du}{d\varphi} + u \frac{d^2u}{d\varphi^2} + \left(\frac{d^2u}{d\varphi^2} \right)^2 \right\} d\varphi - \\
& - 2q_1 r \int_{\pi/2-\alpha/2}^{\pi/2} \left(\frac{du}{d\varphi} \sin^2\varphi - u \sin\varphi \cos\varphi \right) d\varphi - \\
& - 2q_2 r \int_{\pi/2-\beta/2}^{\pi/2} \left(\frac{du}{d\varphi} \sin^2\varphi - u \sin\varphi \cos\varphi \right) d\varphi
\end{aligned}
\tag{7.2-1}
$$

where:

$$w = \frac{du}{d\varphi} \tag{7.2-2}$$

$$\eta = \frac{\Delta\alpha}{\alpha} \qquad (\alpha \text{ is the central angle, Fig. 7.1-4}) \tag{7.2-3}$$

$$q_1 = \frac{Q}{2r \sin \alpha/2} \qquad (\alpha \text{ is the loading angle, Fig. 7.1-6}) \tag{7.2-4}$$

$$q_2 = \frac{Q}{2r \sin \beta/2} \qquad (\beta \text{ is the bearing angle, Fig. 7.1-6}) \tag{7.2-5}$$

$$Q = Q_d + Q_{eq} \tag{7.2-6}$$

$$Q_{eq} = Q_i \frac{2 - \sin \gamma/2}{4 - \sin \alpha/2 - \sin \beta/2} \qquad \text{(for } \alpha, \beta, \gamma \text{ see Fig. 7.1-6)} \tag{7.2-7}$$

Formula (7.2-7) for the equivalent earth pressure has been derived in Section 6.1.2.1.

7.2.2 Further development of the potential energy equation

For developing and further working out equation (7.2-1) a suitable displacement function for u should be chosen:

$$u = \sum_{n=1}^{\infty} a_n \sin n\varphi + \sum_{n=1}^{\infty} b_n \cos n\varphi \tag{7.2-8}$$

For reasons of symmetry the displacement u must be zero for $\varphi = \pi/2$ and $\varphi = 3\pi/2$. This is also the case for $\varphi = 0$ and $\varphi = \pi$ if the loading angle α is equal to the reaction angle β. If α is not equal to β the values of φ for which $u = 0$ will be slightly different from $\varphi = 0$ and $\varphi = \pi$. For the sake of simplicity this difference will be left out of account in the further derivation of the moment-curvature diagram. On the basis of these considerations equation (7.2-8) becomes:

$$u = a_2 \sin 2\varphi + a_4 \sin 4\varphi + a_6 \sin 6\varphi + \ldots \tag{7.2-9}$$

According as more terms are included in this series a more accurate solution is obtained. The so-called bend parameter λ is a criterion for the number of terms required for obtaining a particular accuracy:

$$\lambda = \frac{tR}{r^2} \tag{7.2-10}$$

Rodabaugh and George [3.13] give the following guidance for attaining 10 per cent accuracy:

$\lambda > 0.50 \rightarrow$ one term
$0.40 > \lambda > 0.16 \rightarrow$ two terms
$0.12 > \lambda > 0.08 \rightarrow$ three terms
$0.06 > \lambda > 0.04 \rightarrow$ four terms

In practice the radius of the bend in a buried pipeline is always at least $3D$, while the diameter/wall thickness ratio (D/t) for these (sharply curved) bends is in general not more than 50–70.
For $D/t = 70$ and $R = 3D$ the bend parameter is $\lambda = (t/r) \cdot (R/r) = (1/35) \cdot (6r/r) = 0.171$. This means that for practical purposes it will in general suffice to work with two terms. In [2.3] the limit value for using two terms is given as $\lambda = 0.15$. As a result of restricting the number of terms to two, tolerably convenient formulae are obtained with which a "manual calculation" is possible.

In the BOCHT* computer program developed on the basis of this research a general solution has been employed, the number of terms being a function of λ. This general solution is fully presented in an appendix to [2.3].
With two terms (7.2-9) becomes:

$$u = a_2 \sin 2\varphi + a_4 \sin 4\varphi \tag{7.2-11}$$

When this expression for u is substituted into the potential energy equation (7.2-1), the total potential energy is obtained as a function of the unknowns η, a_2 and a_4:

$$\begin{aligned}
E_{\text{pot}} = {} & \frac{rtE\pi}{2R^2}\left\{(r\eta)^2 + 3a_2 r\eta + \frac{5}{2}a_2^2 - \frac{5}{2}a_2 a_4 + \frac{17}{2}a_4^2\right\} + \\
& + \frac{Et^3\pi}{2r^3}(3a_2^2 + 300a_4^2) - \\
& - M\frac{\eta}{R} + \\
& + 6P\pi(a_2^2 + 20a_4^2) - \\
& - \frac{2q_1 r \sin \alpha/2}{8}\left\{a_2\left(\frac{-3\alpha}{\sin \alpha/2} - 8\cos \alpha/2 - 2\cos \alpha/2 \cos \alpha\right) + 32a_4 \cos^5 \alpha/2\right\} - \\
& - \frac{2q_2 r \sin \beta/2}{8}\left\{a_2\left(\frac{-3\beta}{\sin \beta/2} - 8\cos \beta/2 - 2\cos \beta/2 \cos \beta\right) + 32a_4 \cos^5 \beta/2\right\}
\end{aligned} \tag{7.2-12}$$

The system is in equilibrium if the potential energy is a minimum. Solutions for η, a_2 and a_4 are obtained by differentiating the potential energy equation with respect to the unknowns η, a_2 and a_4 and equating these partial differentials to zero. Next, the deformations, strains and stresses can be determined with the aid of these solutions:

$$\frac{\partial E_{\text{pot}}}{\partial \eta} = \frac{rtE\pi}{2R^2}(2r^2\eta + 3a_2 r) - \frac{M}{R} = 0 \tag{7.2-13}$$

$$\begin{aligned}
\frac{\partial E_{\text{pot}}}{\partial a_2} = {} & \frac{rtE\pi}{2R^2}\left(3r\eta + 5a_2 - \frac{5}{2}a_4\right) + \\
& + \frac{Et^3\pi}{2r^3}(6a_2) + 12P\pi a_2 + \\
& + \frac{2q_1 r \sin \alpha/2}{8}\left(\frac{3\alpha}{\sin \alpha/2} + 8\cos \alpha/2 + 2\cos \alpha/2 \cos \alpha\right) + \\
& + \frac{2q_2 r \sin \beta/2}{8}\left(\frac{3\beta}{\sin \beta/2} + 8\cos \beta/2 + 2\cos \beta/2 \cos \beta\right) = 0
\end{aligned} \tag{7.2-14}$$

* BOCHT is the Dutch word for a BEND.

$$\frac{\partial E_{\text{pot}}}{\partial a_4} = \frac{rtE\pi}{2R^2}\left(-\frac{5}{2}a_2 + 17a_4\right) +$$

$$+ \frac{Et^3\pi}{2r^3}(600a_4) + 240P\pi a_4 -$$

$$- \frac{2q_1 r \sin \alpha/2}{8}(32 \cos^5 \alpha/2) -$$

$$- \frac{2q_2 r \sin \beta/2}{8}(32 \cos^5 \beta/2) = 0 \tag{7.2-15}$$

Putting:

$$\lambda = \frac{tR}{r^2} \tag{7.2-16}$$

$$\psi = \frac{PR^2}{Ert} \tag{7.2-17}$$

$$A = \frac{QR^2}{4rtE\pi}\left(\frac{3\alpha}{\sin \alpha/2} + \frac{3\beta}{\sin \beta/2} + 8 \cos \alpha/2 + 8 \cos \beta/2 + \right.$$

$$\left. + 2 \cos \alpha/2 \cos \alpha + 2 \cos \beta/2 \cos \beta\right) \tag{7.2-18}$$

$$B = \frac{-QR^2}{4rtE\pi}(32 \cos^5 \alpha/2 + 32 \cos^5 \beta/2) \tag{7.2-19}$$

the equations (7.2-13), (7.2-14) and (7.2-15) become:

$$2r^2\eta + 3a_2 r - \frac{2MR}{rtE\pi} = 0 \tag{7.2-20}$$

$$3r\eta + (5 + 6\lambda^2 + 24\psi)a_2 - \frac{5}{2}a_4 + A = 0 \tag{7.2-21}$$

$$-\frac{5}{2}a_2 + (17 + 600\lambda^2 + 480\psi)a_4 + B = 0 \tag{7.2-22}$$

Whence, with some simplifications, the following expressions are obtained for η, a_2 and a_4:

$$\eta = k_p \frac{MR}{EI} + \frac{1.5G_p}{D_p G_p - 6.25}\left(\frac{A}{r} + \frac{5B}{2G_p r}\right) \tag{7.2-23}$$

$$a_2 = \frac{-3G_p}{D_p G_p - 6.25}\left(\frac{MRr}{EI} + \frac{A}{3} + \frac{B}{G_p}\right) \tag{7.2-24}$$

$$a_4 = \frac{-7.5}{D_p G_p - 6.25}\left(\frac{MRr}{EI} + \frac{A}{3} + \frac{B}{G_p}\right) = \frac{2.5}{G_p}a_2 \tag{7.2-25}$$

where:

$$C_p = 5 + 6\lambda^2 + 24\psi \qquad (C_p \text{ is used in (7.2-29) only}) \tag{7.2-26}$$

$$D_p = 0.5 + 6\lambda^2 + 24\psi \tag{7.2-27}$$

$$G_p = 17 + 600\lambda^2 + 480\psi \tag{7.2-28}$$

$$k_p = \frac{C_p G_p - 6.25}{D_p G_p - 6.25} \tag{7.2-29}$$

$$EI = E\pi r^3 t \tag{7.2-30}$$

while:

$$C_0 = 5 + 6\lambda^2 \tag{7.2-31}$$

$$D_0 = 0.5 + 6\lambda^2 \tag{7.2-32}$$

$$G_0 = 17 + 600\lambda^2 \tag{7.2-33}$$

$$k_0 = \frac{C_0 G_0 - 6.25}{D_0 G_0 - 6.25} \tag{7.2-34}$$

The expressions C_0, D_0 and G_0 play a part in the derivation of the maximum moment in the plastic range in Section 7.3. By elimination of M from (7.2-24) and (7.2-25) it is possible also to express a_2 and a_4 as functions of η:

$$a_2 = \frac{-3G_p}{D_p G_p - 6.25}\left\{\frac{r\eta}{k_p} - \frac{1.5G_p}{C_p G_p - 6.25}\left(A + \frac{5}{2}\frac{B}{G_p}\right) + \frac{A}{3} + \frac{B}{G_p}\right\} \tag{7.2-35}$$

$$a_4 = \frac{2.5}{G_p}\, a_2 \tag{7.2-36}$$

7.2.3 Moment-curvature diagram

From (7.2-23) follows for the linearly elastic solution:

$$M = \frac{EI}{R}\left\{\frac{\eta}{k_p} - \frac{1.5G_p}{C_p G_p - 6.25}\left(\frac{A}{r} + \frac{5B}{2G_p r}\right)\right\} \tag{7.2-37}$$

where k_p is called the flexural stiffness factor. It indicates the ratio between the stiffness of a straight pipe (with the same r and t) and that of the bend under consideration. Comparative calculations have shown that k_p as expressed by (7.2-29) is in good agreement with the factor k_p according to ANSI [1.7] (provided that $\lambda > 0.15$). It further appears that the moment-curvature diagram for a smooth bend subjected also to earth pressure is parallel to the moment-curvature diagram for that bend not subjected to earth pressure. This is already shown in Fig. 7.1-3.

Formulae (7.2-37) and (7.2-29) do not take account of:

- the influence of the change in curvature due to bending and earth pressure;
- the influence of the straight pipes to which the bend is connected;
- the influence of ovalization.

On introducing these influences, (7.2-37) and (7.2-29) become:

$$\boxed{M = \frac{EI}{R'}\left\{\frac{\eta}{k'_p} - \frac{1.5G_p}{C_pG_p - 6.25}\left(\frac{A}{r} + \frac{5}{2}\frac{B}{G_p r}\right)\right\} \cdot f_3} \tag{7.2-38}$$

where:

$$R' = \frac{1}{1+\eta} R \tag{7.2-39}$$

$$\eta = \frac{\Delta\alpha}{\alpha} \tag{7.2-40}$$

$$k'_p = k_p \cdot \frac{k'_0}{k_0} \tag{7.2-41}$$

$$k_p = \frac{C_pG_p - 6.25}{D_pG_p - 6.25} \tag{7.2-42}$$

$$k_0 = \frac{C_0G_0 - 6.25}{D_0G_0 - 6.25} \tag{7.2-43}$$

$$k'_0 = 1 + (k_0 - 1)\sqrt{1 - \left(\frac{\gamma - \alpha}{\gamma}\right)^2} \tag{7.2-44}$$

$$\gamma = 1200\left(\frac{t_r}{t_b}\right)^2 \sqrt{\frac{t_b}{D_u}} \tag{7.2-45}$$

$$f_3 = \left(\frac{r + w_h}{r}\right)^{4.5} \tag{7.2-46}$$

The values of C_0, D_0, G_0, C_p, D_p, G_p can be taken from (7.2-26) et seq., substituting instead of R the value R' as expressed by (7.2-39).
The following explanatory comments are offered:

Influence of change in curvature on M
In consequence of bending and earth pressure, R becomes R'. This is indicated in Fig. 7.1-4. Formula (7.2-39) follows directly from the geometry.

Influence of connected straight pipes on M
According as the angle of the bend is smaller, the influence of the connected straight pipes is greater. Differences in wall thickness, if any, between the bend and the straights likewise affect the behaviour of the bend. Finally, the length over which the influence of the straight pipe manifests itself in the bend plays a part. This length is approximately proportional to $\sqrt{t_b/D_u}$.
The formulae (7.2-41), (7.2-44) and (7.2-45) for k'_p, k'_0 and γ have been established on the basis of these considerations and in the light of the test results.

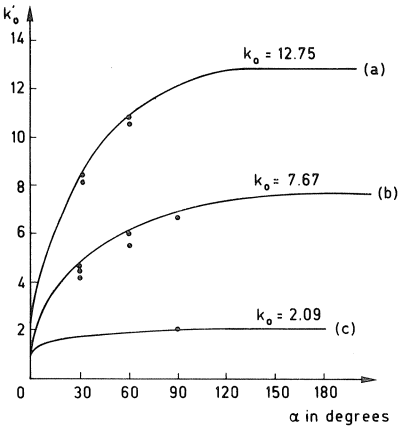

Fig. 7.2-1. Comparison between the measured flexural stiffness factors k_0' and the calculated values.

In Fig. 7.2-1 the measured flexural stiffnesses of the pipe bends tested in the research are compared with the calculated results obtained with the aid of the formulae given above. The formulae have deliberately been so established that in virtually all cases higher values are obtained for the factors k_0' and k_p' than those measured experimentally. For practical purposes this constitutes a situation which is on the safe side, because the higher flexural resistance which is actually available ensures that the deformations and strains will be less than the calculated ones.

Table 7.2-1. Data relating to the pipe bends that were tested

	(a), [2.8]	(b), [2.8]	(c), [2.8]
D_u in mm	261	160	322
t_b in mm	2.9	2.9	6.4
D_u/t_b	90	55	51
t_r in mm	3.0	3.0	6.4
R in mm	772	480	3040
λ	0.134	0.226	0.779
k_0	12.75	7.67	2.09
γ in degrees	135	173	169

In recent years, theoretical and experimental research on the influence of the connected straight pipes has been carried out in various other places as well. An overview of those investigations is given by Thomson and Spence in [3.14]. The theoretical work relates to calculations in which the variation of u along the bend has been included in the derivations. Finite element analyses have also been performed.
Comparison of these theoretical results and the test results reported in this research and elsewhere with the approximate formulae given above reveals reasonably good agreement. In the range of values which is of interest with reference to buried steel pipelines the differences are not more than about ± 10 per cent and are of the same order of magnitude as the scatter in the test results.

Influence of ovalization on M

When pipe bends are subjected to bending, ovalization will occur, as is proven theoretically and can be demonstrated with the aid of the equilibrium model with ovalization forces f presented in Section 6.1.2.1 The forces dg acting in the wall have components df which have an effect similar to that of external earth pressure Q (see Fig. 7.2-2). With straight pipes the ovalization due to earth pressure is proportional to r^3. If the horizontal diameter increases by an amount $2w_h$, the resistance to ovalization will change by

$$f_1 = \left(\frac{r + w_h}{r}\right)^3 \tag{7.2-47}$$

For bends there is a linear relation between ovalization and the additional curvature. Hence it is most appropriate to take account of the effect of ovalization on the flexural stiffness of the bend by means of the factor f_1 as expressed by (7.2-47).

Furthermore, ovalization affects the moment of inertia of the bend. A factor f_2 applies to straight pipes:

$$f_2 = \left(\frac{r - w_v}{r}\right)^{1.5} \tag{7.2-48}$$

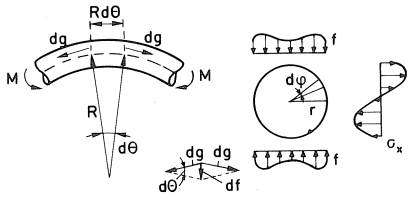

Fig. 7.2-2. Ovalization forces and stress distribution in the longitudinal direction.

This factor is assumed to be applicable also to bends, while w_v in (7.2-48) is replaced by $-w_h$ for sake of simplicity, so that the overall effect of ovalization on flexural stiffness is given by:

$$EI_{bo}(:) f_3 = \left(\frac{r + w_h}{r}\right)^{4.5} \tag{7.2-49}$$

7.2.4 Ovalization-curvature diagram

The relationship between u and w is:

$$w = \frac{du}{d\varphi}$$

so that with (7.2-11) it follows that:

$$w = 2a_2 \cos 2\varphi + 4a_4 \cos 4\varphi \tag{7.2-50}$$

Taking account of the influence of the change in curvature and the change in the angle of the bend (see Section 7.2.3), it follows with (7.2-35) and (7.2-36) that:

$$w = -\frac{6G_p \cos 2\varphi + 30 \cos 4\varphi}{D_p G_p - 6.25} \left\{ \frac{r\eta}{k_p} - \frac{1.5 G_p}{C_p G_p - 6.25} \left(A + \frac{5}{2} \frac{B}{G_p} \right) + \frac{A}{3} + \frac{B}{G_p} \right\} \cdot f_w \qquad (7.2\text{-}51)$$

The values adopted for f_w are:
- for the middle of the bend:

$$f_w = f_{wm} = \left(\frac{k_p}{k_p'} \right)^{0.25} \qquad (7.2\text{-}52)$$

- and for the edges:

$$f_w = f_{wr} = 0.75 \frac{k_p}{k_p'} \quad \text{with} \quad f_{wr} \geq 1.0 \qquad (7.2\text{-}53)$$

The influences mentioned in Section 7.2.3 which are of importance here have been taken into account in (7.2-51) as follows:

Influence of the change in curvature on w
This influence is taken into account in the same way as in Section 7.2.3, namely, by replacing the radius R of the bend by R' from (7.2-39) in the formulae for C_p, D_p, G_p, A and B.

Influence of the connected straight pipes on w
The connected straight pipes are virtually without effect on the relationship between the deformation parameters w and η, except that the ovalization in the middle of the bend will be greater than at the edges. This is shown in Fig. 7.2-3.

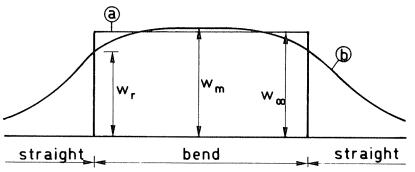

Fig. 7.2-3. Distribution of the ovalization along the bend and the connected straight pipes.
a = if no connected straight pipes were present
b = with connected straight pipes
w_∞ = ovalization in situation "a" according to (7.2-51), with $f_w = 1.0$
w_m = max. ovalization in situation "b", with $f_w = f_{wm}$
w_r = ovalization at the edge of the bend in situation "b", with $f_w = f_{wr}$.

7.2.5 Strain in longitudinal direction ε_x

In [2.3] the strain due to bending and earth pressure was found to be:

$$\varepsilon_{xb} = \frac{1}{R'} \{r\eta \sin \varphi + (2a_2 + 20a_4) \sin^3 \varphi - 24a_4 \sin^5 \varphi\} \tag{7.2-54}$$

In addition there is the strain due to the pressure P. If it is assumed that the pipe is longitudinally unrestrained, then with $\nu = 0.3$ we get:

$$\varepsilon_{xp} = \frac{1}{E}\left(\frac{Pr}{2t} - \nu \frac{Pr}{t}\right) = 0.2 \frac{Pr}{t} \tag{7.2-55}$$

so that:

$$\varepsilon_x = \varepsilon_{xb} + \varepsilon_{xp} \tag{7.2-56}$$

The values of φ for which ε_{xb} attains a maximum can be found by differentiation of (7.2-54) with respect to φ or, more simply, by the application of a numerical procedure whereby ε_{xb} is calculated for any value between 0 and $\pi/2$.
The influences mentioned in Section 7.2.3 which are of importance in the present context are the change in curvature and the influence of the connected straight pipes. These influences can be taken into account by replacing in the relevant formulae for C_p, D_p, etc. the radius R by R' according to (7.2-39) and the factor k_p by k_p' according to (7.2-40).

7.2.6 Strain in circumferential direction ε_y

In [2.3] the strain due to bending and earth pressure was found to be:

$$\varepsilon_{yb} = \pm \frac{3t}{r^2} (-a_2 \cos 2\varphi - 10a_4 \cos 4\varphi) \tag{7.2-57}$$

In addition there is the strain due to the pressure P. With the same assumption as in Section 7.2.5, we get for the inside of the bend:

$$\varepsilon_{yp} = \frac{1}{E}\left(\frac{Pr}{t} - \nu \frac{Pr}{2t}\right) \cdot \frac{R - r/3}{R - r} = 0.85 \frac{Pr}{Et} \cdot \frac{R - r/3}{R - r} \tag{7.2-58}$$

and for the outside of the bend:

$$\varepsilon_{yp} = \frac{1}{E}\left(\frac{Pr}{t} - \nu \frac{Pr}{2t}\right) \cdot \frac{R + r/3}{R + r} = 0.85 \frac{Pr}{Et} \cdot \frac{R + r/3}{R + r} \tag{7.2-59}$$

so that:

$$\varepsilon_y = \varepsilon_{yb} + \varepsilon_{yp} \tag{7.2-60}$$

The values of φ for which ε_{yb} attains a maximum can be found by differentiation of (7.2-57) with respect to φ:

$$\frac{d\varepsilon_{yb}}{d\varphi} = 0 = 2a_2 \sin 2\varphi + 20a_4 \sin 4\varphi \tag{7.2-61}$$

The following solutions are obtained:

$$\varphi_1 = 0 \text{ and } \pi \tag{7.2-62}$$

$$\varphi_2 = \frac{\pi}{2} \text{ and } \frac{3\pi}{2} \tag{7.2-63}$$

$$\varphi_3 = 0.5 \arccos \frac{-a_2}{40a_4} = 0.5 \arccos \frac{-G_p}{100} \tag{7.2-64}$$

The solution φ_3 is possible only if $G_p \leqslant 100$. Otherwise the maxima occur only for φ_1 and φ_2.
With (7.2-35) and (7.2-36), and taking account of the influences mentioned in Section 7.2.3, the following expression for ε_{yb} is obtained:

$$\varepsilon_{yb} = \pm \frac{3t}{r^2} \cdot \frac{f_8 f_w}{D_p G_p - 6.25} \left\{ \frac{r\eta}{k_p} - \frac{1.5 G_p}{C_p G_p - 6.25} \left(A + \frac{5}{2} \frac{B}{G_p} \right) + \frac{A}{3} + \frac{B}{G_p} \right\} \tag{7.2-65}$$

where:

$$f_8 = -3G_p \cos 2\varphi - 75 \cos 4\varphi \tag{7.2-66}$$

The factor f_w can be obtained from (7.2-52) and (7.2-53).
The various maxima of ε_{yb} (namely, ε_{ybm}) are determined by substitution of the correct value of f_8 into (7.2-65):

- for $\varphi_1 = 0$ and $\pi \rightarrow f_8 = -3G_p - 75$ (7.2-67)

- for $\varphi_2 = \frac{\pi}{2}$ and $\frac{3\pi}{2} \rightarrow f_8 = +3G_p - 75$ (7.2-68)

- for $\varphi_3 = 0.5 \arccos \frac{-G_p}{100} \rightarrow f_8 = \frac{3G_p^2 + 15000}{200}$ (7.2-69)

Here again R' according to (7.2-39) is introduced into the expressions for C_p, D_p, etc. The influence of the variation of the ovalization along the bend due to the connected straights is taken into account by means of f_w.

7.3 *Maximum moment in the plastic range*

7.3.1 Mechanisms

According to plastic theory, it is permissible to choose the most favourable possible stress distribution for determining the maximum plastic moment, provided that:
- the conditions of equilibrium are satisfied;
- the conditions of yielding are satisfied, e.g., the Von Mises criterion;

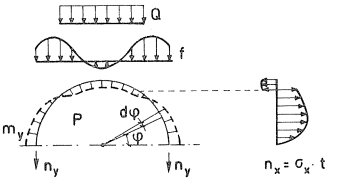

Fig. 7.3-1. Plate forces due to Q, P and M.

- the chosen stress distribution is in reasonably good agreement with the strains and deformations that occur.

Fig. 7.3-1 shows a possible distribution of the longitudinal stresses, the "ovalization forces" f already dealt with, the earth pressure Q and the bending moment distribution in the circumferential direction.

In Chapter 6 the maximum plate force in the longitudinal direction in the presence of a bending moment m_y and a normal force n_y has been calculated:

$$n_x = 0.5 \left(n_y \pm n_p \sqrt{4 - 3 \left(\frac{n_y}{n_p} \right)^2 - 2\sqrt{3} \left| \frac{m_y}{m_p} \right|} \right) \tag{7.3-1}$$

The ovalization forces f are dependent on the radius of curvature of the bend and on n_x, while m_y in turn is dependent on f and thus also on n_x. This interdependence is the reason why it is no simple matter to find an optimum stress distribution. To overcome the difficulty, an approximate method has been established. The results obtained in this way are found to be in good agreement with the test results.

The starting point of the approximate method is that there exist two mechanisms which determine the magnitude of the maximum moment in the bend. These mechanisms are:

a. The occurrence of *plastic hinges in the circumferential direction:* This will be the governing mechanism if the bend is sharply curved (low value of λ), the internal pressure has a low value and the earth pressure is large and causes ovalization in the same direction to the bending moment.
b. The occurrence of *yielding in the longitudinal direction:* This will be the governing mechanism if the bend is less sharply curved (high value of λ), the internal pressure has a high value and the earth pressure is large and causes ovalization in the opposite direction to the bending moment. It ties up with the design rules for straight pipes given in Chapter 6.

Design rules for both these mechanisms are derived and presented in Sections 7.3.2 and 7.3.3.

7.3.2 Maximum moment M_{pbo} determined by plastic hinges in the circumferential direction

7.3.2.1 Fundamental points

In Section 7.2 the formulae have been derived with which the longitudinal stresses σ_x

and the bending moments m_y in the pipe wall can be calculated. With increasing load the moments m_y will increase until m_e is attained at the maxima. With further load increase the value m_p will finally be attained, resulting in the formation of a plastic hinge. If a sufficient number of plastic hinges in the circumferential direction have been formed, a mechanism develops. The bending moment and the earth pressure acting on the pipe bend can then undergo no further increase. The following fundamental points are adopted in developing the procedure; explanatory comments are given after point e:

a. For calculating the maximum bending moments m_y in the wall of the pipe in the circumferential direction the formulae given in Section 7.2 may be used.
b. The places where the moments m_y have their maxima in the plastic range are the same as those in the elastic range.
c. The maximum load on the bend is attained when the plastic moment has developed in at least four places around the circumference of the pipe wall.
d. The longitudinal stresses σ_x will so adjust themselves that they are zero at the plastic hinges.
e. As in the preceding section, formulae in which two terms of the expansion in a series are used will be derived here. The BOCHT computer program makes use of the general solution [2.3].

The fundamental points mentioned in a. and b. mean that in the case of this mechanism the distribution of the stresses in the longitudinal direction in the plastic range is not significantly different from those in the elastic range. In the elastic range the stresses σ_x at those points where m_y has its maximum values are relatively small, so that the redistribution of the stresses envisaged in point d. is not very considerable. In fact point d. states the criterion relating to the two mechanisms mentioned in Section 7.3.1, because if the longitudinal stresses are of such magnitude that this redistribution cannot take place, it means that the second mechanism (mechanism b) will be the governing one. This can be checked by also calculating M_{pbo} in accordance with this mechanism b (Section 7.3.3). The lower of the two values should be taken into account.

7.3.2.2 Location of the plastic hinges

The plastic hinges will occur where the strain in the circumferential direction has its maximum values. In Section 7.2.6 it was shown that the maxima occur at:

$$\varphi_1 = 0 \text{ and } \pi \tag{7.3-2}$$

$$\varphi_2 = \frac{\pi}{2} \text{ and } \frac{3\pi}{2} \tag{7.3-3}$$

If $G_p < 100$, a maximum also occurs at:

$$\varphi_3 = 0.5 \arccos \frac{-G_p}{100} \tag{7.3-4}$$

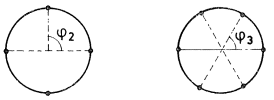

Fig. 7.3-2. Plastic hinges: (a) for $G_p > 100$; (b) for $G_p < 100$.

In this last-mentioned case the maximum strain ε_{ybm} for φ_2 is smaller than ε_{ybm} for φ_3. The foregoing means that if $a_4 < a_2/40$ or $G_p > 100$, the pattern of plastic hinges develops as shown in Fig. 7.3-2a; otherwise it develops as shown in Fig. 7.3-2b.

7.3.2.3 Maximum moment M_{pbo} for $P = P_l - P_u = 0$

The maximum bending moment M_{pbo} occurs when a sufficient number of plastic hinges have been formed. This means that the sum of the absolute values of m_y for $\varphi_1 = 0$ and φ_2 or φ_3 must be equal to twice the plastic moment $= 2 \times 1.15 m_p = 2.3 m_p$.
First, m_y will now be calculated:
With (7.2-57), (7.2-24) and (7.2-25) the following expression can be written for the strains $\varepsilon_{yb}(P=0)$:

$$\varepsilon_{yb} = \pm \frac{3t}{r^2} \cdot \frac{3G_0 \cos 2\varphi + 75 \cos 4\varphi}{D_0 G_0 - 6.25} \left(\frac{MRr}{EI} + \frac{A}{3} + \frac{B}{G_0} \right) \tag{7.3-5}$$

With due regard to the influences mentioned in Section 7.2.3, the maximum values of m_y are found to be:

$$m_y = f_4 \frac{Et^3}{2r^2} \cdot \frac{f_8}{D_0 G_0 - 6.25} \left(\frac{1}{f_5 f_6} \cdot \frac{MR'' r}{EI} + \frac{A}{3} + \frac{B}{G_0} \right) \tag{7.3-6}$$

where:

f_8 = factor according to (7.2-67) or (7.2-68) or (7.2-69)

$$f_4 = 1 - \frac{w_h}{r} \tag{7.3-7}$$

$$f_5 = 1 - \frac{2w_v}{3r} \tag{7.3-8}$$

$$f_6 = \frac{k_p}{k_p'} \left(\text{with } P = 0 \rightarrow f_6 = \frac{k_0}{k_0'} \right) \tag{7.3-9}$$

The following explanatory comments are offered to show how the influences envisaged in Section 7.2.3 have been taken into account:

Influence of the change in curvature
As shown by the tests, the plastic zones occur chiefly on the compression side of the bend. The greatest additional curvatures occur there. In connection with this, the modified radius R'' is employed in the plastic range (see Fig. 7.3-3).

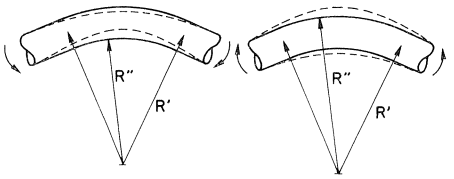

Fig. 7.3-3. Radius of the bend R'' to be taken into account in the case of bending in the plastic range.

For positive bending:

$$R'' = R' - r \tag{7.3-10}$$

For negative bending:

$$R'' = R' + r \tag{7.3-11}$$

R'' according to (7.3-10) or (7.3-11) should be used for calculating C_0, D_0, G_0, etc.

Influence of the connected straight pipes
Part of the ovalization forces will be transmitted by shell action via the connected straights. This is similar to the situation in the elastic range, where a reduced flexural stiffness factor k' was introduced. To take account of the strengthening effect of the straight pipes, the plastic moment is increased by the factor f_6 according to (7.3-9).

Influence of ovalization
In consequence of ovalization, for equal bending moment and imposed load on the bend, the moments in the pipe wall are increased by the factor f_4 according to (7.3-7). Furthermore, ovalization will cause the section modulus of the cross-section to decrease by the factor f_5 according to (7.3-8).

The maximum bending moment is attained when the sum of the absolute values of the maxima of m_y is equal to $2.3m_p$. Two situations are to be distinguished with regard to this:

a. $a_4 < a_2/40$ or $G_0 > 100$, alternatively $\lambda > 0.37$
In this case the plastic hinges occur at $\varphi_1 = 0$ and π and at $\varphi_2 = \pi/2$ and $3\pi/2$. With the absolute values of (7.2-67) and (7.2-68) in (7.3-6) it follows that:

$$2.3m_p = f_4 \frac{Et^3}{2r^2} \cdot \frac{6G_0}{D_0G_0 - 6.25} \left(\frac{1}{f_5 f_6} \cdot \frac{MR''r}{EI} + \frac{A}{3} + \frac{B}{G_0} \right) \tag{7.3-12}$$

b. $a_4 > a_2/40$ or $G_0 < 100$, alternatively $\lambda < 0.37$
In this case the plastic hinges occur at $\varphi_1 = 0$ and π and at $\varphi_3 = 0.5 \arccos - G_0/100$. With the absolute values of (7.2-67) and (7.2-69) in (7.3-6) it follows that:

$$2.3m_p = f_4 \frac{Et^3}{2r^2} \cdot \frac{3G_0^2 + 600G_0 + 30000}{200(D_0G_0 - 6.25)} \left(\frac{1}{f_5 f_6} \cdot \frac{MR''r}{EI} + \frac{A}{3} + \frac{B}{G_0} \right) \tag{7.3-13}$$

On rewriting (7.3-12) and (7.3-13) the following formula is obtained for the maximum moment M_{pbo} for $P=0$:

$$M_{pbo}=f_5 f_6 \frac{EI}{R''r}\left\{\frac{D_0 G_0-6.25}{3G_0}\left(\frac{2.3m_p}{f_4}\cdot\frac{r^2}{Et^3}\cdot f_7\right)-\frac{A}{3}-\frac{B}{G_0}\right\} \tag{7.3-14}$$

where:

- for $a_4 \leqslant a_2/40$ or $G_0 \geqslant 100$, alternatively $\lambda \geqslant 0.37$:

$$f_7 = 1.0 \tag{7.3-15}$$

- for $a_4 > a_2/40$ or $G_0 < 100$, alternatively $\lambda < 0.37$:

$$f_7 = \frac{400G_0}{G_0^2+200G_0+10000} \tag{7.3-16}$$

7.3.2.4 Maximum moment M_{pbo} for $P \neq 0$

If the internal pressure is greater than the external pressure, the earth pressure and the ovalization forces f due to M are also resisted by the internal pressure acting additionally to bending of the pipe wall.
The average of the bending contributions for $\varphi=0$ and $\varphi=\pi/2$ will, on putting:

$$n_y \approx n_{yp} = Pr \tag{7.3-17}$$

be equal to:

$$m_{yp} = Pr\frac{|w_h|+|w_v|}{2} \tag{7.3-18}$$

The maximum value of m_y in the pipe wall ($=m_{pr}$) is found by putting $n_x=0.5n_y$ in (7.3-1):

$$4-3\left(\frac{n_y}{n_p}\right)^2-2\sqrt{3}\left|\frac{m_{pr}}{m_p}\right|=0 \tag{7.3-19}$$

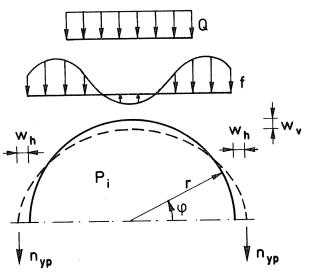

Fig. 7.3-4. In the case of an ovalized section the pressure makes a contribution to the load-carrying capacity with respect to f and Q.

so that:

$$m_{pr} = 1.15 m_p \left\{1 - 0.75 \left(\frac{n_y}{n_p}\right)^2\right\} \tag{7.3-20}$$

where:

$$n_p = t\sigma_e \tag{7.3-21}$$

$$m_p = 0.25 t^2 \sigma_e \tag{7.3-22}$$

The total "resistance" to ovalization is found to be:

$$m_{tot} = 1.15 m_p \left\{1 - 0.75 \left(\frac{Pr}{t\sigma_e}\right)^2\right\} + Pr \frac{|w_h| + |w_v|}{2} \tag{7.3-23}$$

The maximum bending moment acting on the bend can now be calculated by replacing in the formulae of Section 7.3.2.3 the term $2.3 m_p$ by $2 m_{tot}$, so that the following expression is obtained for the maximum moment, inclusive of the effect of the pressure:

$$M_{pbo} = f_5 f_6 \frac{EI}{R'' r} \left\{\frac{D_0 G_0 - 6.25}{3 G_0} \left(\frac{2 m_{tot}}{f_4} \cdot \frac{r^2}{E t^3} \cdot f_7\right) - \frac{A}{3} - \frac{B}{G_0}\right\} \tag{7.3-24}$$

where M_{pbo} denotes the maximum moment acting on the bend when the plastic hinges have fully developed. The transition from the elastic range to the fully plastic range will be considered in Section 7.4.

It is to be noted that for the calculation of a_2, a_4, D, G, etc. it is necessary to substitute $P = 0$ into the relevant formulae, the reason being that the extra loadbearing capacity due to P has here been incorporated in the formula for m_{tot}. If $P < 0$, i.e., if the external pressure exceeds the internal pressure, the second term of the formulae for m_{tot} becomes negative. This means that the pressure P then increases the ovalization and reduces the loadbearing capacity of the bend M_{pbo}.

The ovalization values w_h and w_v are calculated in Section 7.3.2.6.

According as the internal pressure is greater, M_{pbo} as expressed by (7.3-24) will likewise be greater. For this reason, for high values of P the second mechanism will in general be the governing one (i.e., yielding in the longitudinal direction: Section 7.3.3).

7.3.2.5 Influence of normal force, shear force and torsion

The part of the cross-section that is not utilized for bending, for earth pressure and for pressure P is available for the normal force, shear force and torsion.

If the normal force, shear force or torsion exceeds the resistance capacity of the part of the cross-section thus available, the bending moment will be reduced. In fact, the second mechanism will then occur (yielding in the longitudinal direction). This will be treated in Section 7.3.3, where the effect of the normal force, shear force and torsion are also taken into account.

In view of what has been said above, with respect to the mechanism "plastic hinges in the circumferential direction" it is not necessary to carry out a check on the effect of normal force, shear force and torsion.
Finally, it is to be noted that torsion is attended by bending outside the plane of the pipe bend. For further information on this the reader is referred to [2.3].

7.3.2.6 Ovalization of the cross-section

If the mechanism characterized by circumferential plastic hinges constitutes the governing condition, the stresses in the longitudinal direction will not yet, or not yet everywhere, have attained the yield point. Having regard to the mechanism in question, these longitudinal stresses cannot further increase, which means that, with increasing curvature of the bend, the longitudinal strains will undergo no, or hardly any, further change. The curvatures will then develop as a result of progressive further increase in ovalization.
According to [2.3], the relationship between the longitudinal strain and the ovalization is:

$$\varepsilon_{xb} = \frac{1}{R}\left(\eta r \sin\varphi - \frac{du}{d\varphi}\sin\varphi + u\cos\varphi\right) \tag{7.3-25}$$

For $\eta > \eta_e$ the strain ε_{xb} will be constant for $\varphi = 90°$. It then follows from (7.3-25) with $\varphi = 90°$:

$$\frac{du}{d\varphi} = (\eta - \eta_e)r \tag{7.3-26}$$

where $du/d\varphi$ is the additional ovalization δw_v, so that:

$$\delta w_v = (\eta - \eta_e)r \tag{7.3-27}$$

Taking account of the second order, it follows that:

$$\delta w_v = (\eta - \eta_e)(r - dw_v) \tag{7.3-28}$$

$$\boxed{\delta w_v = \frac{\eta - \eta_e}{1 + \eta - \eta_e} r} \tag{7.3-29}$$

The additional horizontal ovalization follows from the consideration that, after the plastic hinges have developed, the distribution of the moments in the pipe wall does not

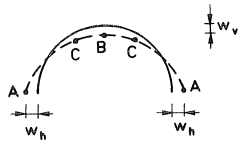

Fig. 7.3-5. Ovalizations w_v and w_h of the cross-section.

change when further ovalization occurs. This means that the distance between the plastic hinges remains unchanged. Besides being the case for AC, this will also very nearly be the case for AB. Hence it follows that (with the appropriate signs for δw_v and δw_h; in Fig. 7.3-5: w_v is positive and w_h is negative):

$$(r-\delta w_v)^2+(r-\delta w_h)^2=\text{constant}\simeq 2r^2$$

$$\delta w_h^2-2r\delta w_h-2r\delta w_v+\delta w_v^2=0$$

$$\boxed{\delta w_h=r-\sqrt{r^2+2r\delta w_v-\delta w_v^2}} \qquad (7.3\text{-}30)$$

7.3.2.7 Elastic-plastic range

Bending moment

The end of the elastic range is deemed to have been reached as soon as the bending moments in the circumferential direction anywhere attain m_e. The full plastic moment M_{pbo} is attained when a mechanism has developed.

In Fig. 7.3-6 the line m_{pbo} indicates the maximum moment when the mechanism described in the preceding sections has been developed. In reality this mechanism is formed gradually (the line M). This situation is analogous to that for straight pipes in Section 6.3.1.

In Fig. 7.3-6 it is assumed that the load Q was first applied and the bending moment then increased. Because "plastification" occurs here chiefly through bending of the wall of the pipe, it is an obvious choice to base the transition curve between M_e and M_{pbo} on that for a rectangular section.

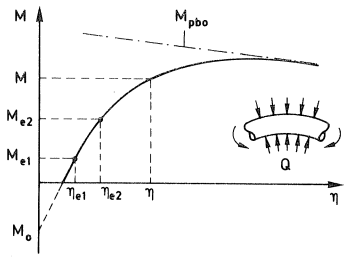

Fig. 7.3-6. Transition between the elastic range and the fully plastic situation on reaching M_{pbo}.

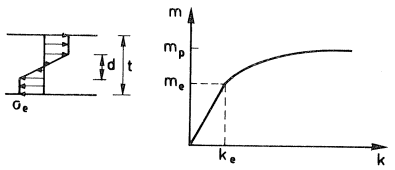

Fig. 7.3-7. Moment-curvature diagram for a rectangular section.

$$m = \tfrac{1}{4}t^2\sigma_e - \tfrac{1}{12}d^2\sigma_e$$

$$k = \frac{\sigma_e}{E}\cdot\frac{2}{d}$$

$$m_p = \tfrac{1}{4}t^2\sigma_e$$

$$m_e = \tfrac{1}{6}t^2\sigma_e$$

$$k_e = \frac{\sigma_e}{E}\cdot\frac{2}{t}$$

On eliminating d we obtain:

$$m = m_p - \frac{m_e}{c}\left(\frac{k_e}{k}\right)^c \tag{7.3-31}$$

where:

$$c = \frac{m_e}{m_p - m_e} \tag{7.3-32}$$

For the rectangular section: $c = 2$.
In analogy with this, the following procedure is followed for the elastic-plastic branch for the bending of the pipe bend:

$$c_1 = \frac{M_{e1} - M_0}{M_{pbo} - M_{e1}} \tag{7.3-33}$$

$$c_2 = \frac{M_{e2} - M_0}{M_{pbo} - M_{e2}} \tag{7.3-34}$$

$$M = M_{pbo} - 0.5\,\frac{M_{e1} - M_0}{c_1}\left(\frac{\eta_{e1}}{\eta}\right)^{c_1} - 0.5\,\frac{M_{e2} - M_0}{c_2}\left(\frac{\eta_{e2}}{\eta}\right)^{c_2} \tag{7.3-35}$$

where:

M_0 = the moment which develops when, on applying Q, the angular rotation is kept zero: see Fig. 7.3-6
M_{e1} = the moment at which the value m_e is first attained anywhere in the circumferential direction of the wall of the pipe; in general this occurs at $\varphi = 0$
M_{e2} = the moment at which the value m_e is attained in the circumferential direction for the second time
η_{e1} = the η associated with M_{e1}
η_{e2} = the η associated with M_{e2}
η = the value of η for which M is calculated

If M_{e1} exceeds $0.9M_{pbo}$, then, in order to avoid difficulties in the calculation process, M_{e1} is taken as equal to $0.9M_{pbo}$. The same applies to M_{e2}.

Ovalization

For the relation between the additional curvatures and ovalizations there will likewise be an elastic-plastic branch. For the type of bend considered here (mechanism "a") the elastic and the fully plastic branch for the ovalizations do not differ much from each other. This being so, it is proposed, with regard to the ovalizations after the attainment of M_{el} and η_{el} according to Fig. 7.3-6, to pass directly to the fully plastic branch (Section 7.3.2.6).

7.3.3 Maximum moment M_m determined by longitudinal yielding

7.3.3.1 Maximum moment

If the maximum moment is determined by yielding in the longitudinal direction (mechanism "b" in Section 7.3.1), the distribution of the ovalization forces f, the bending moments m_y and the longitudinal stresses σ_x will be approximately as shown in Fig. 7.3-8. The distributions of m_y and σ_x which occur in this case are substantially similar to those which occur in straight pipes.

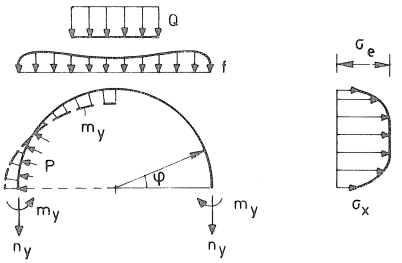

Fig. 7.3-8. Plate forces due to bending and due to pressure.

For this reason the method of analysis given in Chapter 6 will be used for determining the moment-curvature diagram and the relation between the additional curvature and the ovalization. The formulae presented in the preceding section can be used for the determination of m_y. Since the favourable effect of the initial curvature of the pipe on the strength and rigidity of the pipe wall have been taken into account in these last-mentioned formulae, they will give lower values for m_y than the formulae in Chapter 6. The relation between m_y and the maximum moment M_m calculated with the formulae of Chapter 6 is presented in Fig. 7.3-9, as is also the relation between m_y and M_{pbo} calculated with the formulae of Section 7.3.2.

For the value of m_y to be introduced into the calculation of M_m is adopted the average of the absolute values of m_y at the two extremes. In Fig. 7.3-8 these are the values of m_y for $\varphi = 0$ and $\varphi = \pi/2$.

The procedure for determining the correct moment M_{max} is as follows:

a. Calculate with the formulae of Section 7.3.2 the moment M_{pbo} (mechanism "a"). In Fig. 7.3-9 this is M_{pbo1}.

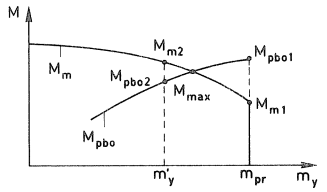

Fig. 7.3-9. Determination of the maximum moment if yielding in the longitudinal direction is the governing condition.

b. Calculate with the formulae of Chapter 6 for m_y = maximum the moment M_m (mechanism "b"). In Fig. 7.3-9 this is M_{m1}.
c. If M_{m1} is *greater* than M_{pbo1}, then mechanism "a" (plastic hinges) is the governing mechanism. The calculated value of M_{pbo1} is then the maximum moment that the bend can resist.
d. If M_{m1} is *smaller* than M_{pbo1}, then mechanism "b" (yielding in the longitudinal direction) is the governing mechanism.
   If m_y is chosen as having a smaller value than that for which M_{pbo1} and M_{m1} have been calculated, then M_{pbo1} decreases and M_m increases. The correct moment is located at the intersection of the lines for M_m and M_{pbo}. In Fig. 7.3-9 this moment is called M_{max}.

If longitudinal yielding is the governing condition, the strengthening effect of the connected straight pipes will be less than in the case where the occurrence of plastic hinges in the circumferential direction is the governing condition. In connection with this the factor f_6 applied in Section 7.3.2.3 for the calculation of M_{pbo} will be replaced by f_6' as expressed by:

$$f_6' = 1 + (f_6 - 1)\frac{m_y}{m_{pr}} \tag{7.3-36}$$

where:

$$m_{pr} = 1.15 m_p \left\{1 - 0.75\left(\frac{Pr}{t\sigma_e}\right)^2\right\} \tag{7.3-37}$$

7.3.3.2 Ovalization

If longitudinal yielding is the governing condition, the additional curvature will comprise two portions:

a. Increase in ovalization causes an increase in curvature, for which the same formulae as those in Section 7.3.2.6 are valid.
b. Longitudinal yielding produces longitudinal strains and therefore also causes a change in curvature, which can be calculated with the aid of the formulae given for straight pipes in Chapter 6.

The above considerations can be expressed as follows:

$$\delta K_{tot} = \delta K_0 + \delta K_v \tag{7.3-38}$$

where:

δK_{tot} = total increase in curvature in the deformation step concerned
δK_0 = increase in curvature due to ovalization
δK_v = increase in curvature due to longitudinal yielding

Longitudinal yielding produces a change in the curvature and also a change in the ovalization of the pipe (see formula (6.2-30) in Section 6.2):

$$\delta w_v = -\frac{r^3}{t} \cdot 2\psi_m \cdot \delta K_v \tag{7.3-39}$$

where:

δw_v = change in ovalization due to longitudinal yielding
ψ_m = slope of the yield surface

The ovalization δw_v at its turn produces an increase in the curvature of the pipe (see point a above). With the formulae of Section 7.3.2.6 it follows that:

$$\delta w_v = \delta\eta\,(r - w_v) \tag{7.3-40}$$

$$\delta\eta = R'' \cdot \delta K_0 \tag{7.3-41}$$

From (7.3-39), (7.3-40) and (7.3-41):

$$\frac{r^3}{t} \cdot 2\psi_m \cdot \delta K_v + R''(r - w_v)\delta K_0 = 0 \tag{7.3-42}$$

With (7.3-38) is obtained:

$$\delta K_0 = \frac{2\dfrac{r^3}{t}\psi_m \cdot \delta K_{tot}}{2\dfrac{r^3}{t}\psi_m - R''(r - w_v)} \tag{7.3-43}$$

$$\delta w_v = \delta K_0 \cdot R''(r - w_v) \tag{7.3-44}$$

The increase in the horizontal ovalization can be calculated with (7.3-30) given in Section 7.3.2.6.
If internal pressure is acting, with increasing ovalization more and more of the earth pressure and ovalization forces will be supported by the internal pressure: cf. Section 6.4. This means that the contribution made by the pipe wall becomes smaller and smaller, finally diminishing to zero. At that instant the bending moment acting on the bend is equal to M_m for $m_y = 0$ (Fig. 7.3-9). When $m_y = 0$ the equilibrium condition (6.4-1) determines the magnitude of the ovalization (see Section 6.4). For the average of absolute values of m_y due to bending (m_{yk}) and earth pressure (m_{yq}) we obtain with (7.3-6), (7.2-67) and the governing formula (7.2-68):

$$m_{yk}+m_{yq}=\frac{Et^3}{2r^2}\cdot\frac{-3G_0}{D_0G_0-6.25}\left(\frac{1}{f_5f_6'}\cdot\frac{MR''r}{EI}+\frac{A}{3}+\frac{B}{G_0}\right)\cdot f_4 \tag{7.3-45}$$

The contribution due to the pressure P is:

$$m_{yp}=-Pwr \tag{7.3-46}$$

With (6.4-1), (7.3-45) and (7.3-46) and because $m_y=0$ the value of f_6' according to (7.3-36) is equal to 1, we obtain for the average value of the ovalization:

$$w=\frac{Et^3}{2Pr^3}\cdot\frac{3G_0}{D_0G_0-6.25}\left(\frac{1}{f_5}\cdot\frac{MR''r}{EI}+\frac{A}{3}+\frac{B}{G_0}\right)\cdot f_4 \tag{7.3-47}$$

In this situation w_v and w_h will not differ much from each other; they will therefore be taken as equal, except for the algebraic sign.
Since ψ_m is dependent on m_y, it is necessary to perform the calculations step by step - up to and including (7.3-44) - so long as m_y has not yet become zero. After each δK_{tot} the increase in ovalization should be calculated, then the new value of m_y and the new value of ψ_m.
The computational model described here has been incorporated in the BOCHT computer program [2.3].

7.4 *Variations in the pressure P*

In an ovalized bend of a pipe there will occur variations in the bending moment, the curvature and the ovalization when variations occur in the pressure. Two extreme situations are to be distinguished in connection with this:

a. The pipe bend is subjected to bending into the plastic range while the internal pressure $P_i=0$. The pressure is then raised.
b. The pipe bend is subjected to bending into the plastic range while the internal pressure is equal to the maximum working pressure. The pressure is then reduced.

In the first situation the ovalization at the commencement of the pressure variations will in general be considerably greater than in the second situation. In fact, the first situation implies that during a substantial part of the envisaged service period the pressure is zero and subsequently alternates between zero and the working pressure, while the settlements undergo no further increase. But if the settlements do increase while the pressure is acting, the stresses and strains will, after some further settlements, be so redistributed that the maximum resistance to the imposed flexural deformation is developed. This means that then the second situation, as envisaged in point (b), is reached.
In view of what has been said above, in fact only the second situation is of importance with regard to the limit states "alternate yielding" and "fatigue". For calculating the effect of the pressure variations it is presupposed in the TGSL guidelines [2.1] that throughout the envisaged service period the pressure is constantly equal to the average

working pressure (= 0.5 times the maximum working pressure). The forces and deformations to which the bend is subjected are calculated for this pressure, and on the basis of this is then calculated the effect of varying the pressure.
Suppose that for a certain value of the angular rotation of the bend the pressure is changed (by and amount ΔP). Then changes will also occur in the magnitude of the moment (by ΔM), the angular rotation (by $\Delta\eta$), the ovalization (by Δw) and the earth pressure (by ΔQ). The extent to which these changes occur depends not only on the properties of the pipe bend itself but also on, among other factors, the rigidity of the surrounding soil and the rigidity of the connected straight pipes.
The relation between M, η, P and w is indicated qualitatively in Figs. 7.4.-1 and 7.4-2. It is to be noted that, at the first change in pressure for a certain angular rotation, in general yielding will occur, in which case the stresses and strains will so adjust themselves that further pressure variations will, for the same differences in settlement, occur in the elastic range (provided that the conditions as to alternate yielding and of course also the equilibrium conditions are satisfied).

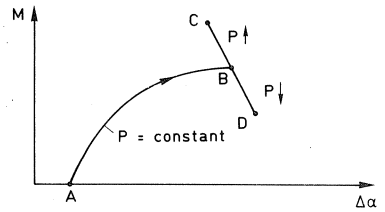

Fig. 7.4-1. Moment-angular rotation diagram for variation of the pressure (qualitative).

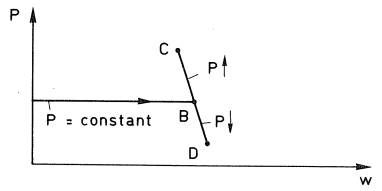

Fig. 7.4-2. Pressure-ovalization diagram for variation of the pressure (qualitative).

Because the relation between M, η, P and w is also dependent on the rigidity of the soil and of the connected straight pipes, the anaysis is rather complicated. For this reason it is stated in the TGSL guidelines [2.1] that we may confine ourselves to analysing the following two situations:

- The bending moment does not change during the variation of the pressure (load-controlled situation).
- The curvature does not change during the variation of the pressure (deformation-controlled situation).

7.4.1 Calculation of ΔM, $\Delta\eta$, Δw due to ΔP

Elastic branches BC and BD in Figs. 7.4-1 and 7.4-2

For this calculation the load exerted by P on an ovalized section is conceived as replaced by a load due to an equivalent earth pressure Q'_d with $\alpha = \beta = 180°$.

In Fig. 7.4-3a the load due to the pressure on an ovalized section is indicated. It produces moments in the pipe wall which are equal to:

$$m_{yp} = -n_{yp} w \tag{7.4-1}$$

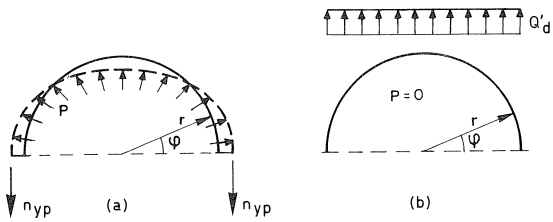

Fig. 7.4-3. Calculation of an equivalent earth pressure Q'_d for an ovalized section loaded by pressure $P = P_i - P_u$.

Because the ovalization w is substantially described by a cos 2φ function, the distribution of the bending moment that occurs in consequence of ovalization is virtually similar to that occurring in consequence of a uniformly distributed load Q'_d with loading angle and bearing angle equal to 180° (Fig. 7.4-3b):

$$m_{yq} = 0.125 Q'_d r \cos 2\varphi \tag{7.4-2}$$

By equating m_{yp} to m_{yq} it follows from (7.4-1) and (7.4-2) that:

$$Q'_d = -\frac{8 n_{yp} w}{r \cos 2\varphi} \tag{7.4-3}$$

For n_{yp} and w we can write:

$$n_{yp} = Pr \tag{7.4-4}$$

$$w = w_{max} \cos 2\varphi \tag{7.4-5}$$

so that (7.4-3) becomes:

$$Q'_d = -8 P w_{max} = -8P(w_v - w_h)/2 \tag{7.4-6}$$

In this equation the average of w_v and w_h at the instant when the pressure is present is adopted for w_{max}. In the further derivation, w_{max} is designated as w for the sake of simplicity.

For $\alpha = \beta = 180°$ it follows for the constants A and B according to (7.2-18) and (7.2-19), taking account of the change in the radius of the bend due to the additional curvature, that:

$$A' = \frac{3 Q'_d (R')^2}{2rtE} = \frac{-12 P w (R')^2}{rtE} \tag{7.4-7}$$

$$B' = 0 \tag{7.4-8}$$

For the relationship between ΔM, $\Delta\eta$ and ΔP, taking account of the effect of the changing radius of curvature and of ovalization, we now obtain with (7.2-38):

$$\Delta M = \frac{EI}{R'}\left\{\frac{\Delta\eta}{k_0'} + \frac{1.5G_0}{C_0G_0 - 6.25}\left(\frac{12(R')^2}{r^2tE}\,\Delta P\, w_p - \frac{\Delta A}{r} - \frac{5}{2}\frac{\Delta B}{G_0 r}\right)\right\}\cdot f_3 \tag{7.4-9}$$

The quantities C, G and k' in this formula should be determined for $P = 0$ because the effect of the pressure has been separately taken into account.
The ovalization w_p in (7.4-9) is the ovalization associated with the eventual pressure P:

$$w_p = \frac{w_v - w_h}{2} \tag{7.4-10}$$

In the case of positive bending (reduction of the curvature radius) w_p should be taken as positive. ΔP is positive when the pressure increases. If the earth pressure increases then ΔA and ΔB are positive too.
The ovalization w_p is composed of the ovalization in the initial situation plus the additional ovalization Δw due to $\Delta\eta$ and ΔP. Making use of (7.2-35), taking account of the influences of Section 7.2.3 and of the fact that w_p is, according to (7.4-10), equal to twice a_2, it follows that:

$$\Delta w = 2\Delta a_2 = \frac{6G_0}{D_0G_0 - 6.25}\left\{\frac{r\Delta\eta}{k_0} - \frac{1.5G_0}{C_0G_0 - 6.25}\left(\frac{12(R')^2}{rtE}\,\Delta P w_p + \right.\right.$$

$$\left.\left. + \Delta A + \frac{5}{2}\frac{\Delta B}{G_0}\right) + \frac{4(R')^2}{rtE}\,\Delta P w_p + \frac{\Delta A}{3} + \frac{\Delta B}{G_0}\right\}\cdot f_w \tag{7.4-11}$$

The signs follow the same rules as those for the formula for ΔM. If the earth pressure remains unchanged, then $\Delta A = \Delta B = 0$. For the sake of simplicity, the value adopted for w_p in (7.4-11) is the value associated with the higher of the two pressures considered. For the same reason as in the case of the formula for ΔM, here C_0 and G_0 have likewise been adopted. Because it is the relation between the deformation parameters w and η with which we are here concerned, the flexural stiffness factor is introduced as k_0 and not k_0' as in the case of ΔM in (7.4-9).
For the change (Δm_y) of the average of m_y for $\varphi = 0$ and $\varphi = \pi/2$ it follows with (7.2-57) that:

$$\Delta m_y = \frac{Et^2}{6}\,\Delta\varepsilon_{yb} = \frac{Et^3}{2r^2}\,\Delta a_2 \tag{7.4-12}$$

With (7.4-12) we obtain:

$$\Delta m_y = \frac{Et^3}{4r^2}\,\Delta w \tag{7.4-13}$$

By adding Δm_y to the old m_y we obtain the new m_y. In the case of a rise in pressure the algebraic sign of Δm_y is negative, so that the new m_y is smaller than the old m_y. According to (7.3-37) the maximum m_y is m_{pr}:

$$m_{pr} = 1.15 m_p \left\{1 - 0.75 \left(\frac{Pr}{t\sigma_e}\right)^2\right\} \tag{7.4-14}$$

If $m_y > m_{pr}$, then yielding will occur; in that case m_{pr} should be introduced into the further calculation.
With m_y known, the maximum moment M_{max} can be calculated as indicated in Sections 7.3.2 and 7.3.3.
If the original moment increased by ΔM according to (7.4-9) is greater than M_{max}, then yielding will occur and the ovalization becomes less. ΔM according (7.4-9) will then be reduced. This is possible by adopting in (7.4-9) a smaller value of w of such magnitude that the original M increased by ΔM becomes just equal to M_{max}. This smaller value of w is the ovalization after yielding.

7.5 *Calculation of the strains - plastic*

7.5.1 Longitudinal direction

For the plastic range a distinction can be drawn between the two yield mechanisms of Section 7.3.1:

a. Occurrence of *plastic hinges* in the *circumferential* direction: With this mechanism the additional curvatures are made possible by further increase in ovalization. The strains in the longitudinal direction undergo no, or hardly any, change. For this reason the longitudinal strains can be determined from the "elastic" formulae given in Section 7.2.5.
b. Occurrence of *yielding* in the *longitudinal* direction: In this case the additional curvatures develop as a result of longitudinal yield *and* of ovalization. The additional curvature due to ovalization (δK_0) can be determined with (7.3-40) and (7.3-41):

$$\delta K_0 = \frac{\delta w_v}{R''(r - w_v)} \tag{7.5-1}$$

The additional curvature δK_v due to longitudinal yielding is found by subtracting δK_0 from the total additional curvature in the plastic range (δK_{tot}):

$$\delta K_v = \delta K_{tot} - \delta K_0 \tag{7.5-2}$$

The plastic strains caused by δK_v are:

$$\varepsilon_{xpl} \approx \delta K_v \cdot y \tag{7.5-3}$$

where y is the distance from the fibre under consideration to the neutral axis.
To the plastic strains the elastic strains according to Section 7.2.5 should be added.

7.5.2 Circumferential direction

A reasonable estimate can be obtained by following the same procedure as that described for straight pipes in Section 6.5.

7.6 *Experimental verification*

The design rules which had been established were incorporated in a computer program designated as BOCHT*, with which the tests performed were analysed.

7.6.1 Overview of tests performed

a. Bends ø 160–2.9 mm with $R = 480$ mm, $\sigma_e = 380$ N/mm^2, loaded by combinations of bending and internal pressure.
b. Bends ø 261–2.9 mm with $R = 772$ mm, $\sigma_e = 380$ N/mm^2, loaded by combinations of bending and internal pressure.
c. A bend ø 160–2.9 mm, $R = 480$ mm, $\alpha = 90°$, $\sigma_e = 380$ N/mm^2, loaded by out-of-plane bending and internal pressure.
d. A bend ø 322–6.4 mm, $R = 3040$ mm, $\sigma_e = 330$ N/mm^2, $\alpha = 90°$, loaded by earth pressure Q_d and bending.

It would be outside the scope of the present publication to include all the test results. Instead, only test 75 and the test referred to in point d, above, will be dealt with.

Table 7.6-1. Overview of the ø 160–2.9 mm pipe bends tested

No.	α degrees	P_i (bar)	$\frac{\sigma_{yp}}{\sigma_e}$	direction of bending (see sign conventions in Section 7.1)
70	30°	0	0	positive
71	30°	0	0	negative
72	60°	0	0	positive
73	60°	0	0	negative
74	30°	86	0.60	positive
75	30°	86	0.60	negative

Table 7.6-2. Overview of the ø 261–2.9 mm pipe bends tested

No.	α degrees	P_i (bar)	$\frac{\sigma_{yp}}{\sigma_e}$	direction of bending
81	30°	0	0	positive
82	30°	0	0	negative
83	60°	0	0	positive
84	60°	0	0	negative

* BOCHT is the Dutch word for a BEND.

7.6.2 Test 75

Photo 20 shows the test rig employed, with specimen 75, after the test had been completed. The bending action was produced by means of the two hydraulic cylinders seen on the left and right respectively (four-point bending). The change in curvature was measured with the aid of the displacement transducers mounted in the steel frames welded to the pipe bend. The change in the vertical diameter was measured with the dial gauges in the stirrup-type measuring devices ($\Delta D_v = 2w_v$). Because of the internal pressure (86 bar $\approx \sigma_{yp} = 0.6\sigma_e$) the maximum moment in the bend was so large that plastic deformations occurred also in the connected straight pipes (Photo 20).
The measured moment-angular rotation diagram for the bend is presented in Fig. 7.6-1. In the elastic range, bending tests were performed also for $P = 0, 29, 57, 86$ and 115 bar. The result calculated with the aid of the BOCHT computer program is also included in this diagram.
Fig. 7.6-2 gives the measured relationship between ΔD_v in the middle and the angular rotation along the bend. The result of the computer calculation is likewise included. To illustrate the effect of the pressure P, in Figs. 7.6-3 and 7.6-4 moment-angular

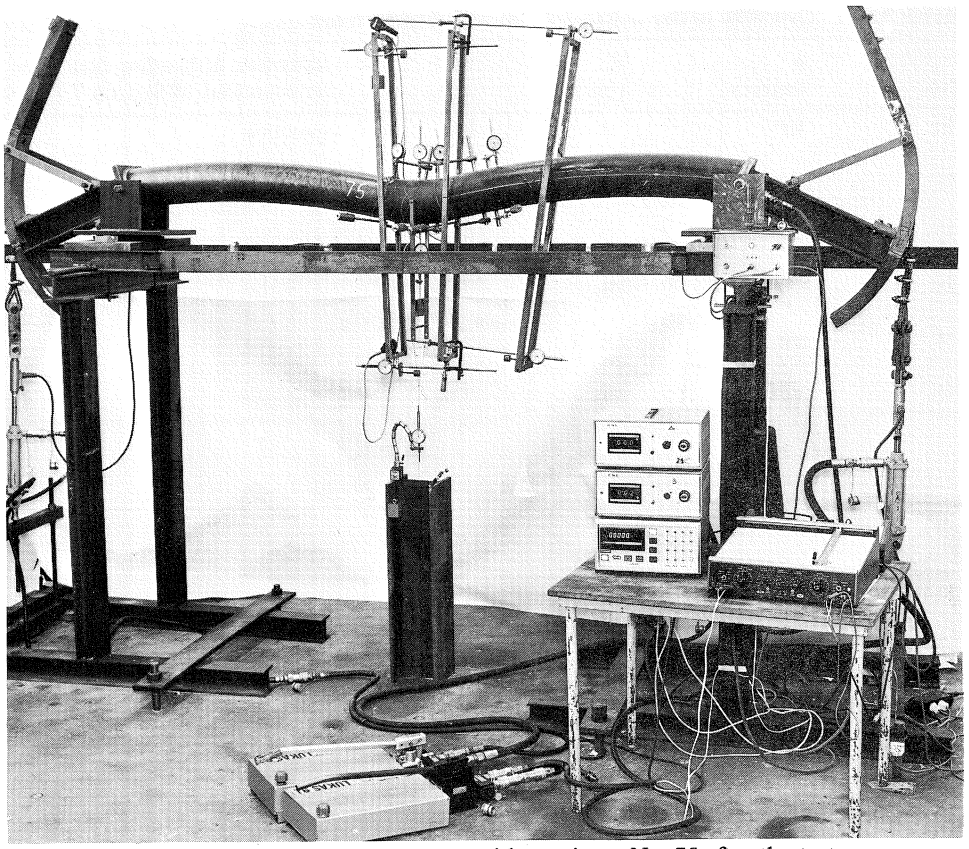

Photo 20. Testing arrangement with specimen No. 75 after the test.

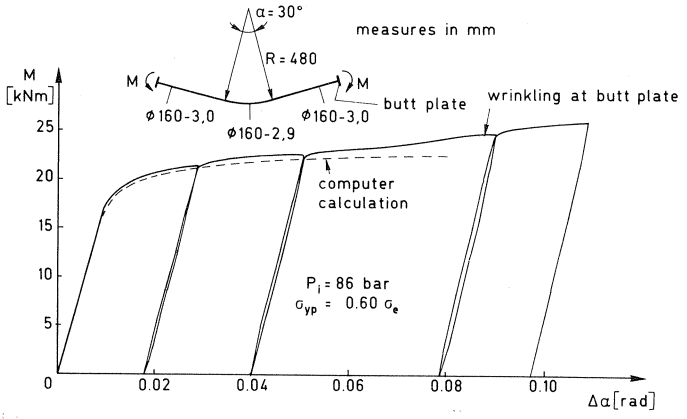

Fig. 7.6-1. Measured and calculated moment-angular rotation diagrams for test 75.

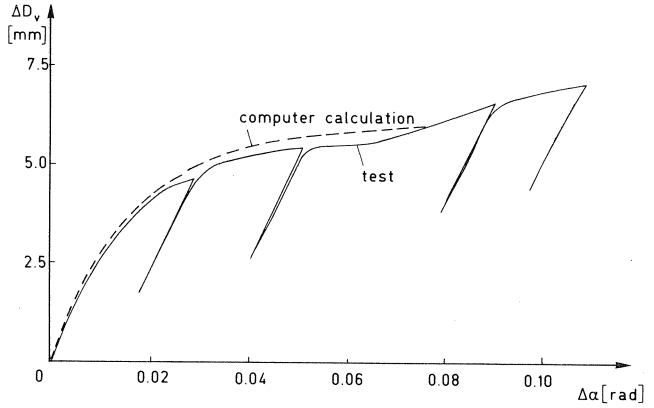

Fig. 7.6-2. Measured and calculated ovalization-angular rotation diagrams for test 75. ΔD_v is the change (increase) in diameter in the plane of bending in the middle of the bend.

rotation diagrams and ovalization-angular rotation diagrams for specimen 75 are given for $P = 0$, 29, 57, 86 and 115 bar. These give the following values for σ_{yp}/σ_e: 0, 0.2, 0.4, 0.6 and 0.8, respectively.

The symbols and abbreviations listed beside Figs. 7.6-3 and 7.6-4 have the following meanings:

DU	external diameter
T-BOCHT	wall thickness of the bend
T-RECHT	wall thickness of the connected straight pipes
R-BOCHT	radius of the bend
B.HOEK	angle of the bend α
SE	yield point
VERSTSP.	stress at the maximum calculated angular rotation ($\Delta\alpha$); in the calculation of M_{max} the maximum stress is taken between SE and VERSTSP., proportional to the angular rotation
P	pressure $= P_i - P_u$; the curve extending farthest relates to the input P
Q	earth pressure $= Q_d + Q_{eq}$

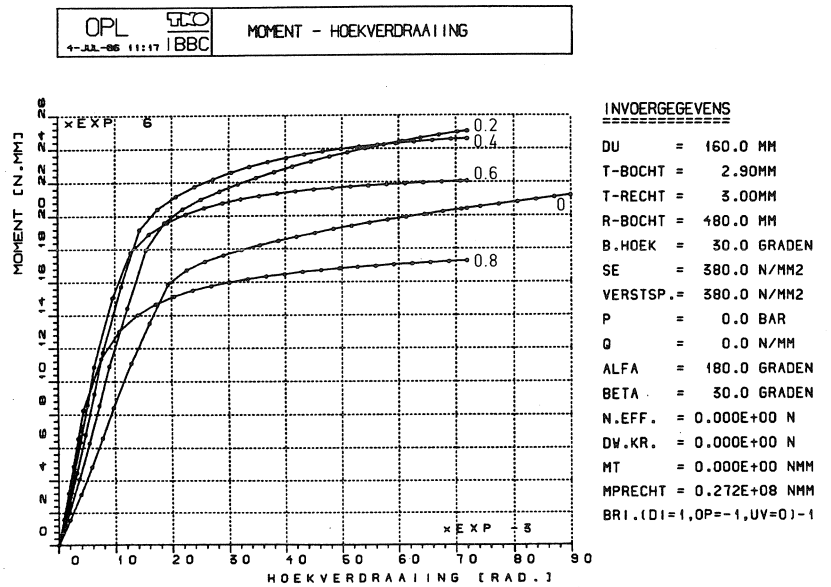

Fig. 7.6-3. Calculated moment-angular rotation diagrams for several values of σ_{yp}/σ_e.

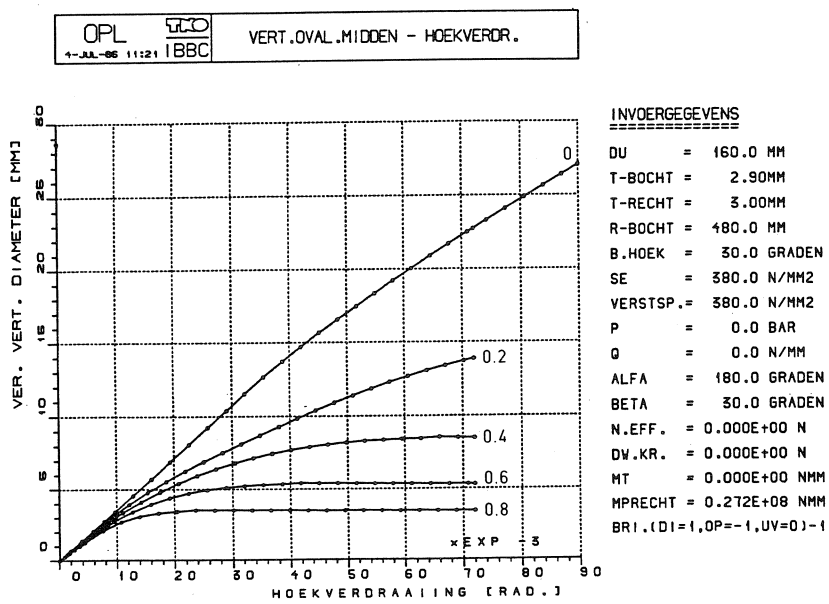

Fig. 7.6-4 Calculated relations between the change (increase) in diameter in the plane of bending in the middle of the bend (ΔD_v) and the angular rotation (Δa) for several values of σ_{yp}/σ_e.

ALFA, BETA	loading angle, bearing angle (α, β)
N.EFF.	effective normal force (Section 6.1.3)
DW.KR.	shear force
MT	torsional moment
MPRECHT	plastic moment of straight pipe with the same r, t and σ_e (MPRECHT $= 4r^2t\sigma_e$)
BRI	direction of bending: BRI $= 1$ when the bend tends to become more curved (DI); BRI $= -1$ when the bend tends to become less curved ("straightens out") (DU); BRI $= 0$ for out-of-plane bending (UV)

Further:

INVOERGEGEVENS	input data
MOMENT	moment
HOEKVERDRAAIING	angular rotation ($\Delta\alpha$)
VERT. OVAL. MIDDEN	change in vertical diameter ($\Delta D_v = \|2w_v\|$)
HOR. OVAL. MIDDEN	change in horizontal diameter ($\Delta D_h = \|2w_h\|$)

7.6.3 Test on bend ø322-6.4 mm

The test arrangement employed is shown in Photos 21 and 22. The "earth pressure" was applied by means of inflated rubber cushions. The loading angle and the bearing angle were 30°. The "earth pressure" Q_d was 49 N/mm. Figs. 7.6-5 and 7.6-6 show the measured moment-angular rotation diagram and the ΔD_h-angular rotation diagram. In analogy with Figs. 7.6-3 and 7.6-4 the computer results for $\sigma_{yp}/\sigma_e = 0$, 0.2, 0.4, 0.6 and 0.8 have likewise been included.

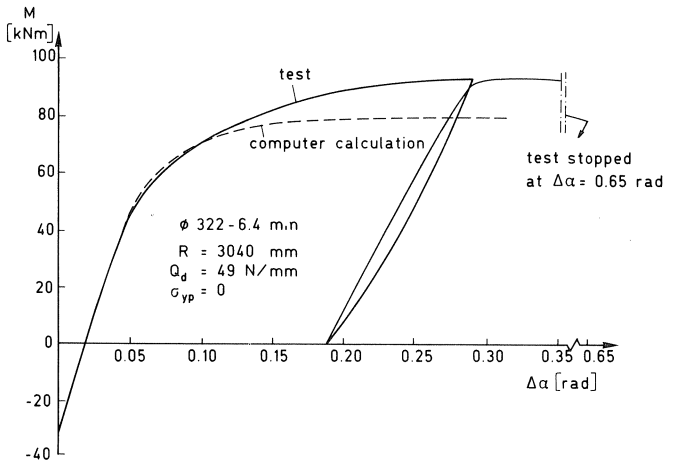

Fig. 7.6-5. Measured and calculated moment-angular rotation diagrams.

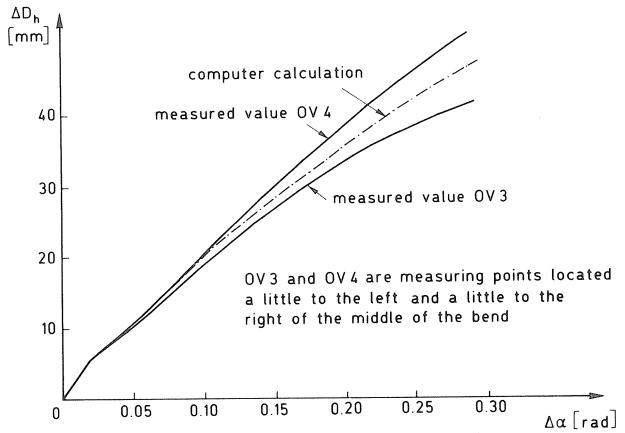

Fig. 7.6-6. Measured and calculated relations between the change (increase) in diameter perpendicular to the plane of bending (ΔD_h) and the angular rotation ($\Delta\alpha$).

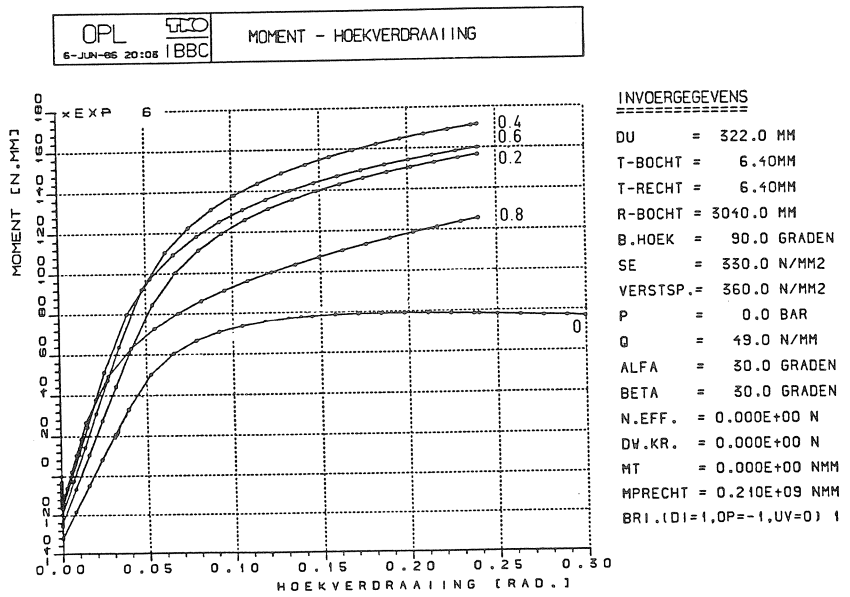

Fig. 7.6-7. Calculated moment-angular rotation diagrams for several values of σ_{yp}/σ_e.

The symbols and abbreviations listed beside Figs. 7.6-7 and 7.6-8 are explained in the preceding Section.

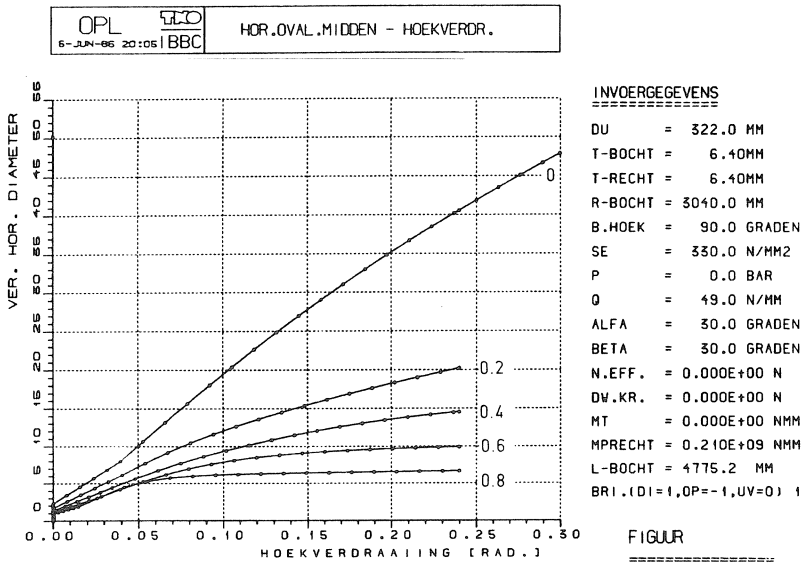

Fig. 7.6-8. Calculated relations between the change (increase) in diameter perpendicular to the plane of bending (ΔD_h) and the angular rotation ($\Delta\alpha$) for several values of σ_{yp}/σ_e.

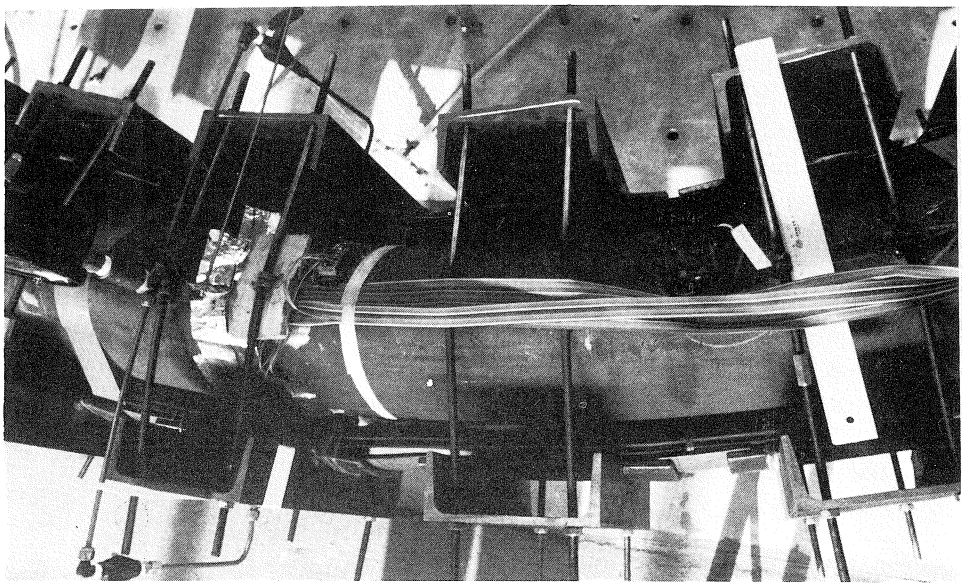

Photo 21. Test arrangement for "earth pressure" by means of inflated rubber cushions for the bend ⌀322-6.4 mm.

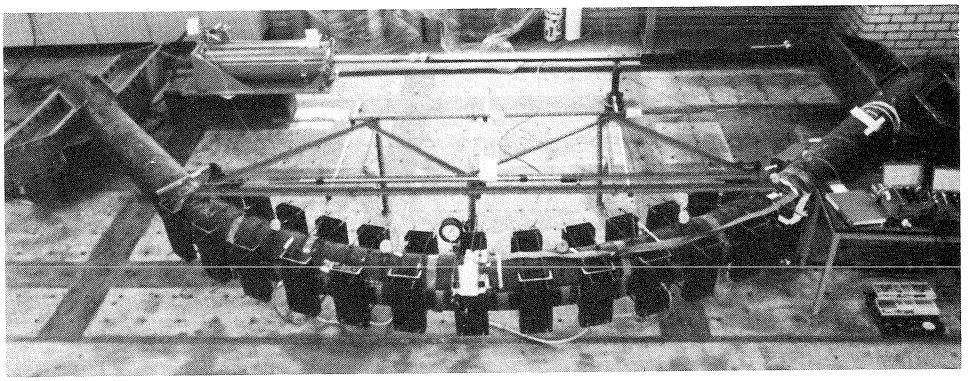

Photo 22. Overview of the test arrangement for "earth pressure" and bending for the bend ø 322-6.4 mm.

8 Practical application; conclusions

8.1 *Practical application*

The results of the research have provided the basis for the "Technical principles for the design of buried steel pipelines" (TGSL-1986) [2.1].
In order to promote acceptance thereof, the TGSL together with the associated reports have been submitted for approval to the "Technical Advisory Committee for Dykes and Flood Defences" (TAW), which was set up by the Netherlands Minister of Transport and Civil Engineering Works. After approval, the TAW will advise the Minister to publish the TGSL as an appendix to the Guidelines [1.1] and [1.2]*.
In anticipation thereof several existing pipeline crossings of the NV Nederlandse Gasunie have been analysed on the basis of the new method. These are crossings which do not satisfy the safety requirements of the present guidelines [1.1] and [1.2].
For performing the calculations, TNO-IBBC has added the required subroutines to DIANA. DIANA (DIsplacement ANAlysis) is an in-house general purpose finite element computer program.
Several of the pipeline crossings that have been re-analysed have turned out to be sufficiently safe just as they are. In the case of some others it has proved possible to attain the desired level of safety by making relatively minor adaptive changes such as partial excavation or the replacement of a small portion of the pipeline crossing. In this way the need for costly replacement schemes (costing between 1 and 2 million guilders per crossing) has been avoided in most cases.

* The TGSL and associated reports have been approved in January 1987 and will be published in June 1987.

8.2 *Conclusions*

To summarize, it can be stated that the research has resulted in a new method of design and analysis which gives a better insight into the actual strength and deformation properties than was possible with the old method. The principal consequences are:

a. *With regard to the properties and safety*
   - In many situations the actual strength and the actual deformation capacity are considerably greater than can be shown by an analysis based on elastic theory.
   - Thanks to the better insight obtained into the actual properties it is possible to attain a more uniform degree of safety. This has been made possible also because the various failure modes (limit states) have been investigated separately, and limit values have been established for them. For example, when the old method was employed, the buckling safety of thick-walled pipes was greater than that of thin-walled pipes. In the new method this is no longer the case.

b. *With regard to economy*
   The application of a new design method can yield substantial economic advantages, both in relation to existing pipeline crossings and to new ones yet to be built:
   - In situations where, with existing crossings, the differential settlement turns out to be greater than that on which the original design was based, or where in response to changes in safety philosophy greater safety margins are required than provided in the original design, in many cases the need for costly replacements can be avoided by re-analysing the pipeline crossings with the new method.
   - In the case of new crossings the better insight provided by the new method can lead to simpler forms of construction. For example, it may be possible to adopt a straight crossing instead of a "reclining arch": in Fig. 1-2, solution "a" instead of solution "b".

9 Summary

Loads acting on buried steel pipelines consist of combinations of internal liquid or gas pressure, earth pressure and temperature differences. Where differential settlements occur along the alignment of a pipeline, the latter is moreover subject to imposed deformations. This occurs more particularly at crossings with dykes, roads and railways. It means that, besides the strength (internal pressure, resistance to earth pressure), the deformation capacity is important.
Design methods based on elastic theory have long been used for pipelines. The actual behaviour up to failure cannot properly be described by those methods, however.
Research has led to the development of a new method of design and analysis based on plastic theory, which does provide a good insight into the actual strength and deformation properties and thus into the actual structural safety available. In many situations the actual strength and actual deformation capacity are found to be considerably greater than can be shown on the basis of an elastic analysis.

Also, greater uniformity in the safety of the pipeline can be attained as a result of a better understanding of the actual properties. This has been made possible partly also because the various modes of failure (limit states) have been investigated separately, and limit values have been established for them. For example, with the old method the buckling safety of thick-walled pipes turned out to be greater than that of thin-walled pipes. In the new method this is no longer the case.
This publication reports in detail on the research which has provided the basis for the "Technical principles for the design of buried steel pipelines" (TGSL) [2.1]. On applying the TGSL to some existing pipeline crossings which were no longer acceptable according to the conventional methods of analysis it was found in several cases that the pipeline in question was in fact sufficiently safe just as it was. As for some of the other pipelines that were re-analysed it emerged that the desired level of safety was attainable by making relatively minor adaptive changes (e.g., partial excavation), so that in most cases it proved unnecessary to have recourse to replacement.
For new pipeline crossings the better insight provided by the new method can lead to different and simpler forms of construction: for example, a straight crossing instead of a "reclining arch".

10 Acknowledgements

The author wishes to thank the "Steering Committee on Pipelines" ("Begeleidingscommissie Pijpleidingen") for their support in carrying out the research. More particularly he wishes to record his indebtedness to the Chairman, Prof. Ir. A. A. van Douwen, who from the outset contributed with his valuable advice to the content and results of the research.
The Steering Committee on Pipelines comprises representatives of the pipeline companies in the Netherlands who have financially supported the research, and further the Delft University of Technology, the Municipality of Rotterdam, the Technical Advisory Committee for Dykes and Flood Defences (TAW), the Government Authority for the Safety of Pressure Vessels (Dienst voor het Stoomwezen), and the TNO Institute for Building Materials and Structures (TNO-IBBC).
At the time of publication of this report the Steering Committee on Pipelines comprised the following members:

Prof. Ir. A. A. van Douwen, Chairman	- Delft University of Technology
Ir. A. M. Gresnigt, Secretary	- TNO-IBBC
Ir. M. J. G. Broekhoven	- Dienst voor het Stoomwezen
Ir. K. C. J. van den Ende	- Rijkswaterstaat (TAW)
Ir. H. de Groot	- Polder Board of Rijnland (TAW)
Ir. J. Hieter	- Water Supply Undertaking of The Hague (VEWIN)
Ing. C. Menzel	- VEG Gas Institute (VEGIN)
Ir. K. Noorlander	- Municipality of Rotterdam

Ir. P. H. A. Rietjens	- N.V. Nederlandse Gasunie (VELIN)
Ir. L. E. B. Saathof	- Rijkswaterstaat (TAW)
Ir. A. de Waal	- SIPM (VELIN)

VELIN = Association of Pipeline Owners in the Netherlands
VEWIN = Association of Water Supply Undertakings in the Netherlands
VEGIN = Association of Gas Supply Undertakings in the Netherlands
Rijkswaterstaat = Netherlands Government Civil Engineering Works Department

11 Notation*

A	cross-sectional area	mm^2
a, b	ovalization of straight pipes	mm
a_2, a_4	coefficients for in-plane bending of smooth bends	-
C_0, C_p	function of λ, and of λ and ψ, respectively (Section 7.2.2)	-
c_1, c_2	coefficients (Sections 6.1.2.2 and 6.1.5)	-
D_u	external diameter	mm
D	$D_u - t$	mm
D, D_p	shear force (Section 6.1.5)	N
D_0, D_p	function of λ, and of λ and ψ, respectively (Section 7.2.2)	-
ΔD_v	change in vertical diameter; the vertical diameter is the diameter in the plane of bending	mm
ΔD_h	change in horizontal diameter; the horizontal diameter is the diameter perpendicular to the plane of bending	mm
E	modulus of elasticity	N/mm^2
EI_{bo}	flexural stiffness of a bend	Nmm^2
EI_{rb}	flexural stiffness of straight pipe connected to a bend	Nmm^2
F	normal (or direct) force in pipeline	N
$f_1, f_2 \ldots f_8$	coefficients in the analysis of bends	-
f_{wm}, f_{wr}	factor for the ovalization in the middle and at the edges of a bend	-
G	shear modulus	N/mm^2
G_0, G_p	function of λ and ψ respectively (Section 7.2.2)	-
g	function of c_1 and c_2 (Section 6.1.5)	-
h	function of a and r (Section 6.1.5)	-
I	moment of inertia	mm^4
K	curvature due to bending	1/mm
k_0, k_p	flexural stiffness factor for $P=0$ and for P respectively	-
k_0', k_p'	reduced value of k_0 and k_p respectively, due to the effect of the connected straight pipes, the additional curvature and the ovalization	-

* Symbols not listed here are explained in the next where they first appear.

M	bending moment in the pipeline conceived as a beam	Nmm
M_m	maximum moment in a straight pipe (Section 6.1.5), or in a bend if longitudinal yielding is the governing mechanism (Section 7.3.3)	Nmm
M_p	plastic moment $M_p = 4r^2 t\sigma_e$	Nmm
M_{pbo}	maximum moment in a bend if the occurrence of plastic hinges in circumferential direction is the governing mechanism (Section 7.3.2)	Nmm
M_t	torsional moment	Nmm
m	plate moment per unit width	Nmm/mm
N	effective normal force in pipeline	N
n	plate normal force per unit width	N/mm
P	difference in pressure between inside and outside of pipeline $P = P_i - P_u$	N/mm^2
P_u	external pressure (liquid)	N/mm^2
P_i	internal pressure (liquid of gas)	N/mm^2
Q	earth pressure	N/mm
Q_d	directly transmitted earth pressure	N/mm
Q_i	indirectly transmitted earth pressure	N/mm
Q_{eq}	equivalent earth pressure	N/mm
q, q_1, q_2	earth pressure per unit area	N/mm^2
R	radius of a non-loaded bend	mm
R'	radius of a bend including additional curvature due to bending	mm
R''	radius of a bend including additional curvature and increased by r for negative bending or reduced by r for positive bending (Section 7.3.2.3)	mm
r	average (or mean) radius $r = D/2$	mm
r'	plate curvature of an ovalized pipeline (Section 4.4.2)	mm
t	pipe wall thickness	mm
t_r	wall thickness of straight pipe connected to bend	mm
t_b	wall thickness of bend	mm
u	displacement of an element of the pipe circumference along the circumference	mm
W	section modulus	mm^3
w	displacement of an element of the pipe circumference perpendicular to the circumference; ovalization in bends $(0.5\,\Delta D)$	mm
w_m	ovalization in the middle of a bend	mm
w_r	ovalization at transition from bend to straight pipe	mm
w_h, w_v	horizontal and vertical ovalization respectively (perpendicular to the plane of bending and in the plane of bending)	mm

α, β, γ	loading angle, bearing angle for Q_d and for Q_i and Q_{eq} respectively (Sections 6.1.2.1 and 7.1)	rad
α	angle of a smooth bend not flexurally loaded (Section 7.1)	rad
$\Delta\alpha$	change of α due to bending	rad
η	relative change of $\alpha \rightarrow \eta = \Delta\alpha/\alpha$	-
δ	displacement; small part of the quantity concerned	mm
ε	strain	-
θ	angular rotation due to torsion per unit length of pipe	rad/mm
λ	bend characteristic $\lambda = tR/r^2$	-
ν	Poisson's ratio	-
ϱ,ρ	radius of curvature due to bending of a straight pipe	mm
σ	stress	N/mm^2
σ_e	yield stress	N/mm^2
σ_t	tensile stress	N/mm^2
τ	shear stress	N/mm^2
τ_e	yield shear stress	N/mm^2
φ	angle; angular rotation	rad
ψ	bend characteristic $\psi = PR^2/Ert$	-
ψ	slope of yield surface	rad
Δ	change of the quantity concerned	-

Subscripts in so far as they are not already indicated above

e	end of elastic range
p	yield force of the quantity concerned
pr, pdtr	reduced value of yield force (Section 6.1)
pl	plastic part of the quantity concerned
cr	critical value associated with buckling
m, max	maximum value
x	in longitudinal direction
y	in circumferential direction
xm, xp, xk, xq	in longitudinal direction due to *M*, *P*, *K*, *Q*
ym, yp, yk, yq	in circumferential direction due to *M*, *P*, *K*, *Q*

12 References

12.1 *Design rules*

1.1* Technische Adviescommissie voor de Waterkeringen. Leidraad voor constructie en beheer van vloeistofleidingen in en nabij waterkeringen. Staatsuitgeverij, 's-Gravenhage (The Hague), 1971.

1.2* Technische Adviescommissie voor de Waterkeringen. Leidraad voor constructie en beheer van gasleidingen in en nabij waterkeringen. Staatsuitgeverij, 's-Gravenhage (The Hague), 1973.

1.3* Provinciale Waterstaat in Zuid-Holland. Pijpleidingcode 1972 (+ latere revisies). 's-Gravenhage (The Hague).

1.4* NEN 1091. Veiligheidseisen voor stalen gasleidingen met een bedrijfsdruk boven 1 bar, 1984.

1.5 Dienst voor het Stoomwezen. Regels voor toestellen onder druk / Rules for pressure vessels. Staatsuitgeverij, 's-Gravenhage (The Hague), 1973 + subsequent supplements and amendments.

1.6 DIN 2413. Stahlrohre, Berechnung der Wanddicke gegen Innendruck. June 1972.

1.7 ANSI/ASME B 31.8 - 1979. Liquid Petroleum Transportation Piping Systems. The American Society of Mechanical Engineers, New York, 1979.

1.8 Published Document 6493. Guidance on some methods for the derivation of acceptance levels for defects in fusion welded joints. British Standards Institution, 1980.

1.9 European Recommendations for Steel Constructions. ECCS-EG-76-1E.

12.2 *TGSL and associated reports*

2.1* Technische grondslagen voor de berekening van ingegraven stalen transportleidingen. (TGSL - 1986), TNO-IBBC Report BI-86-110, 1986.

2.2* GRESNIGT, A. M., Rekenregels voor ingegraven rechte stalen leidingen, TNO-IBBC Report BI-86-112, 1986.

2.3* GRESNIGT, A. M., Rekenregels voor gladde bochten in ingegraven stalen leidingen, TNO-IBBC Report BI-86-113, 1986.

2.4* GRESNIGT, A. M., Rekenregels voor mijterbochten (mitred bends) in ingegraven stalen leidingen, TNO-IBBC Report BI-86-114, 1986.

2.5* COO, P. J. A. DE, A. M. GRESNIGT, Computerprogramma rekenregels voor ingegraven rechte stalen leidingen, TNO-IBBC Report BI-86-121, 1986.

2.6* GRESNIGT, A. M., Vermoeiingsberekening bij ingegraven stalen transportleidingen, TNO-IBBC Report BI-82-31, 1982.

2.7* RIETJENS, P. H. A., Scheurpropagatie in gastransportleidingen, N.V. Nederlandse Gasunie, 1981.

2.8* GRESNIGT, A. M., Ontwerp en berekening van ingegraven stalen leidingen met de plasticiteitsleer. Samenvattend rapport van het onderzoek pijpleidingen - OPL, TNO-IBBC Report BI-86-111, 1986.

2.9* BRISTOLL, P., A. M. GRESNIGT and P. H. A. RIETJENS, Materiaaleisen, eindrapport van de Subgroep Materiaaleisen van de Begeleidingscommissie Pijpleidingen, TNO-IBBC Report BI-82-74, 1982.

2.10 DOUWEN, A. A. VAN, A. M. GRESNIGT and J. W. B. STARK, Plastic design of buried steel pipelines for transport of oil, gas or water, verified by tests on scale models, TNO-IBBC Report BI-74-67, 1974.

2.11*GRESNIGT, A. M., Kritieke stuik en kritieke rotatie in verband met plooien door buiging, normaalkracht en wringing. TNO-IBBC Report BI-86-116, 1986.

2.12*GRESNIGT, A. M., De invloed van uitwendige belastingen op de barstdruk van ingegraven stalen leidingen, TNO-IBBC Report BI-86-115, 1986.

---

* References marked into an asterisk are in Dutch.

12.3 *Other publications*

3.1 REISSNER, E. and H. J. WEINITSCHKE, Finite pure bending of circular cilindrical tubes. Quarterly of applied mathematics, Vol. XX, January 1963.

3.2 ALEXANDER MENDELSON, Plasticity, Theory and Application. The McMillan Company, New York, London, 1968.

3.3 TIMOSHENKO, S. P. and J. M. GERE, Theory of elastic stability, McGraw-Hill.

3.4 SHERMAN, D. R., Tests of circular steel tubes in bending. J. of the Structural Division of the ASCE, November 1976, pp. 2181-2195.

3.5 KATO, B., Local buckling of steel circular tubes in plastic region. Proc. Int. Colloquium on Stability of Structures under Static and Dynamic Loads, SSRC/ASCE, Washington, March 1977.

3.6 MURPHEY, C. E., Ultimate pipe strength under bending, collapse and fatigue. Shell Development Company, Pipeline R & D Laboratory, Deepwater Pipeline Feasibility Study, Section 21-1, April 1975, Houston.

3.7 REDDY, B. D., An experimental study of the plastic buckling of circular cylinders in pure bending. Int. J. Solids Structures, Vol. 15, pp. 669-683.

3.8 KOROL, R. M., Critical buckling strains of round tubes in flexure. Int. J. Mech. Sci., Vol. 21, 1979, pp. 719-730.

3.9 KIMURA, T., S. IDOGAKI, K. TAKADA and Y. FUJITA, Experimental and analytical studies of the elasto-plastic behaviour of offshore pipelines during laying. Offshore Technology Conference, paper 3737, 1980, Houston.

3.10 BOUWKAMP, J. G., Buckling and post-buckling strength of circular tubular sections. Offshore Technology Conference, paper 2204, 1975, Houston.

3.11 ROIK, K. and G. WAGENKNECHT, Traglastdiagramme zur Bemessung von Druckstäben mit doppelsymmetrischem Querschnitt aus Baustahl. Berichte aus dem Institut für Konstruktiven Ingenieurbau der Ruhr-Universität Bochum, Heft 27, January 1977.

3.12 KARMAN, TH. VON, Über die Formänderung dünnwandiger Rohre, insbesondere federnder Ausgleichrohre. Zeitschrift des Vereines deutscher Ingenieure, Band 55, No. 45, 11 November 1911.

3.13 RODABAUGH, E. C. and H. H. GEORGE, Effect of internal pressure on flexibility and stress intensification factors of curved pipe or welding elbows. Trans., ASME, 1957.

3.14 THOMSON, G. and J. SPENCE, Maximum stresses and flexibility factors of smooth pipe bends with tangent pipe terminations under in-plane bending. Journal of Pressure Vessel Technology, November 1983, Vol. 105, pp. 329-335.

3.15 GERARD, G. and H. BECKER, Handbook of Structural Stability, Part III - Buckling of curved plates and shells. N.A.C.A. Technical Note 3783 (1957).

3.16 WARDENIER, J., Hollow Section Joints, Delft University Press, 1983.

3.17* DIJKSTRA, O. D. and A. M. GRESNIGT, Eigenschappen van gladde bochten bij buiging in en uit het vlak van de bocht. Polytechnisch Tijdschrift, Werktuigbouw 34 (1979) No. 12.

3.18 GRESNIGT, A. M., Analysis of pipelines in settlement areas. Paper presented during the pipeline conference "Pipe - pipeline - pipeline system", Utrecht, November 1985.

* References marked into an asterisk are in Dutch.